Final Report on Contract No. NAS 9-15091

NUMERICAL SIMULATION OF DYNAMICS OF BRUSHLESS DC MOTORS FOR AEROSPACE AND OTHER APPLICATIONS

VOLUME (I) - MODEL DEVELOPMENT AND APPLICATIONS - PART (A)

Submitted to NASA-Johnson Space Center

Control Systems Development Division

Houston, Texas 77058

by

Principal Investigator

N. A. O. Demerdash

and

Research Associate

T. W. Nehl

Department of Electrical Engineering

Virginia Polytechnic Institute and State University

Blacksburg, VA 24061

ACKNOWLEGEMENTS

The authors would like to acknowledge the many stimulating discussions with Mr. J. T. Edge of the LBJ NASA Space Flight Center in Houston Texas. These discussions and suggestions were very instrumental in the successful completion of this contract. We would also like to acknowledge that much of the symbolism used in this report, as well as some of the figures were adopted from the final report of the prime contractor, Delco Electronics, References (2), (3), and (4). This was done to assure continuity and consistency between the VPI and Delco efforts.

TABLE OF CONTENTS

1. INTRODUCTION

This document presents the final technical report on work performed at Virginia Polytechnic Institute and State University under the NASA contract NAS9-15091. This contract provided for the development of a detailed and accurate numerical model of the NASA-DELCO Electromechanical Actuator or EMA, References (1), (2), (3), (4).

For convenience, the final report has been divided into two separate volumes: Volume I and Volume II. Volume I deals with the development of a numerical model for the EMA. This topic will be expanded upon in Reference (1). The first volume also contains a comparison between data obtained from the numerical model and data obtained from tests performed on the actual hardware. Volume II describes the function and use of the FORTRAN COMPUTER PROGRAM which implements the numerical EMA model.

The EMA model developed here is based upon the descriptions given in References (2), (3), and (4). Background information and descriptions of the NASA-DELCO EMA are presented next.

1.1 THE NASA-DELCO EMA

At the present time, the positioning of flight control surfaces such as flaps, elevons, and rudders, Figure (1.1-1), is accomplished almost exclusively by hydraulic actuators. The overwhelming preference for the hydraulic actuator is due to the poor past performance of the EMA when compared with its hydraulic counterpart. This poor performance was due mainly to two factors: (1) The lack of practical, fast and reliable high power transistor switches and (2) The lack of a suitable actuator motor.

Recent advances in magnet technology, Reference (6), have made it possible to reduce the size of both the rotor and stator assemblies through

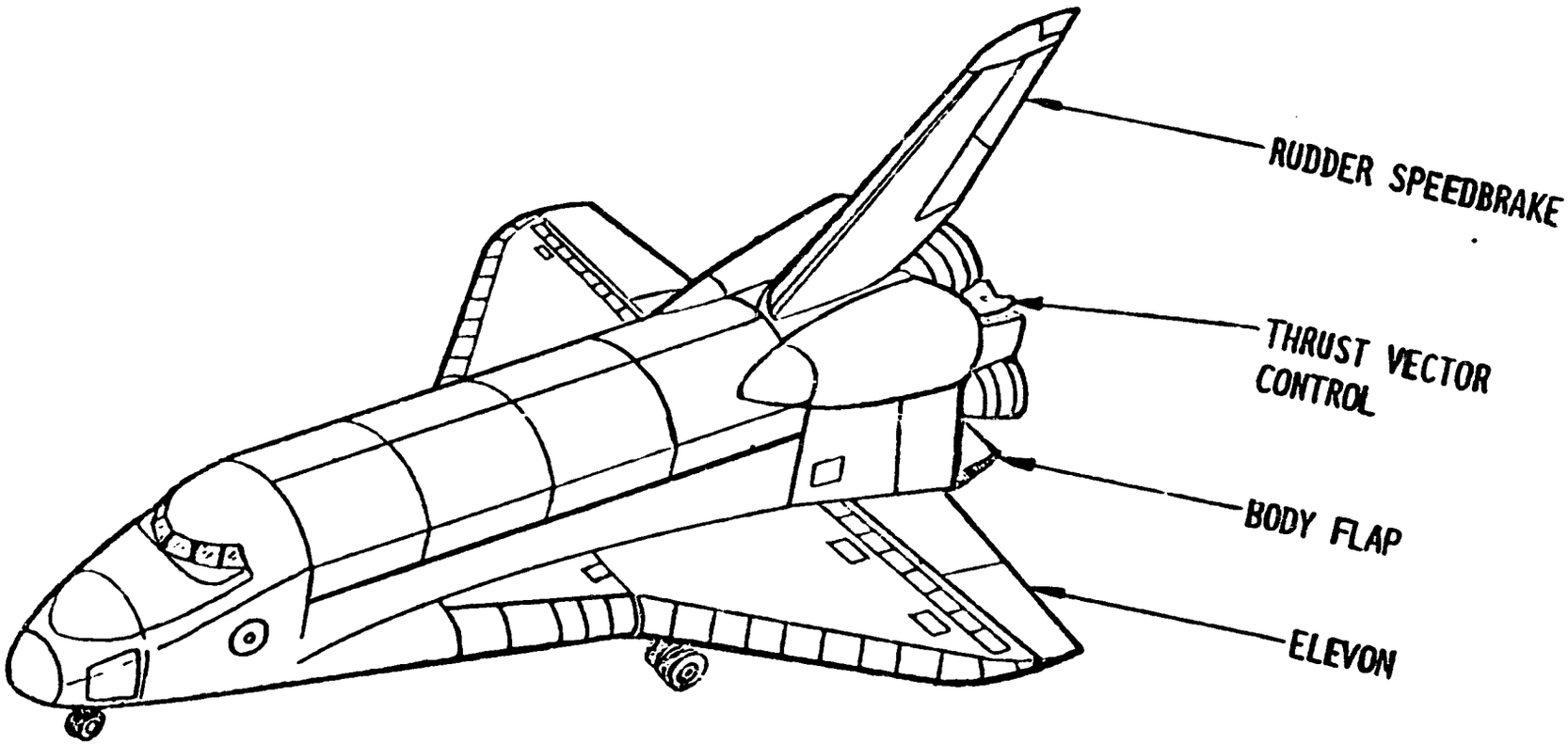

Figure 1.1-1. Applications of Electromechanical Actuators (EMA)

the use of high energy density samarium-cobalt permanent magnets to replace the rotor field winding. The reduction in rotor size and weight (mass) has resulted in improved actuator performance because of the reduced rotor inertia. At the same time, transistor switches capable of switching more than 10 KW in one microsecond or less became available, References (2), (3) and (4).

As a result of these advances, a technology program was initiated by NASA to explore the possibility of replacing existing hydraulic flight control surface actuators with electromechanical ones. The justifications for this program are based upon the possibility of reducing actuator weight, volume, and maintenance requirements as well as increasing reliability.

NASA's interest in the EMA concept resulted in a contract to the DELCO Electronics Division of General Motors; see References (2), (3), and (4). This contract, which has been completed successfully, provided for the development, fabrication, and evaluation of a prototype EMA capable of performing in aerospace applications.

The actual function performed by this prototype EMA is illustrated in Figure (1.1-2). In this figure, the actuator receives a flap position command from an external source (the pilot for instance). The EMA control logic translates this position command into a motor torque of a specified magnitude and orientation. This commanded torque is produced by a power conditioner which drives an eight pole permanent magnet brushless d.c. machine. The resulting flap motion is in the direction of the commanded flap angle. Once the flap reaches the commanded position, it oscillates briefly about this point until the energy of the rotating masses is completely transformed into both heat and electrochemical energy.

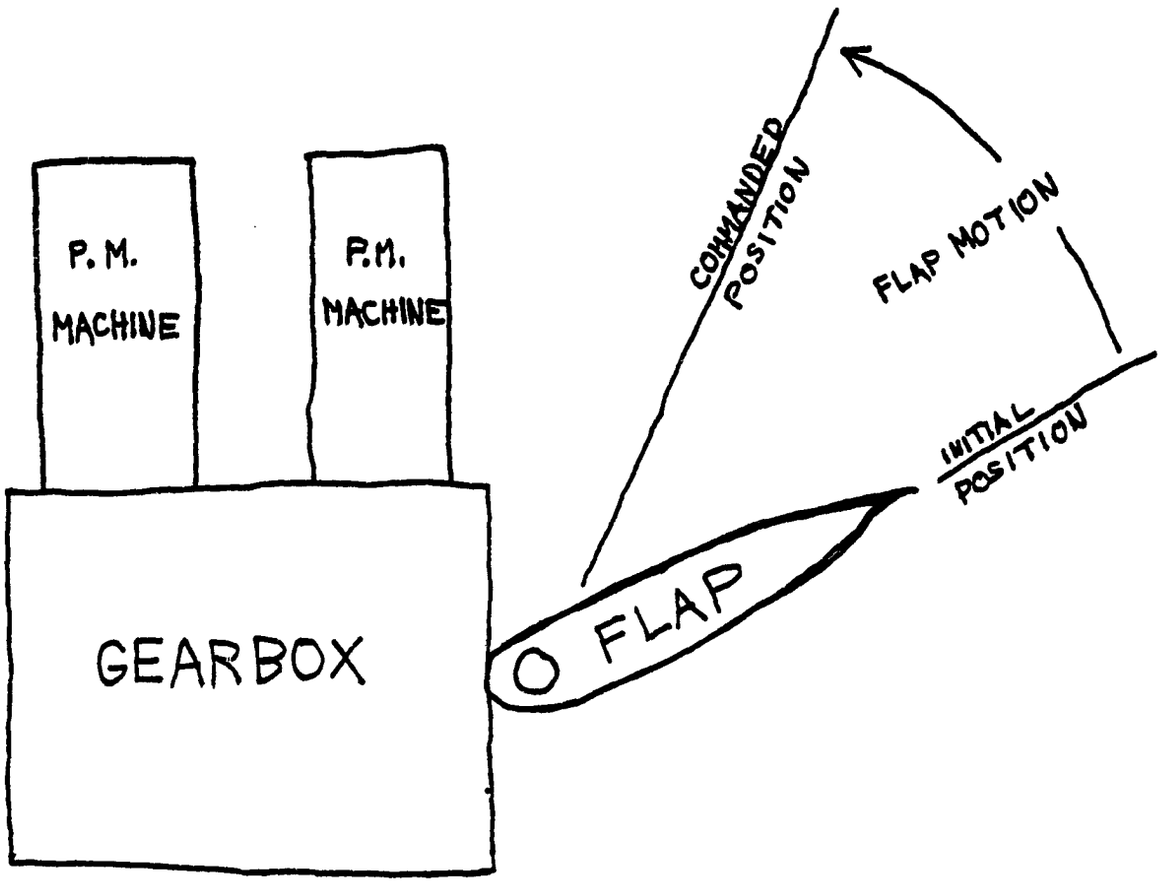

Figure 1.1-2. Applications of Electromechanical Actuators (EMA).

The physical structure of the Delco EMA is given in Figure (1.1-3). Notice that this system utilizes four independent servo loop channels. The four independent channels help to increase the overall reliability because during normal operation two channels are active while the other two are inactive. High reliability is of great importance in aerospace applications since the failure of such components results in reduced or total loss of aircraft control.

The structure of one of these servo loop channels is shown in Figure (1.1-4). At the heart of each servo loop channel there is a power conditioner and machine combination, see Figure (1.1-5), which modulates the power of the supply batteries into the proper actuation energy. In order to achieve this goal, the power conditioner and machine network are operated in any one of three modes by means of transistor switching commands generated by the control electronics. These modes are:

a) Motoring in the Positive and Negative Directions,

b) Regenerative Braking in the Positive and Negative Directions, and

c) Plugging or Braking in the Positive and Negative Directions.

The control electronics determine the proper operating mode at any instant in time based upon the inputs shown in Figure (1.1-4). These inputs are:

a) The Flap Position Command

b) The Three Bit Output of the Rotor Position Sensor or RPS

c) The Machine Velocity

d) The Flap Position

e) The Average Machine Current (Torque)

A typical sequence of mode commands generated during a step response, such as the one in Figure (1.1-2), is shown in Figure (1.1-6). At time

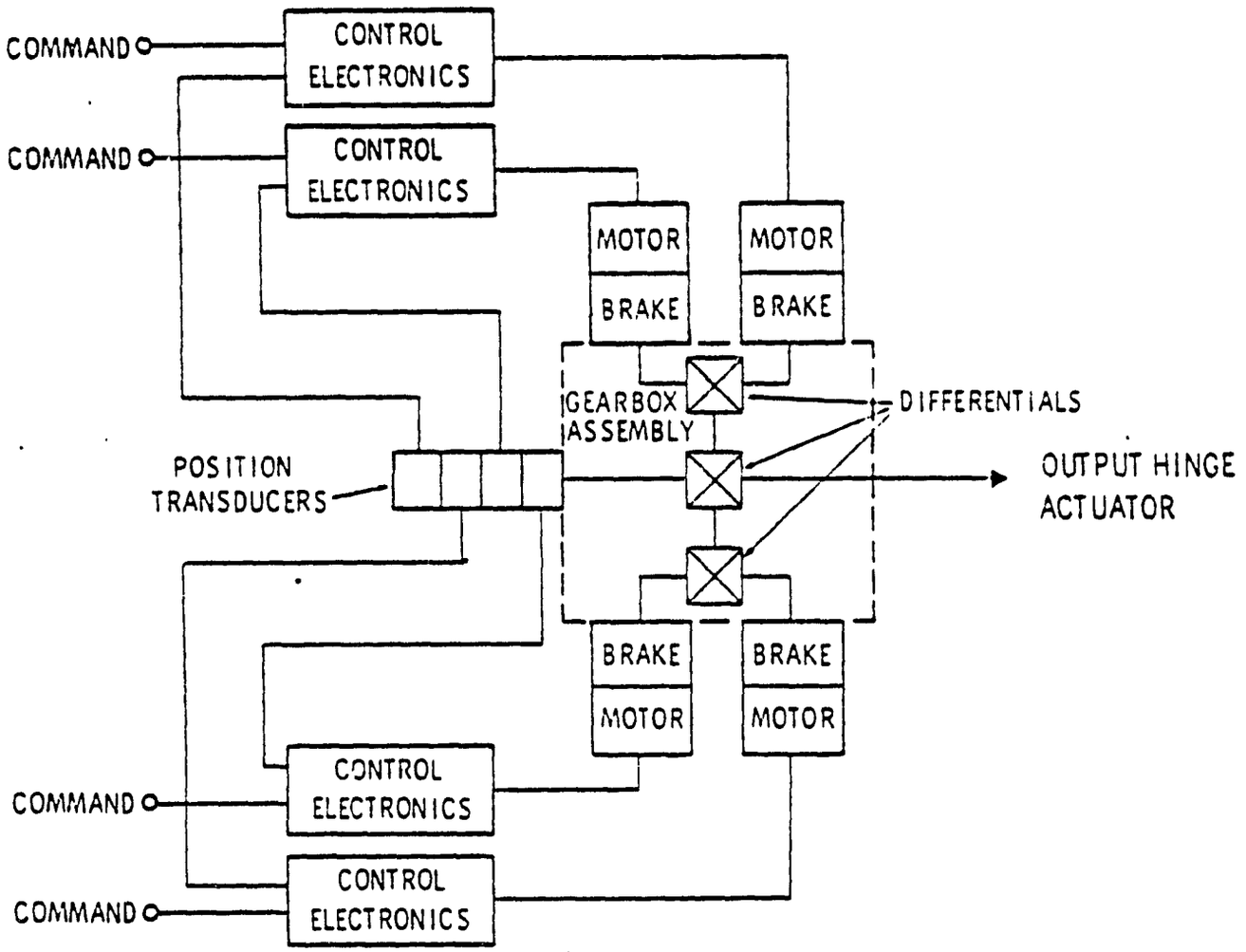

Figure 1.1-3. Functional Diagram of the Delco EMA.

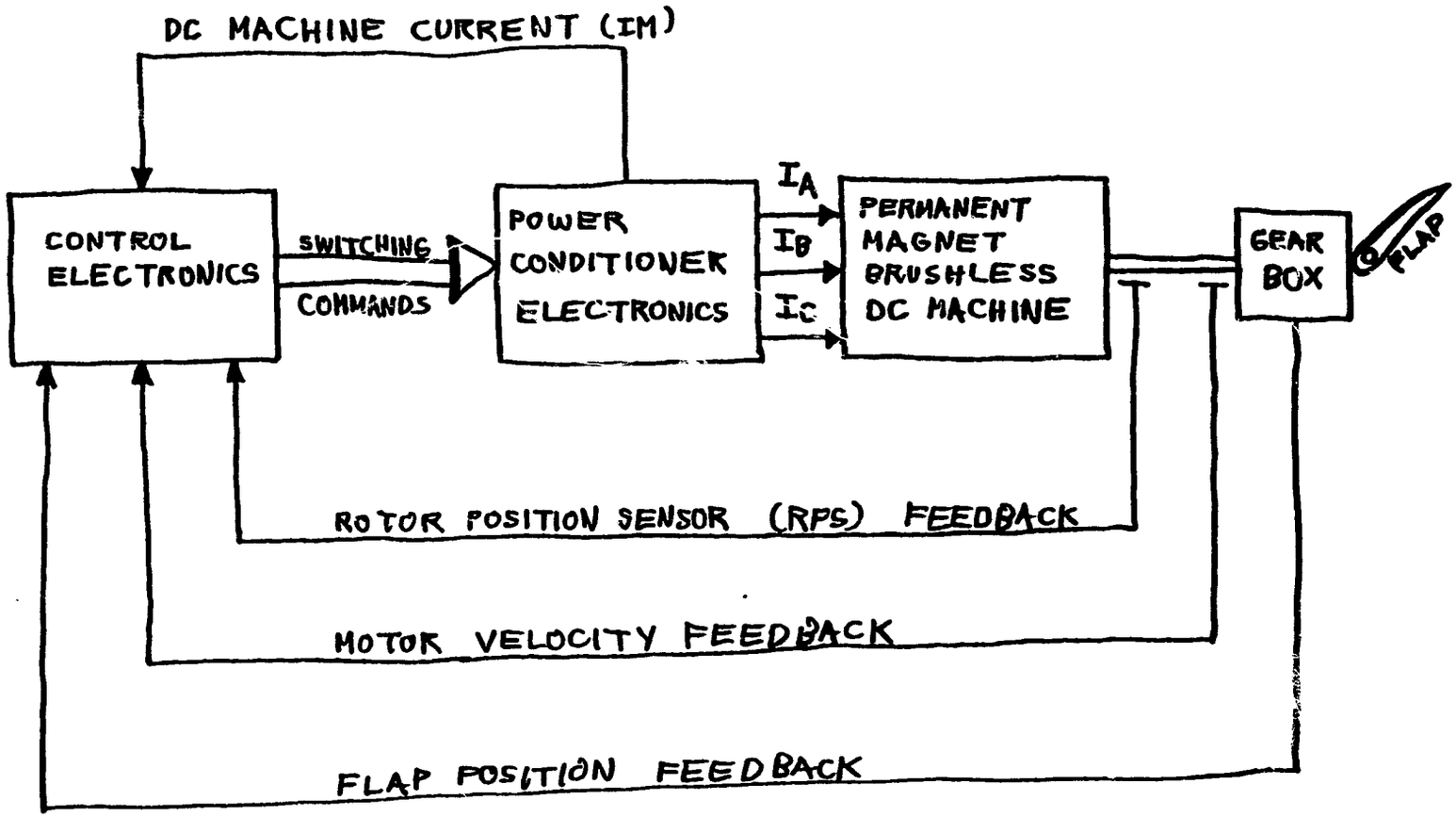

Figure 1.1-4. Functional Diagram of a Single EMA Channel.

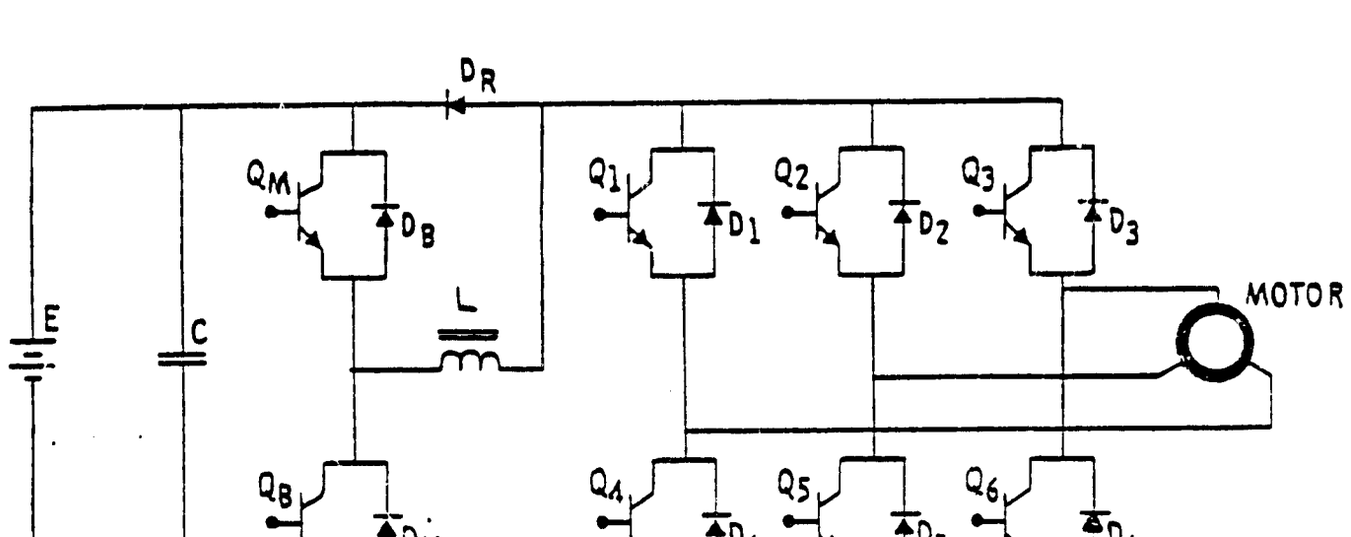

Figure 1.1-5. EMA Power Conditioner Schematic.

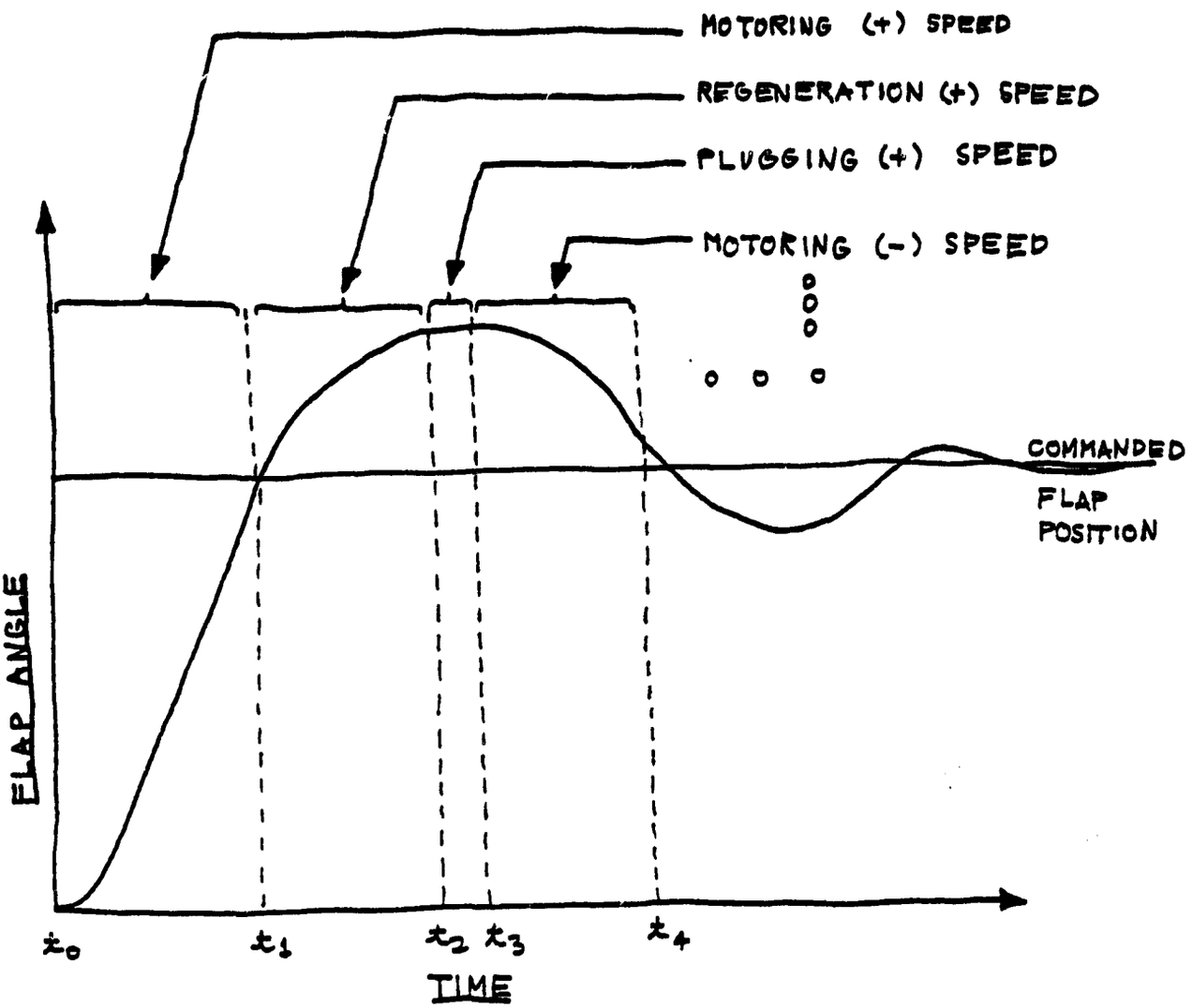

Figure 1.1-6. Idealized EMA Step Response

$t = t_o$ the machine is commanded to motor in the positive direction in response to the step position command. The flap responds with motion in the positive direction, thereby reducing the distance between the actual and commanded flap positions. When the flap reaches the commanded position at some time $t = t_1$, certain logical decisions are made. If the rotor velocity at this point is greater than a specified threshold velocity, then the motor is thrown into the regenerative braking mode, References (1)-(4). During this mode, the machine behaves like a constant field current salient pole generator. When the magnitude of the machine velocity dips below the threshold value, the EMA enters the plugging or braking mode. The machine in this case receives energy from the supply battery which decreases the energy of the rotating masses. When the rotor comes to rest, the position of the flap will exceed the command position. Consequently, the machine is forced to motor in the negative direction. This process is repeated until the commanded flap angle is reached and the flap is at rest.

The velocities of the four machines are summed by a differential gearbox arrangement as shown in Figure (1.1-3). The physical details of this gearbox are pictured in Figure (1.1-7). The advantage of the differential gearbox is the isolation of the rotor inertias of the inactive machines from the inertia of the active machines. The output shaft of the differential gearbox drives a flap hinge actuator. The flap position is fed back continuously to the channel control electronics by position transducers attached to the differential gearbox, Figure (1.1-3).

The rotor velocity is sensed by means of a tachometer attached at the back of the machine. This velocity along with the flap position and the average machine current (or Torque) is processed by the control electronics into a current command for each machine.

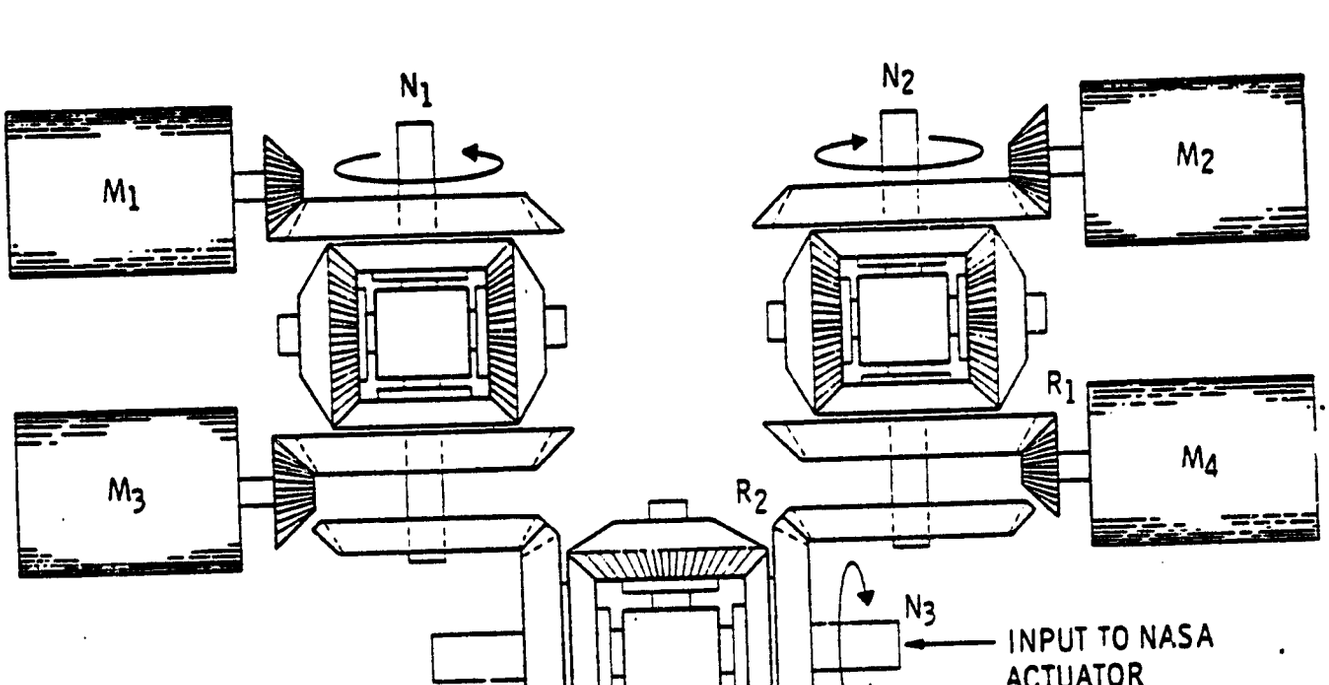

Figure 1.1-7. The Differential Gearbox Arrangement.

The current command is equivalent to a machine torque command because of the linear relationship between the average machine currents and the developed electromagnetic machine torque, due to the equivalent constant field excitation, References (1), (2), (3), and (4).

The EMA described here has been tested and analyzed by Delco Electronics, References (2), (3), and (4). The results of these tests have demonstrated the potential of such actuators for aerospace applications. However, there are still many questions which must be answered before EMA's become serious contenders against existing hydraulic actuators. For example:

(a) Can the switching control for the power conditioner transistors be modified so as to reduce the severity of the switching transients?

(b) How does the timing of the phase commutation affect the overall response and reliability of the EMA?

(c) What are the effects of system parameter changes on the overall system efficiency and performance?

(d) What are the consequences of component failures?

These and other questions are difficult to answer experimentally because of the high costs involved in prototype development. Therefore, the only other alternative is to simulate the EMA dynamics by means of a mathematical model of sufficient detail to allow the accurate calculation of the EMA response under a variety of inputs and configurations. The development and verification of such a model is the topic of the remainder of this first volume.

1.2 PROBLEM DEFINITION AND STATEMENT OF TASKS

The EMA which was introduced in the last section must be examined thoroughly under all possible operating conditions in order to determine the expected ranges of the system state variables. This information is vital in the determination of the stresses experienced by the elements of the power conditioner and hence its reliability. Furthermore, the present design must be carefully evaluated for the purpose of design optimization.

Such knowledge is very costly to obtain by experimental means. In addition, some of this knowledge would require tests which might result in damage to the system. For these reasons a mathematical model of the EMA becomes a necessity.

The EMA actuator unfortunately contains many nonlinearities which greatly complicate the mathematical model. The differential equations which constitute this model are therefore nonlinear. The only practical solution of such equations is by means of a numerical integration scheme. Based upon these observations it becomes evident that a COMPUTER SIMULATION of the EMA on an instantaneous time basis is the only practical modeling approach. The chosen modeling approach can be outlined as follows:

STEP 1. Determine the set of nonlinear differential equations which govern the dynamics of the EMA from the underlying physical principles.

STEP 2. Simulate the control logic by means of equivalent boolean expressions.

STEP 3. Divide the solution period into N equal time increments or steps. These increments are chosen sufficiently small so that the nonlinearities can be linearized during each increment.

STEP 4. Integrate the differential equations forward by one time increment at a time until the entire solution period has been covered. The differential equations are updated, if necessary, after each integration in order to account for the nonlinearities.

These steps are covered in greater detail in Chapters 2, 3, and 4 of this volume. A model of the power conditioner and machine network is derived in Chapters 2 and 3. The equations which describe the control loops, the rotating masses and the control logic are developed in Chapter 4.

The specific requirements of the NASA contract, NAS-15091, are summarized by the statement of tasks below:

TASK 1: Development of a mathematical representation or model for the entire EMA system shown in Figure (1.1-2), under one or two machine operations. This model must include:

(a) A simulation of the logical functions performed by the low level electronics.

(b) A simulation of the linear and nonlinear transfer functions which form the servo loop controller.

(c) A simulation of the nonlinear power conditioner network under all operating configurations.

(d) A simulation of the electromagnetic interactions inside the permanent magnet machines.

(e) A simulation of the rotating masses.

TASK 2: Implementation of the numerical EMA model, developed under Task 1, in terms of a FORTRAN computer program.

TASK 3: Verification of the numerical model by means of test results obtained from the actual hardware.

TASK 4: Determination of the commutation transients under various operating regimes.

TASK 5: Development of a USER's guide for the FORTRAN program.

These tasks have been completed successfully; and together they form the basis for this report. Tasks 1 through 4 are covered in the first volume of this report while Task 5 constitutes Volume II.

The upcoming chapter introduces the actuator motor and models which describe its performance.

2. ELECTRICAL MODEL OF THE PERMANENT MAGNET BRUSHLESS D.C. MACHINE

Chapter 2 deals with the four permanent magnet brushless d.c. motors which power the Delco EMA. An electrical network model of these motors is developed. This model includes the effects of magnetizing and demagnetizing mmf's of the stator winding. Later, in Chapter 3 this model is incorporated with the power conditioner model to form the power conditioner and machine network model.

This chapter is divided into four sections. The first section describes the mechanical and electrical characteristics of this machine. The three different modes of operation: Motoring, Regeneration, and Plugging, are described in terms of the electromagnetic interactions which take place inside the machine in Section 2.2. The electrical network model of the machine is developed in Section 2.3 which follows. In the last section of this chapter, the calculations of the machine back emfs and the developed electromagnetic torque are presented.

2.1 MACHINE DESCRIPTION

The electromechanical actuator, introduced earlier in Section 1.1, derives its actuation energy from four identical permanent magnet brushless d.c. motors. This type of machine was chosen because of its reliability, low rotor inertia, low weight and volume per KW, negligible rotor eddy current losses, and excellent torque characteristics. These factors are important if this type of actuator is to compete successfully with conventional hydraulic systems. These machines owe many of their excellent performance characteristics to the recent advances in the field of high energy product permanent magnets. Such magnets have made it possible to reduce the size of the rotor without risk of demagnetizing the magnetic pole pieces, see Reference (2).

Each one of these four machines has a rating of 17 hp at 9000 rpm with an output torque of 13.558 nt-m (120 in-lb). These ratings are achieved with a permanent magnet rotor of only 0.1335 m (5.25 in) in length and 0.472 m (1.858 in) in diameter, see Reference (2). More detailed mechanical and electrical information about these machines is presented in sections 2.1.1 and 2.1.2 which follow immediately.

2.1.1 Mechanical Description

A relatively complete description of the Delco permanent magnet brushless d.c. motor can be found in Reference (1.1-1). However, for the sake of completeness, a brief description will be given in this section. The major components of the permanent magnet brushless d.c. motor are:

a) The Rotor Assembly,

b) The Stator Assembly,

c) The electromechanical Brake,

d) The Rotor Position Sensor,

e) The Tachometer,

and

f) The Cooling System.

These components are clearly shown in Figure (2.1-1) which gives a cross sectional view along the rotor axis. The outside diameter of the motor frame shown in this figure is 0.09525 m (3.75 inches). The total weight of the motor including the brake, tachometer, and rotor position sensor is only 9.025 kg (19.9 lbs).

The rotor assembly consists of 48 blocks of magnetic samarium cobalt material which has an energy product of 18 million gauss oersteds. These blocks are bonded, six in a row, onto the faces of an octagonal rotor shaft, Figure (2.1-2), creating an eight pole magnetic structure, Figure (2.1-3). Brass and disks are bonded to this assembly to reduce windage losses and to provide removable material for dynamic balancing, see Reference (2). The rotor assembly is then banded by a fiberglass material, Figure (2.1-4), in order to increase the mechanical strength of the assembly and to decrease windage losses. This assembly

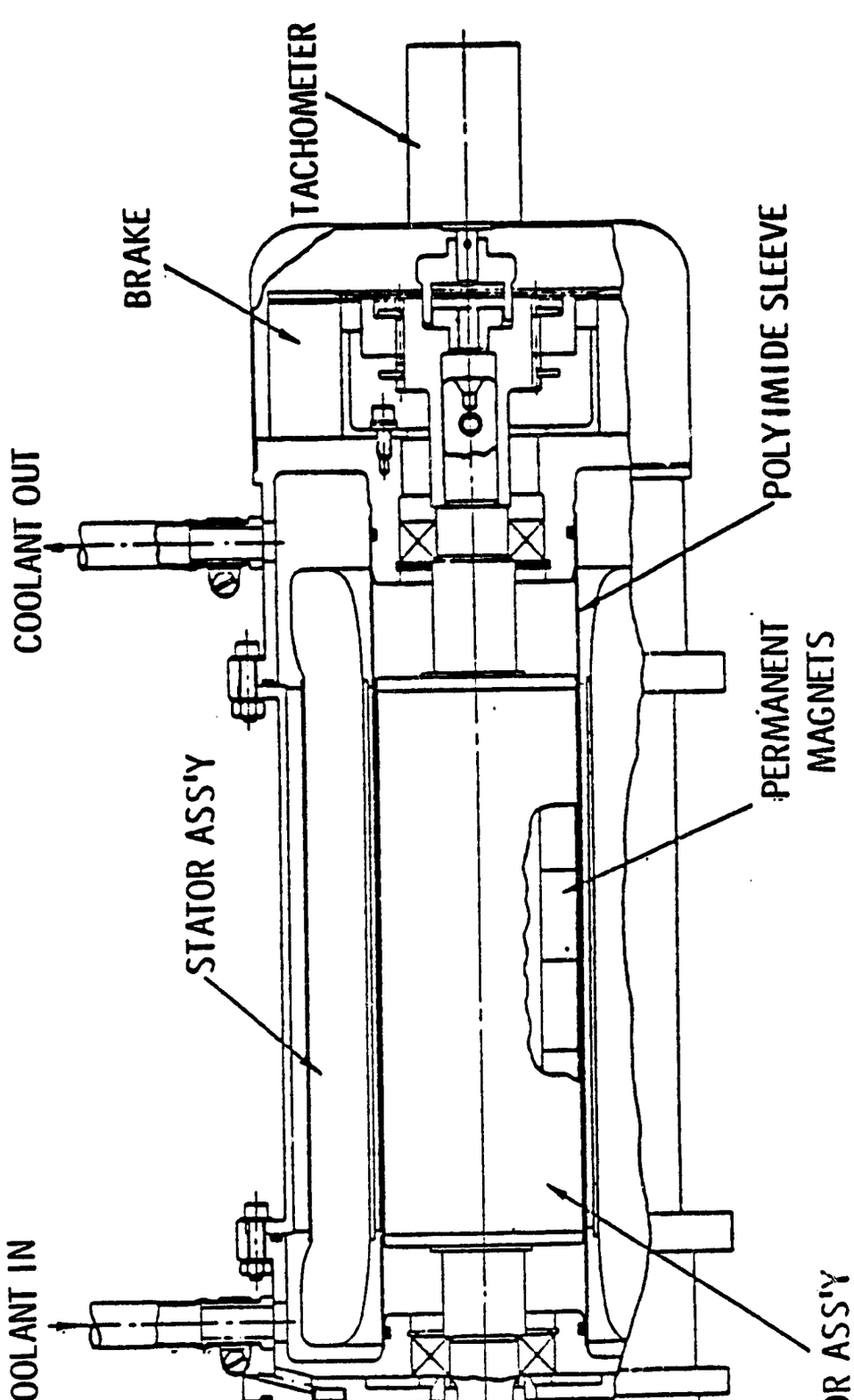

Figure 2.1-1. Cross Sectional View of the EMA Motor Along the Rotor Axis

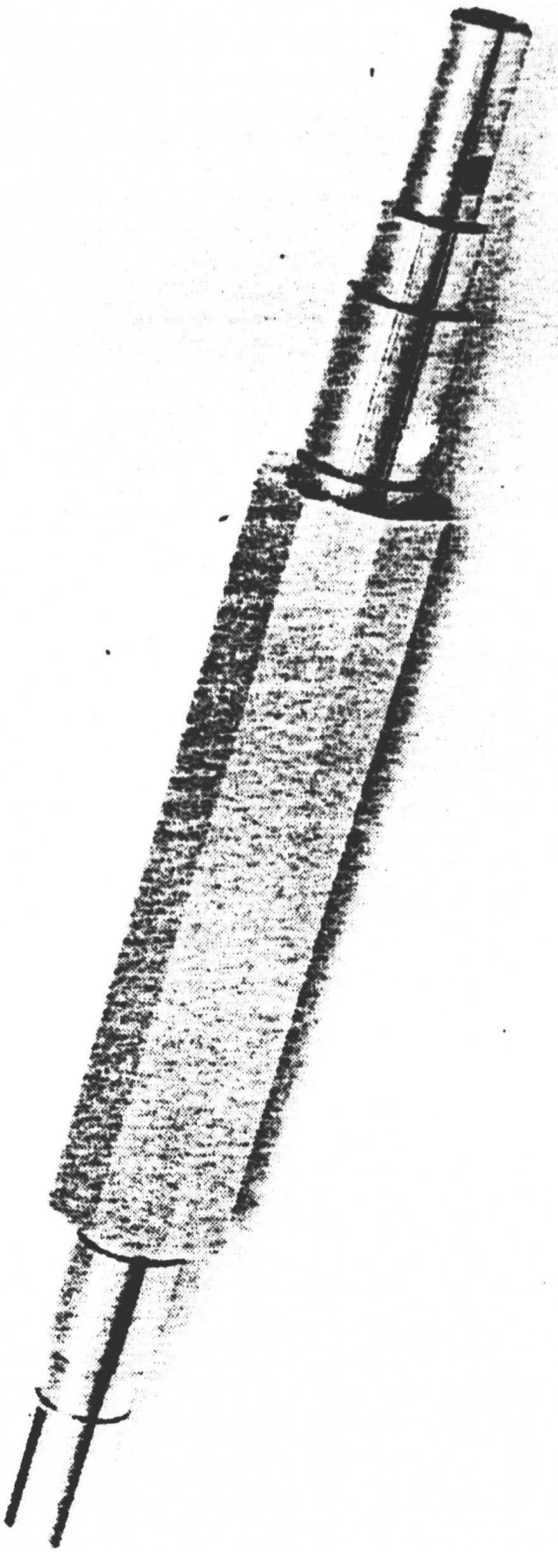

Figure 2.1 2. Rotor Shaft and Core Assembly

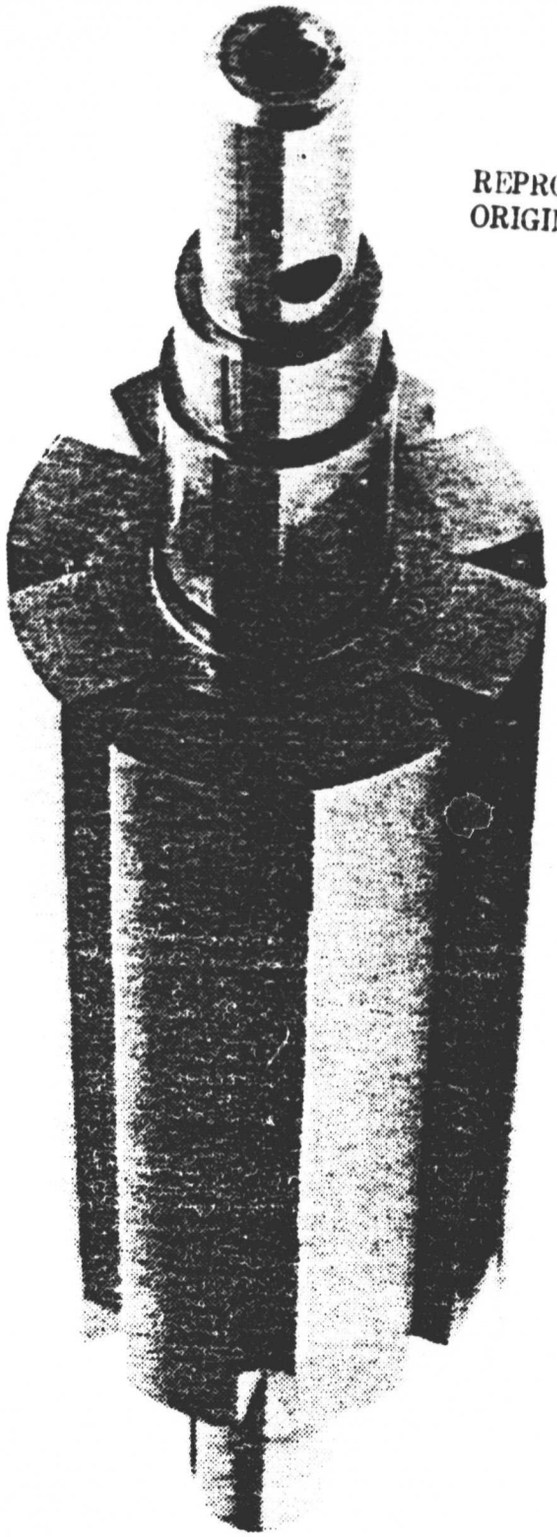

Figure 2.1-3. Permanent Magnet Rotor

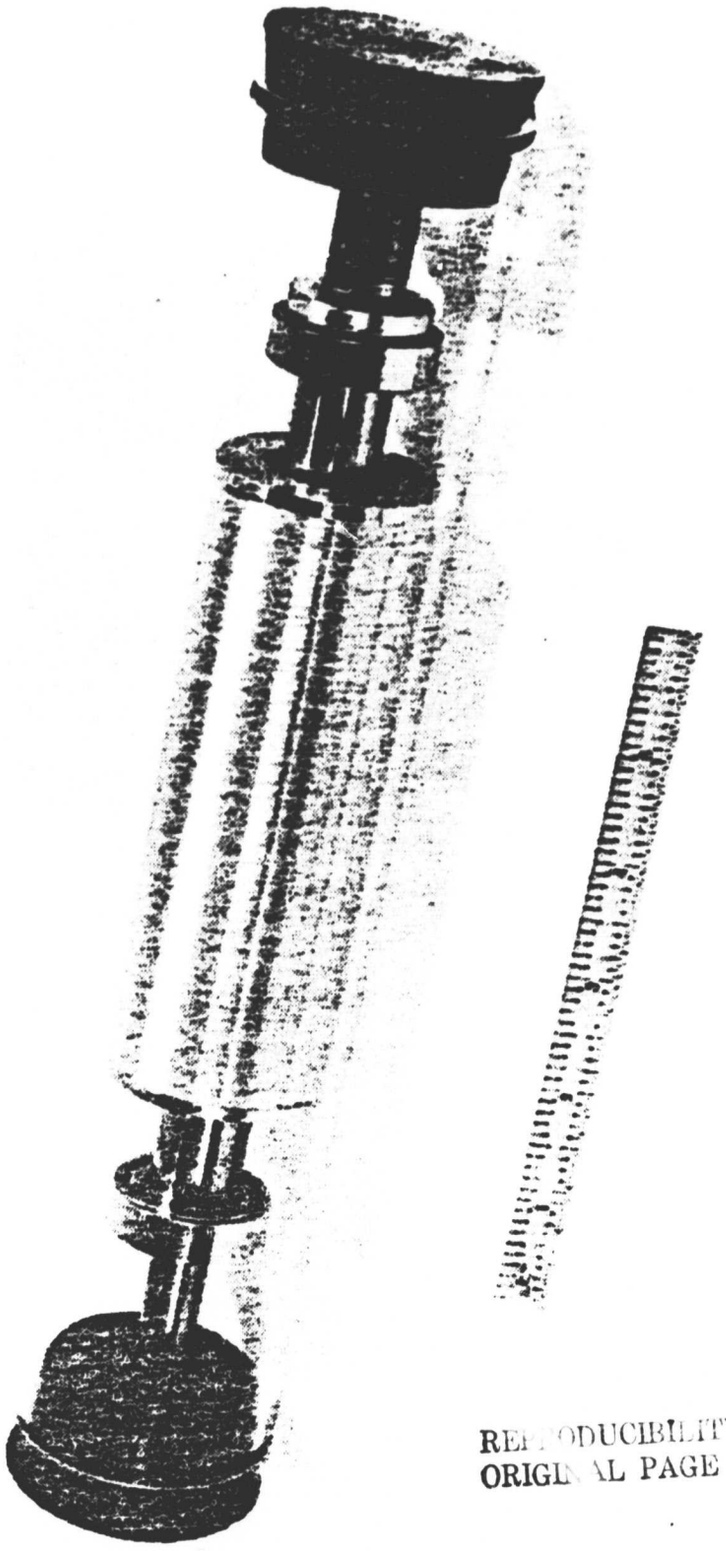

Figure 2.1-4. Rotor Assembly After Banding

has been spin tested by Delco at speeds greater than 30,000 rpm without failure. This is greater than three times the rated speed of 9,000 rpm. The small size of this machine is readily apparent in the actual sized cross section of the motor shown in Figure (2.1-5).

The stator assembly consists of a stack of 7 mil Vanadium Permendur punchings, see Figure (2.1-6). Each stator punching consists of 24 slots and 24 teeth, Figure (2.1-7). The slots are only partially filled in order to allow the circulation of the coolant. A nonmagnetic sleeve covers the inside of the stator bore thereby isolating the stator cooling system as well as reducing windage losses.

A mechanical brake is provided with each motor in order to prevent rotor motion whenever the machine is turned off. This brake makes use of a solenoid actuated braking mechanism, see Reference

At the other end of the rotor shaft lies the rotor position sensor or RPS which is used to control the switching of the inverter transistors. The RPS consists of a laminated rotor, containing four lobes, which operates in conjunction with an electrical sensor composed of nine coils on a laminated stator. The nine coils are arranged into three groups of three coils each. The resolution of the RPS is 60 electrical or 15 mechanical degrees. The logical output signals of these three coil groups (i.e. AA, BB and CC) versus rotor angle are shown in Figure (2.1-8). The RPS output at some angle Θ can be simulated by comparing to zero the values of the three sinusoids shown as dashed lines in Figure (2.1-8) as follows:

$$AA = \begin{cases} 0 & \text{IF} \quad \text{SIN}[4(\Theta_s + \Theta)] < 0 \\ 1 & \text{IF} \quad \text{SIN}[4(\Theta_s + \Theta)] \geq 0 \end{cases} \qquad (2.1\text{-}1)$$

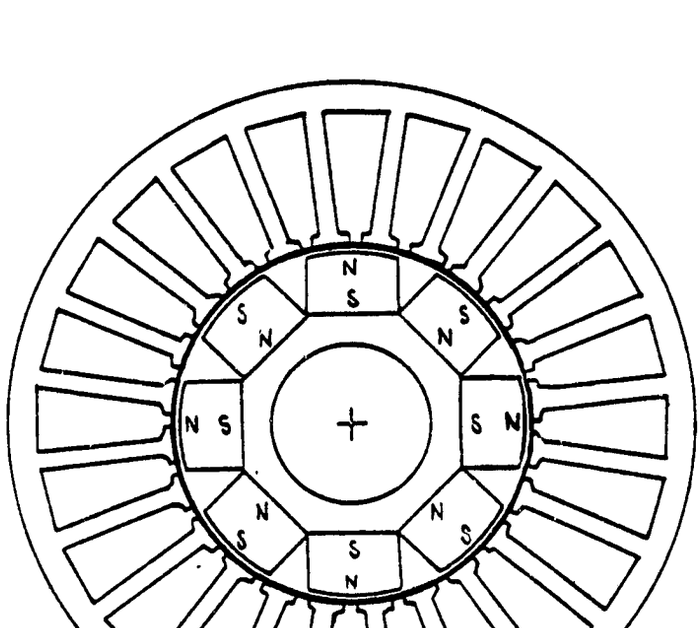

Figure 2.1-5. Actual Sized Cross Section of the EMA Motor

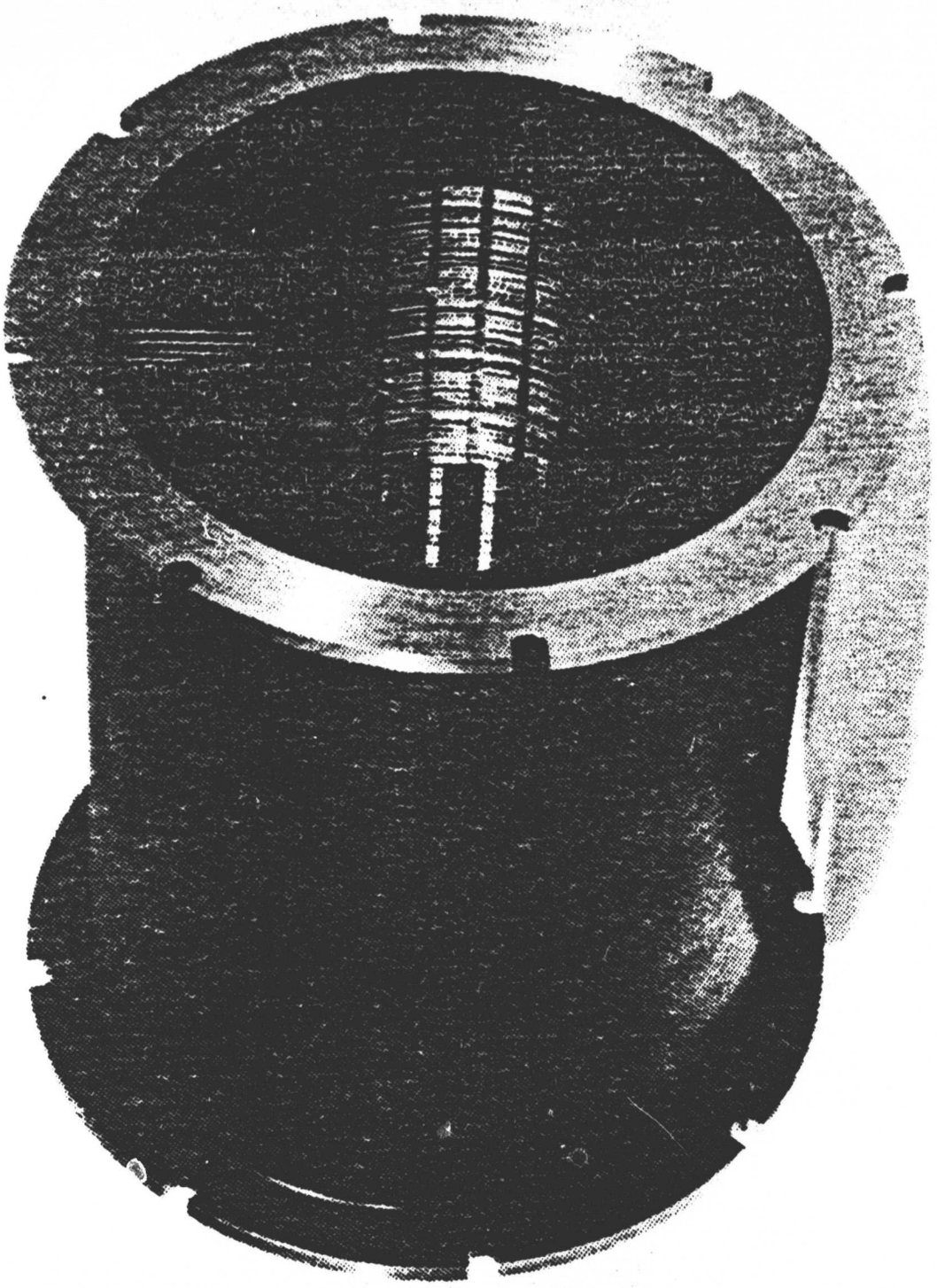

Figure 2.1-6. Stator Assembly

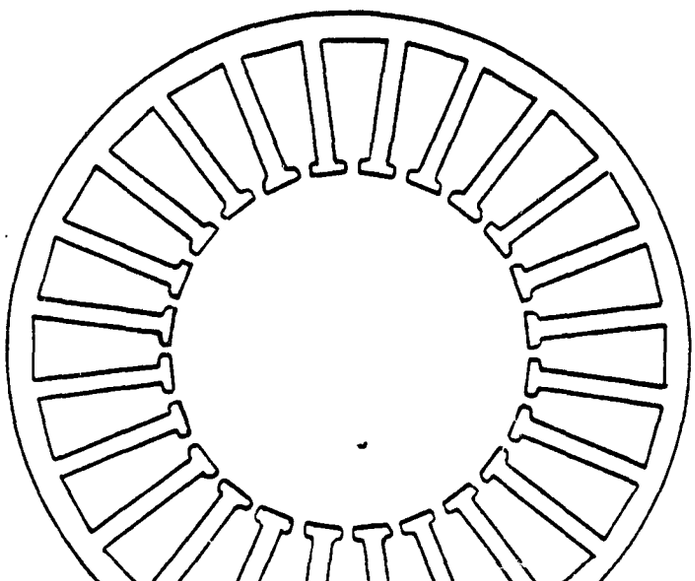

Figure 2.1-7. Stator Punching (Actual Size) for the EMA Motor

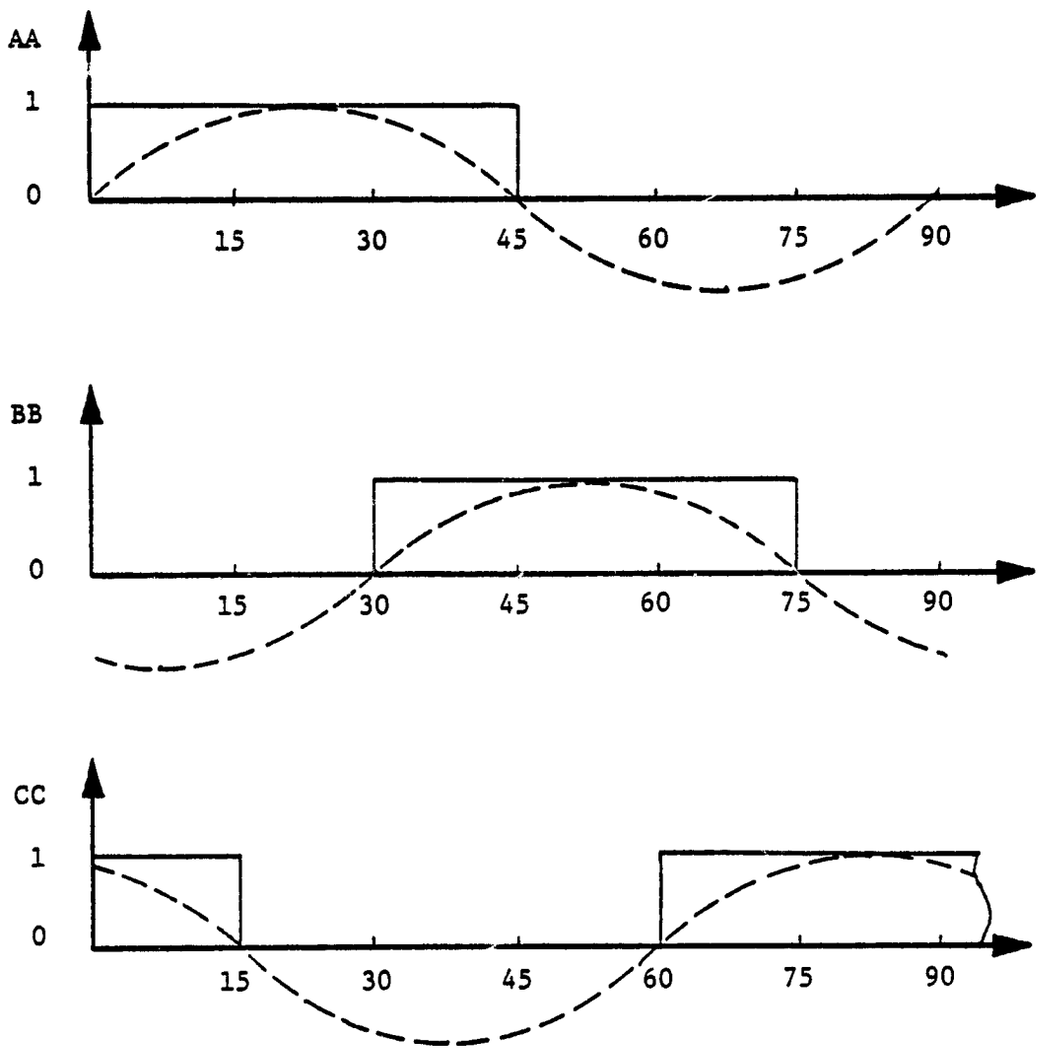

Figure 2.1-8. RPS Output Versus Rotor Angle

$$BB = \begin{cases} 0 & \text{IF} \quad \text{SIN}[4(\Theta_s + \Theta - 30°)] < 0 \\ 1 & \text{IF} \quad \text{SIN}[4(\Theta_s + \Theta - 30°)] \geq 0 \end{cases} \qquad (2.1\text{-}2)$$

and

$$CC = \begin{cases} 0 & \text{IF} \quad \text{SIN}[4(\Theta_s + \Theta - 60°)] < 0 \\ 1 & \text{IF} \quad \text{SIN}[4(\Theta_s + \Theta - 60°)] \geq 0 \end{cases} \qquad (2.1\text{-}3)$$

The angle Θ_s represents a constant shift in the output of the RPS. Figure (2.1-8) shows the RPS output versus rotor angle for $\Theta_s = 0°$.

A tachometer is attached to that end of the rotor shaft which is opposite to the end containing the RPS. The output voltage of the tachometer versus motor speed follows a gradient of 7.0 volts per 1000 revolutions per minute. This output signal is fed back to the channel control electronics where it is processed along with other data to generate the EMA control signals.

2.1.2 Electrical Description

The permanent magnet brushless d.c. motor is rated at 270 volts peak line to line and 60 amperes phase current at rated speed and torque. The electrical configuration of this machine is determined by the eight pole permanent magnet rotor assembly described in the previous section. Consequently, the relationship between electrical and mechanical angles is given by:

$$\Theta_e = P\Theta_m/2$$

or

$$\Theta_e = 4\Theta_m \qquad (2.1\text{-}4)$$

where

P = Number of Poles

Θ_e = Electrical Angle

Θ_m = Mechanical Angle.

The stator has 24 slots which means that there are six slots per pole pair or three slots per pole pitch and two slots per phase. Figure (2.1-9) gives a developed view of a cross section of the stator and rotor. The angular reference for the stator is taken from the phase (a) MMF axis farthest from the right hand side. The rotor angular references are taken at the centers of the north poles.

The structure of the stator phase windings per pole pair is shown in Figure (2.1-10). Each phase winding consists of a series connection of four sets of two-coil groups connected in parallel. Each coil group consists of 11 turns of two AWG #18 heavy ML wires connected in parallel which results in a total of 44 AWG #18 HML conductors per slot. However, there are only 11 independent conductors per slot since the 44 conductors are connected into 11 groups of four conductors in parallel. These 11

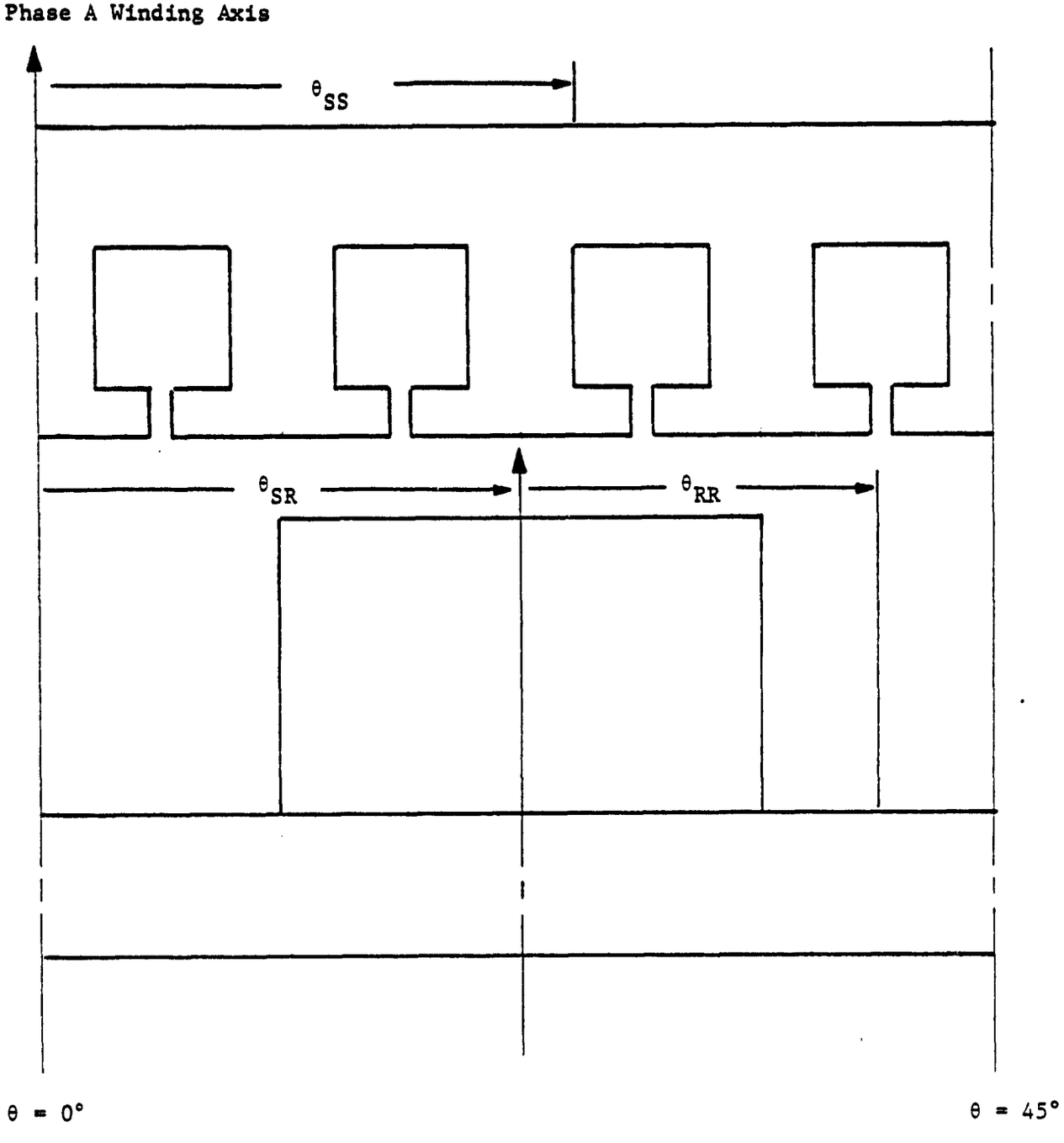

$$\theta_{SS} = \theta_{SR} + \theta_{RR}$$

Figure 2.1-9. Stator and Rotor Angular References

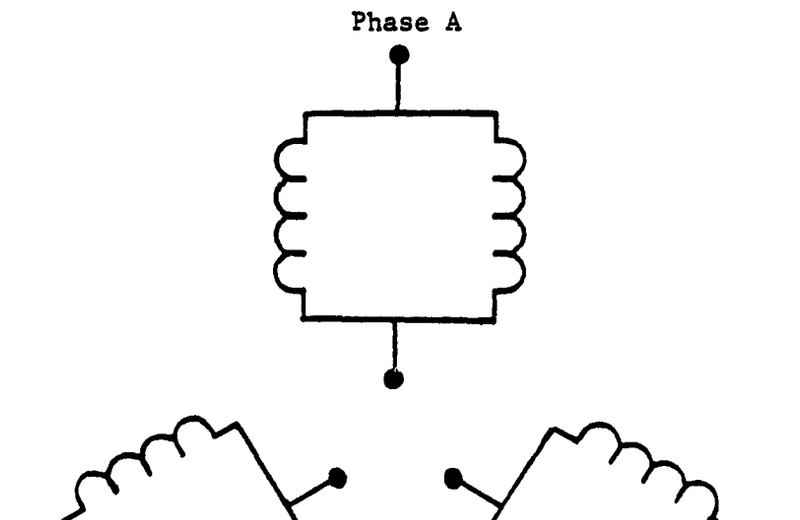

Figure 2.1-10. Stator Winding Schematic Per Pole Pair

groups of conductors are equivalent to 11 turns per pole pair of a conductor with a cross sectional area equivalent to four AWG #18 HML conductors. The phase windings of the four pole pairs are connected together in series resulting in an equivalent phase winding of 44 turns.

The open circuit voltages at various speeds, as determined through tests performed by Delco, Reference (2), are given in Table (2.1-1). A typical open circuit voltage waveform is shown in Figure (2.1-11). Based upon Table (2.1-1) the relationship between the open circuit voltage between the open circuit voltage and the rotor speed is given approximately by:

$$E_{oc} = 0.01555\ n \qquad (2.1\text{-}5)$$

where

E_{oc} = Peak open circuit phase voltage in volts

n = rotor speed in rpm

The electrical operating modes or regimes of this machine are analogous to those of conventional synchronous machines. These operating modes are: motoring, regenerative braking, and plugging. The configurations of this machine and the power conditioner during these modes are the topics of the next section.

Table (2.1-1) Open Circuit Phase Voltages

Motor Speed (rpm)	Phase Voltage (volts peak)
900	14
4500	68
9000	140

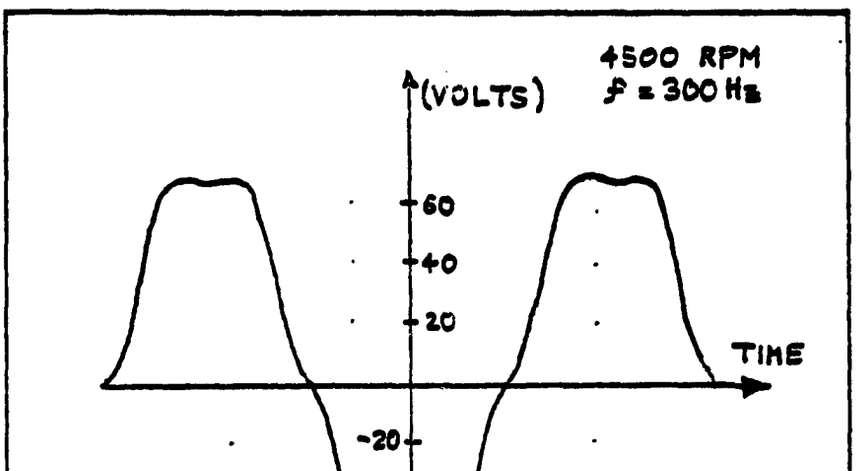

Figure 2.1-11. Open Circuit Phase to Neutral EMF Waveform.

2.2 MACHINE MODES OF OPERATION

The EMA motors during an actuation maneuver can function in any one of three possible operating modes. The operating regions of these modes in the torque-speed plane are shown in Figure (2.2-1). The modes outlined in this figure are:

a) The Motoring Mode - Quadrants I and III,

b) The Regenerative Braking Mode - Quadrants II and IV, and

c) The Braking Mode - Quadrants II and IV.

An analysis of these operating modes is the topic of the three sections which follow. This analysis is based upon the sample data presented in Table (2.2-1) which was obtained from the VPI EMA computer model.

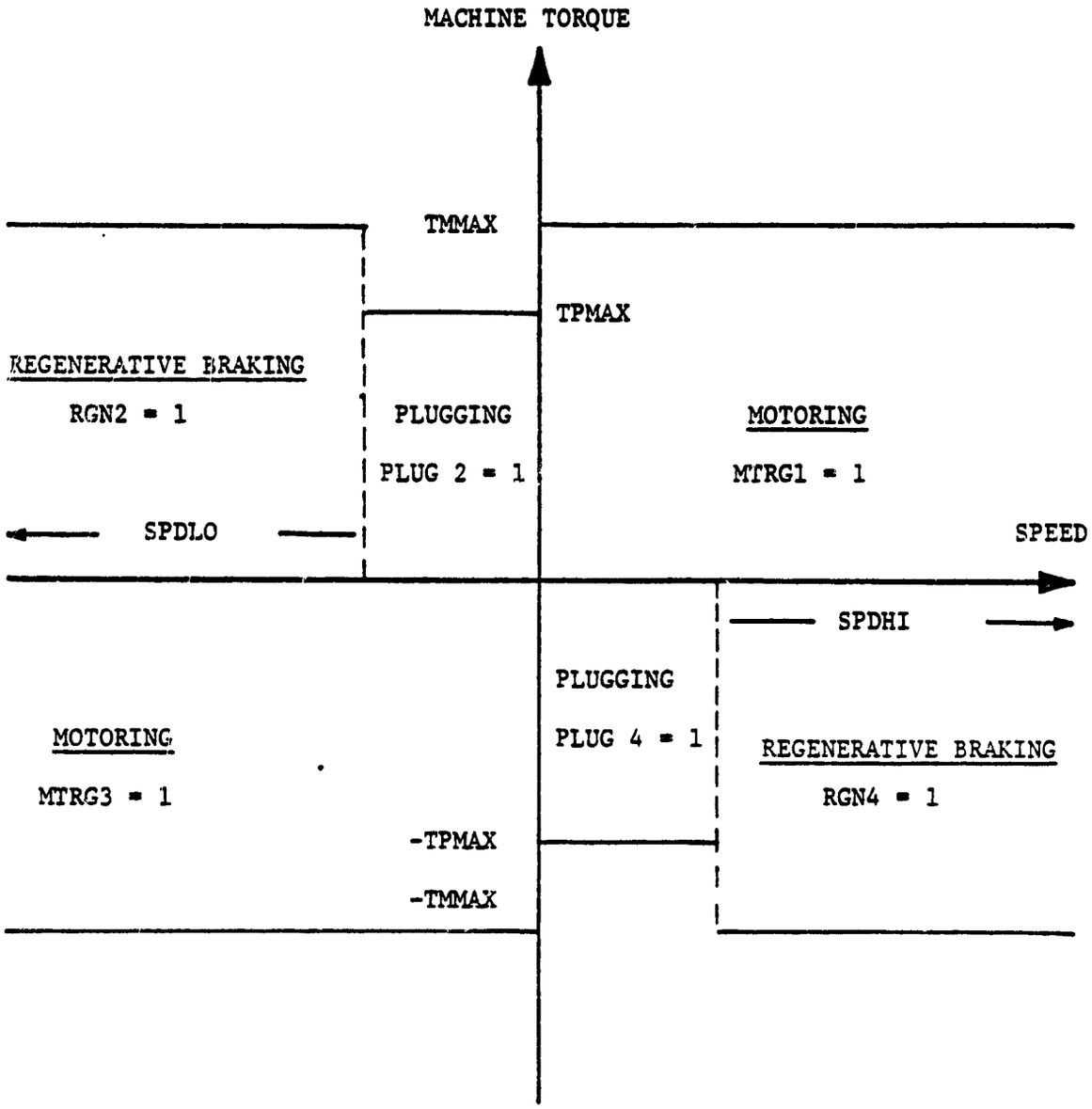

Figure 2.2-1. EMA Operating Regions or Modes

Table (2.2-1) The Status of the Inverter during the Motoring, Regenerative Braking and Plugging Modes at a Rotor Angle of 16.7°.*

I. Motoring Mode

Speed = 4000 rpm Rotor Angle = 16.788° (mech)
Q1 = ON, Q2 = OFF, Q3 = OFF, Q4 = OFF, Q5 = OFF, Q6 = ON
D1 = OFF, D2 = ON, D3 = OFF, D4 = OFF, D5 = OFF, D6 = OFF
Phase A Current = 60.67472841 Amperes
Phase B Current = -23.76844021 Amperes
Phase C Current = -36.90628439 Amperes

II. Regenerative Braking Mode

Speed = 4000 rpm Rotor Angle = 16.788° (mech)
Q1 = OFF, Q2 = OFF, Q3 = OFF, Q4 = OFF, Q5 = OFF, Q6 = OFF
D1 = ON, D2 = OFF, D3 = ON, D4 = OFF, D5 = ON, D6 = OFF
Phase A Current = -22.34997178 Amperes
Phase B Current = 25.27216082 Amperes
Phase C Current = -2.922189036 Amperes

III. Plugging Mode

Speed = 240 RPM Rotor Angle = 16.740° (mech)
Q1 = OFF, Q2 = ON, Q3 = OFF, Q4 = ON, Q5 = OFF, Q6 = OFF
D1 = OFF, D2 = OFF, D3 = ON, D4 = OFF, D5 = ON, D6 = OFF
Phase A Current = -44.47176035
Phase B Current = 62.56684007
Phase C Current = -18.09507972

*This data was obtained from typical computer simulations.

2.2.1 Motoring Mode

The motoring mode is used to accelerate the system inertia in the direction of motion, or in other words, the motor output torque is in the direction of motion (quadrants I and III as shown in Figure (2.2-1)). There is, of course, a practical limit to the amount of torque and speed which can be produced in this mode because of the following three factors:

a) The chosen power supply voltage limits the maximum speed at which the machine can deliver the rated torque. This is due to the increase in the phase back emfs with increases in speed. These back emfs oppose the power supply voltage. Consequently when the speed is such that the two voltages are equal, the current can no longer be driven into the machine phase windings resulting in reduced torque and speed.

b) The volt-ampere rating of the switches limits the amount of power which may be injected into the machine phase windings.

c) The volt-ampere rating of the machine itself sets the upper bound on machine torque.

The maximum obtainable torque in this machine is basically limited by the volt-ampere rating of the switches (item (b) above). This maximum torque is symbolized by the constant TMMAX in Figure (2.2-1). Presently, TMMAX is set at 9.0387 nt-m (80 in-lb) which is approximately equivalent to a phase current of 40 amperes.

In order to gain insight into the operation of this electromechanical actuator one must examine the behavior of the power conditioner switches as well as the interaction of the electromagnetic fields inside the motor. Figures (2.2-2) and (2.2-3) display typical current paths in the power conditioner with the chopper transistor QM on and off respectively and with Q1 and Q6 on, see item (I) in Table (2.2-1). The chopper transistor QM switches on and off in order to maintain the current in the coupling inductor within a specified band about a commanded current level. With QM on, Figure (2.2-2), the battery is connected to the

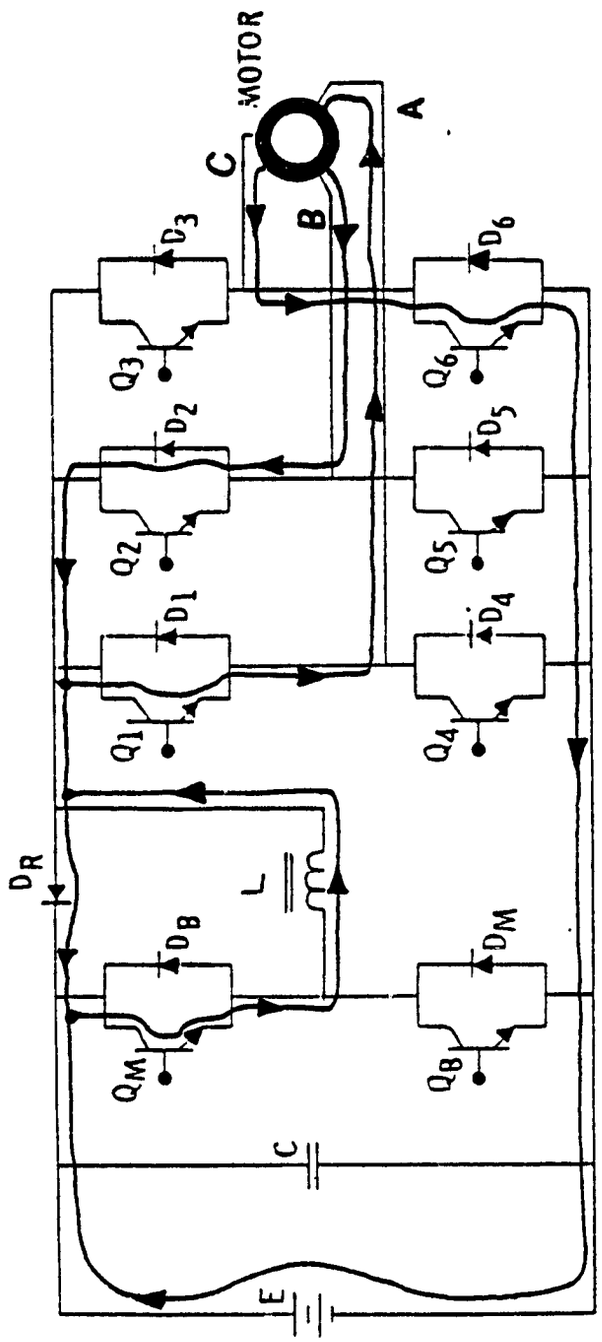

Figure 2.2-2. Current Paths during Motoring Mode with QM and DR both ON

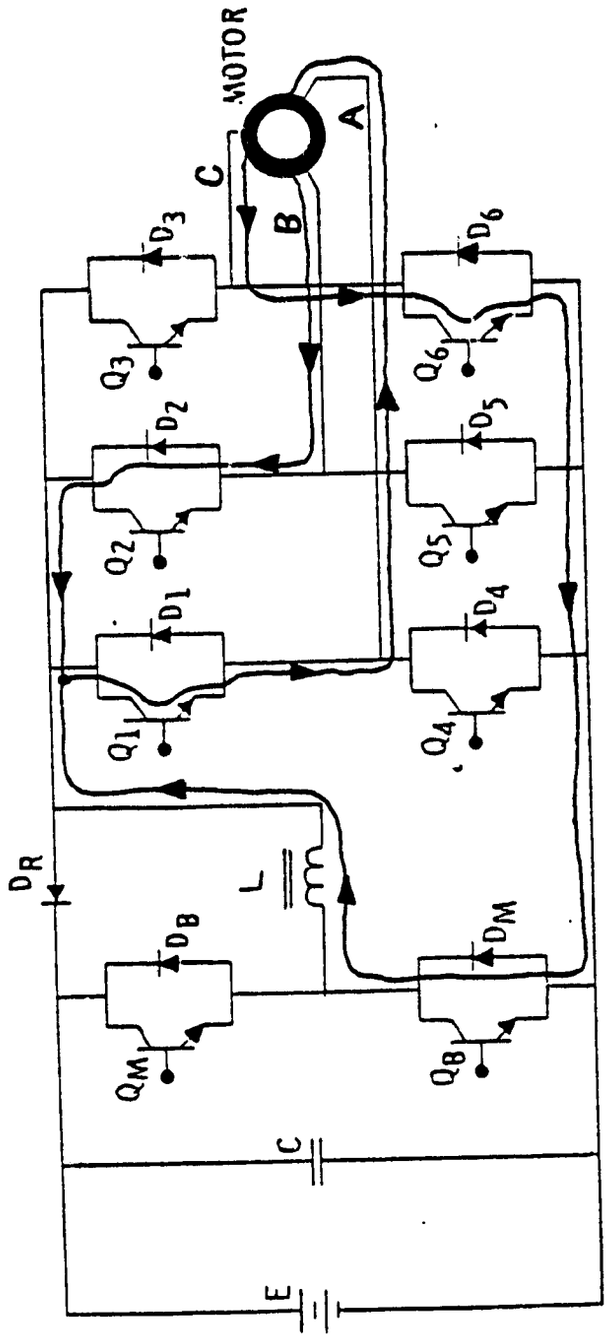

Figure 2.2-3. Current Paths during Motoring Mode with QM OFF

coupling inductor which results in an increase in the inductor current. Transistor QM is turned off when this current reaches a specified level above the commanded current, see Figure (2.2-3). The current then decreases until the inductor current drops to a specified point below the commanded current; at which point QM is switched on again thereby repeating the cycle.

The controlled coupling inductor current is then injected into the proper phase windings of the machine via the six transistor and six diode inverter bridge (Q1 - Q6 and D1 - D6). The firing of these transistors is controlled by the output of the rotor position sensor or RPS. The logic which translates the RPS signals into commands to switch the inverter transistors on or off is described in detail in Section (4.2.4) and in Reference (2).

As an example, consider the two typical network configurations shown in Figures (2.2-2) and (2.2-3). In both cases, Q1 and Q6 are on which means that coupling inductor current is flowing into phase (a) and out of phase (c). These two phase currents result in a motor torque which accelerates the system inertia in the direction of motion. The current out of phase (b) is in the process of decaying through diode D2 because of the recent cutoff of transistor Q5. Diode DR is also on in this case in order to provide a path for the excess current resulting from this commutation process.

The electromagnetic interactions inside the permanent magnet brushless d.c. motor for the case shown in Figure (2.2-2) and listed under item (I) of Table (2.2-1) are displayed in Figure (2.2-4) for a single turn of phase (a). The symbols used in this diagram are defined as follows:

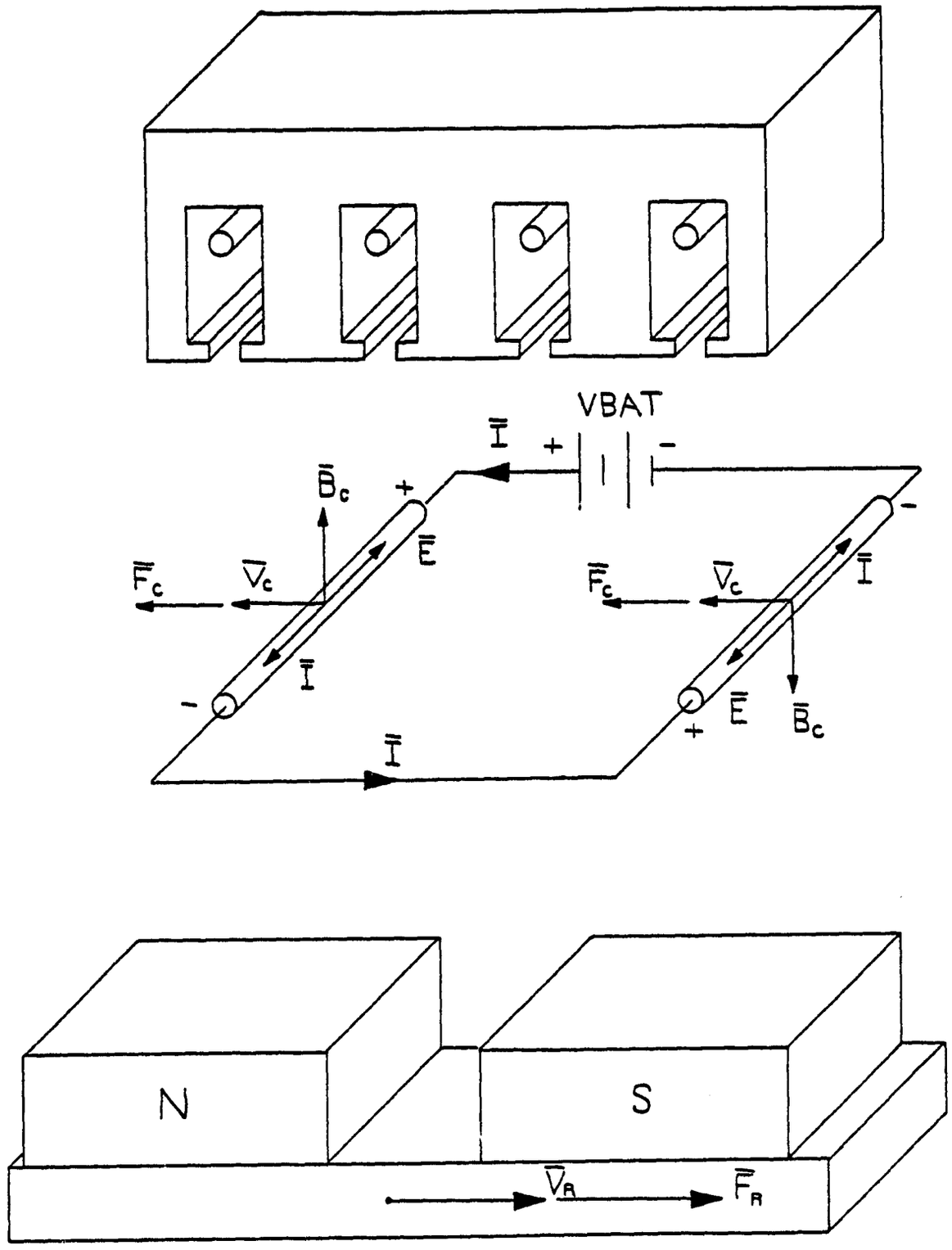

MOTORING MODE

Figure 2.2-4. Electromagnetic Interactions Inside the Delco Machine during Motoring

VBAT = Battery voltage (volts)

$\bar{I}$ = Conductor Current Vector (Amperes)

$\bar{B}_C$ = Conductor Flux Density Vector (Webers/Meter^2)

$\bar{V}_C$ = Velocity Vector of the Conductors with respect to $\bar{B}_C$ (Meters/Second)

$\bar{E}$ = Induced Conductor Back Emf Vector (Volts/Meter)

$\bar{F}_C$ = Conductor Force Vector (Newtons/Meter)

$\bar{F}_R$ = Rotor Force Vector (Newtons)

$\bar{V}_R$ = Rotor Velocity Vector (Meters/Second)

The force per unit length, $\bar{F}_C$, which is experienced by a conductor having the current vector, $\bar{I}$, and a flux density vector, $\bar{B}_C$, is given by

$$\bar{F}_C = (\bar{I} \times \bar{B}_C)\ell_C \quad \text{(Newtons)} \qquad (2.2\text{-}1)$$

where ℓ_C is the active conductor length. For the two conductors shown in Figure (2.2-4) the forces $\bar{F}_C$ are both in the negative direction. Since the stator is fixed and according to the action and reaction principle, the sum of these conductor forces is translated into a rotor force, $\bar{F}_R$, which is in the direction of rotation and is opposite in direction to the rotor conductor force vector, $\bar{F}_C$. The orientation and magnitude of the induced back emf, $\bar{E}$, per unit length for a conductor experiencing a flux density $\bar{B}_C$(wb/m^2) and having a velocity $\bar{V}_C$ (m/s) with respect to the field is given by the vector product

$$\bar{E} = \bar{V}_C \times \bar{B}_C. \quad \text{(Volts/Meter)} \qquad (2.2\text{-}2)$$

In the example shown in Figure (2.2-4), the induced back emf opposes the flow of the phase current, $\bar{I}$, as would be expected in the motoring mode.

2.2.2 Regenerative Braking Mode

The regenerative braking mode utilizes the fact that these permanent magnet machines when operated without the power conditioners look like salient pole synchronous generators. During this mode, the permanent magnet machine is operated as a generator thereby converting the energy of the rotating masses into electrical energy. This energy is used to control the braking torque as well as to recharge the supply batteries. In this mode the rotor torque and velocity vectors point in opposite directions which results in a deceleration of the rotating masses. This relationship between torque and speed is graphically displayed in Figure (2.2-1). The regenerative braking mode is confined by the control system to the speed regions designated by SPDLO and SPDHI in Figure (2.2-1). This is necessary because outside of these speed regions the machine is turning too slowly to produce the back emf necessary to maintain the commanded braking torque (line current).

When the actuator motors are operated in this fashion all six inverter switches (Q1 - Q6) are turned off. Consequently, the phase currents must pass through the six inverter diodes (D1 - D6) which together act as a full wave rectifier bridge. Figures (2.2-5) and (2.2-6) show some typical current paths during this mode of operation, with QB on and off respectively (see item (II) in Table (2.2-1). In Figure (2.2-5) diodes D1, D3 and D5 are on and the chopper transistor, QB, is off. Consequently, the line and phase currents will increase. With QB on, the battery receives no current from the machine. This changes as soon as QB is turned off. When QB is off, Figure (2.2-6), current flows from the inverter bridge through the braking diode, DB, and into the battery. In this configuration the EMA actually converts the externally applied load

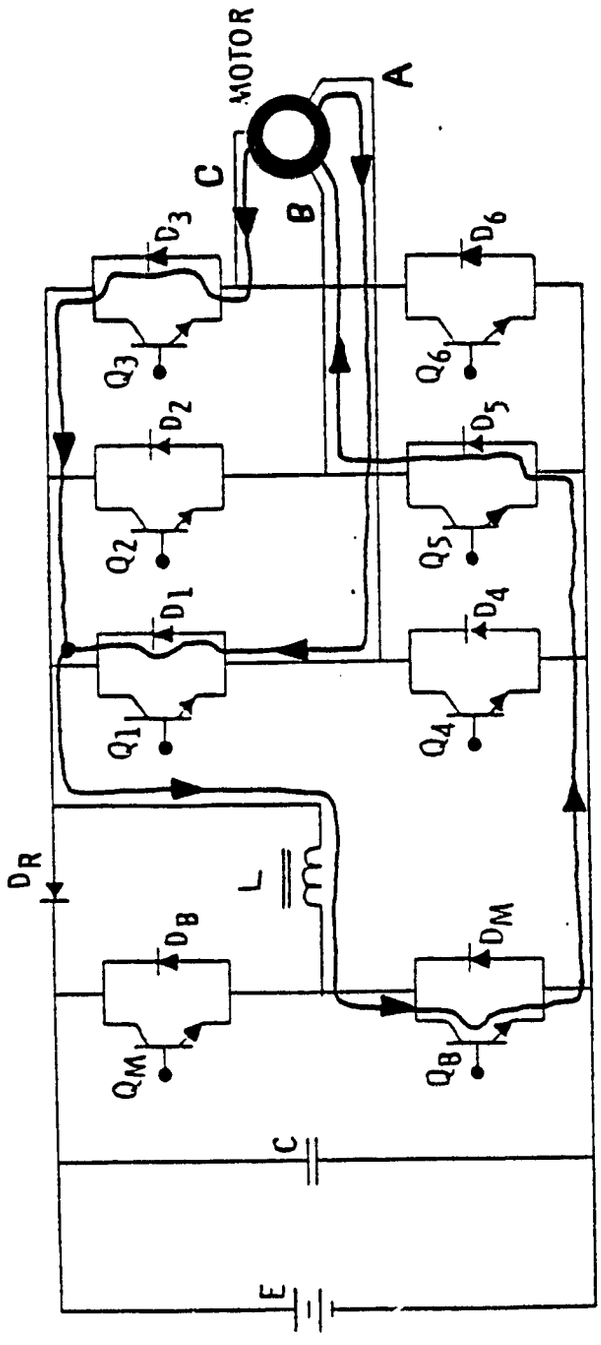

Figure 2.2-5. Current Paths during Regenerative Braking Mode with QB ON

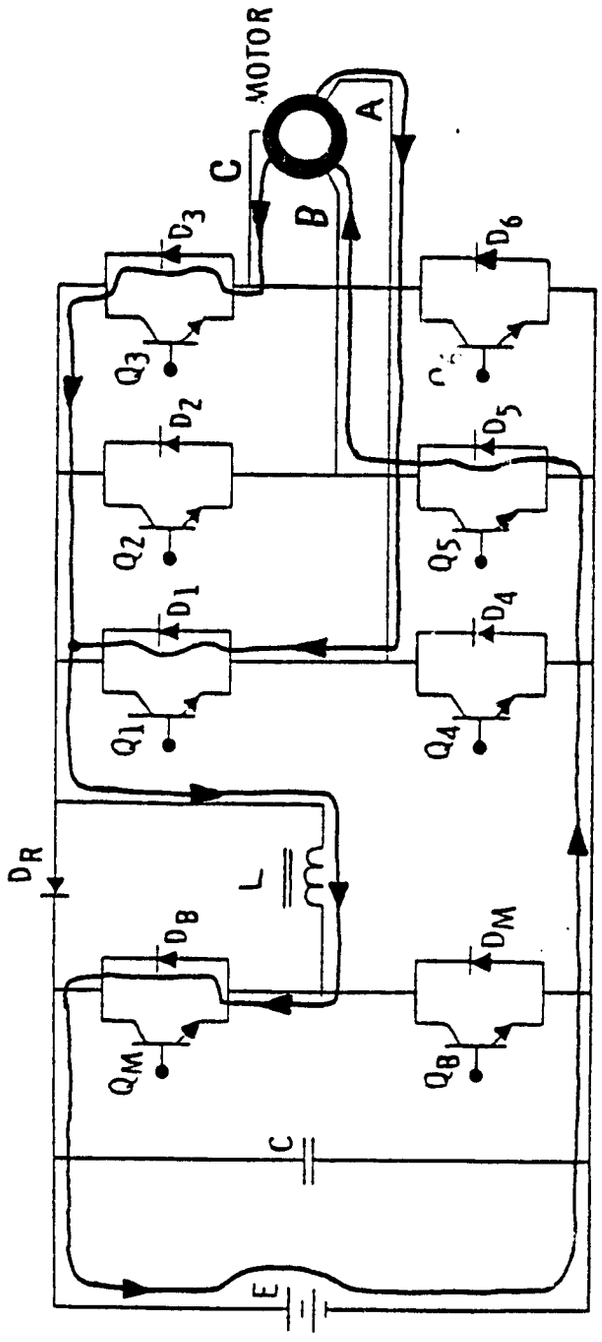

Figure 2.2-6. Current Paths during Regenerative Braking Mode with DB ON

torque into electrical energy which is used to recharge the system batteries.

The electromagnetic interactions between a single turn of a stator phase winding carrying a current, $\bar{I}$, and one north-south pole pair are shown in Figure (2.2-7) for the case given in Figure (2.2-6). The rotor velocity $\bar{V}_R$, the induced back emf $\bar{E}$, and the flux density, $\bar{B}_C$, all have the same orientation as in the motoring mode, Figure (2.2-4). The difference lies in the direction of the phase current $\bar{I}$. In Figure (2.2.7) the phase current exits through the positive terminal of phase (a) and enters the positive terminal of the battery. In other words, the stator winding acts as a source of power while the battery acts like a load. This is opposite to the motor case discussed earlier. The majority of the energy received by the battery is stored and can later be made available. The negative phase current results in a conductor force, $\bar{F}_C$, which points in a direction opposite to $\bar{V}_C$. Consequently, the rotor force vector, $\bar{F}_R$, and the rotor velocity vector, $\bar{V}_R$, point in opposite directions which results in a deceleration of the system inertia as expected.

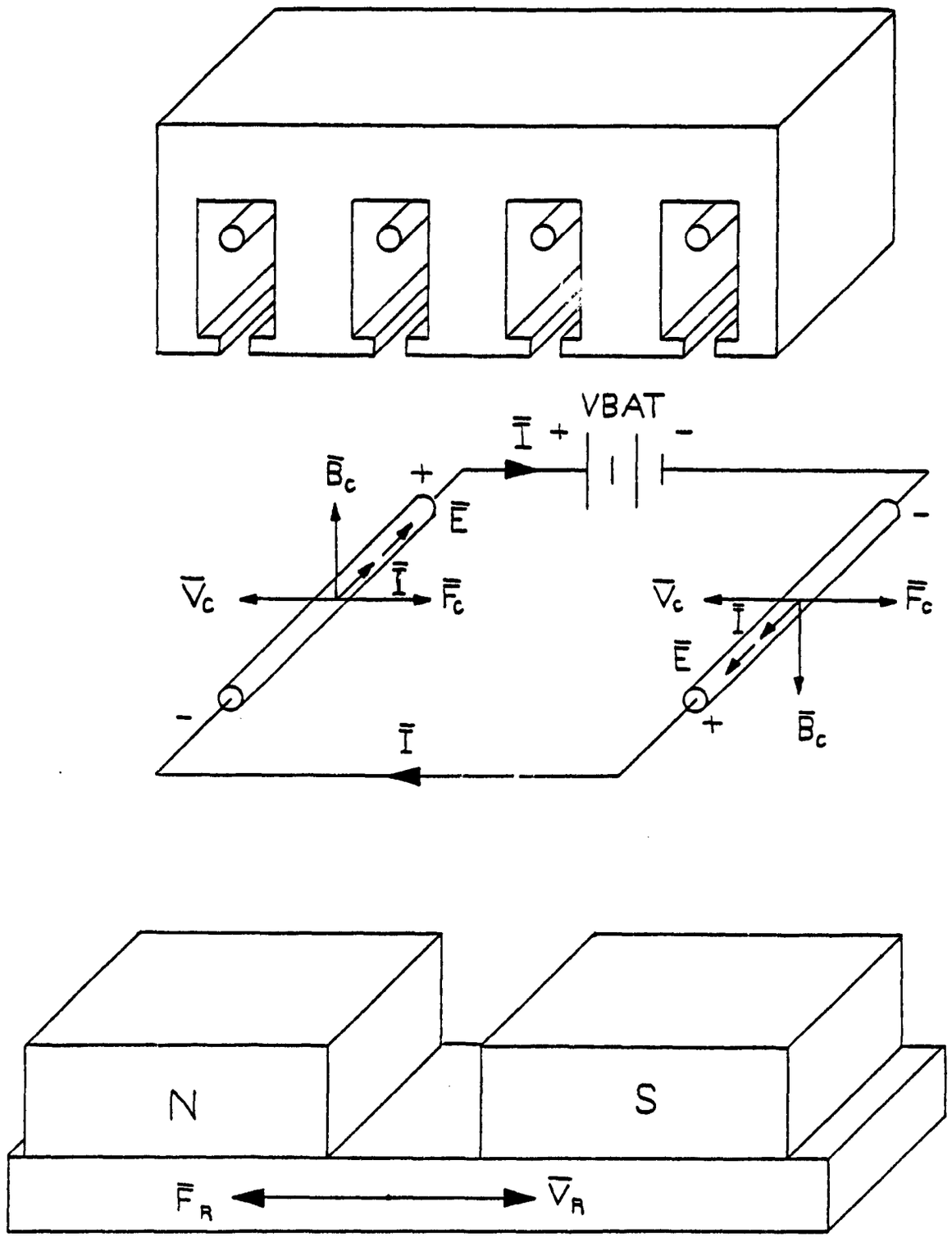

Figure 2.2-7. Electromagnetic Interactions Inside the Delco Machine during Regenerative Braking

2.2.3 Plugging Mode

The EMA operates in the plugging mode whenever the motor speed is too low for the regenerative mode to supply the commanded braking torque. The operating regions for the plugging mode in the torque-speed plane are shown in Figure (2.2-1).

Figures (2.2-8) and (2.2-9) show some typical current patterns in the power electronics during the plugging mode with the chopper transistor QM on and off respectively. Notice that in both cases Q2 and D5 are both on. This effectively sets the voltage of the node formed by the intersection of the coupling inductor and the switches DR, Q1, Q2, Q3, D1, D2 and D3 close to ground potential. This switch configuration allows circulating currents in the inverter switches and machine phase windings, see loops ℓ_1 and ℓ_2 in Figure (2.2-8). These currents do not pass through the chopper transistor or coupling inductor and consequently they cannot be controlled by the EMA control system. For this reason the current in the coupling inductor is limited to 25 amperes in order to keep the currents in the inverter switches below the 60 ampere maximum. This limit on in the maximum chopper current results in a reduced maximum braking torque which is symbolized by TPMAX in Figure (2.2-1).

The electromagnetic interactions between the rotor and stator circuits during the plugging mode are depicted in Figure (2.2-10) for the case listed under item (III) in Table (2.2-1). The plugging mode looks almost identical to the regenerative braking mode, Figure (2.2-7), in terms of the electromagnetic interactions inside the machine. The difference lies in the polarity of the battery with respect to the induced back emfs. In the regenerative braking case, Figure (2.2-7), the battery is connected so that it opposes the machine back emfs. Consequently, rotational energy of the rotating mass is converved into electrical energy. In the plugging

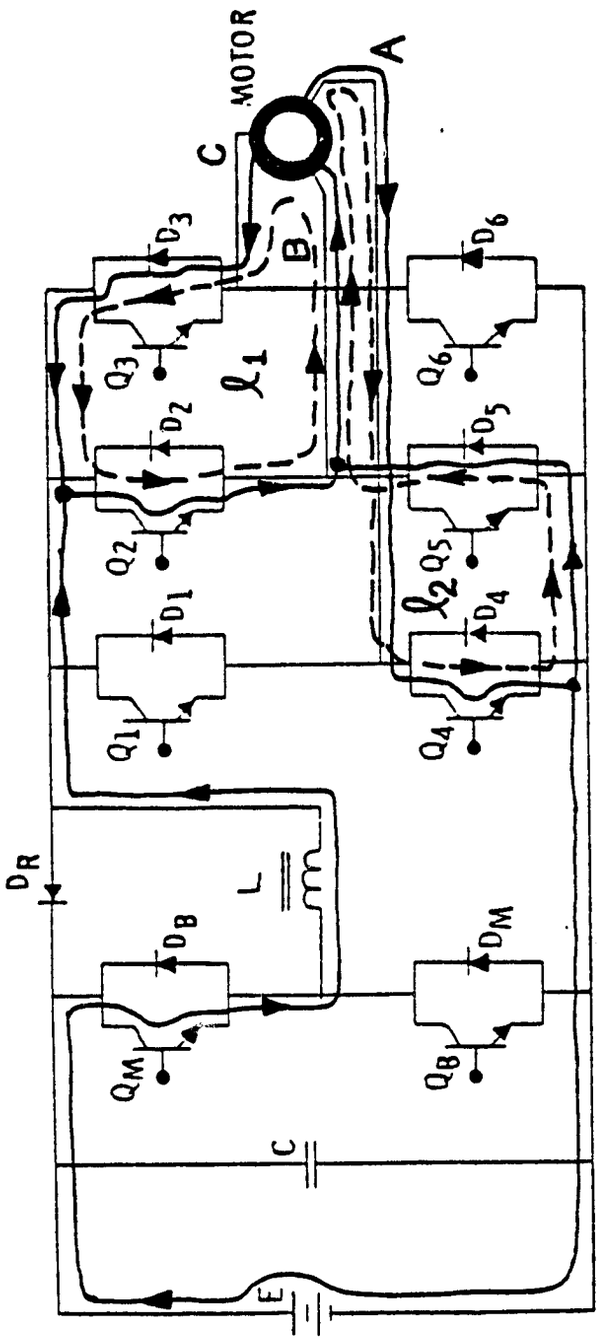

Loops ℓ_1 and ℓ_2 outline the paths of the circulating inverter bridge currents

Figure 2.2-8. Current Paths during Plugging with QM ON

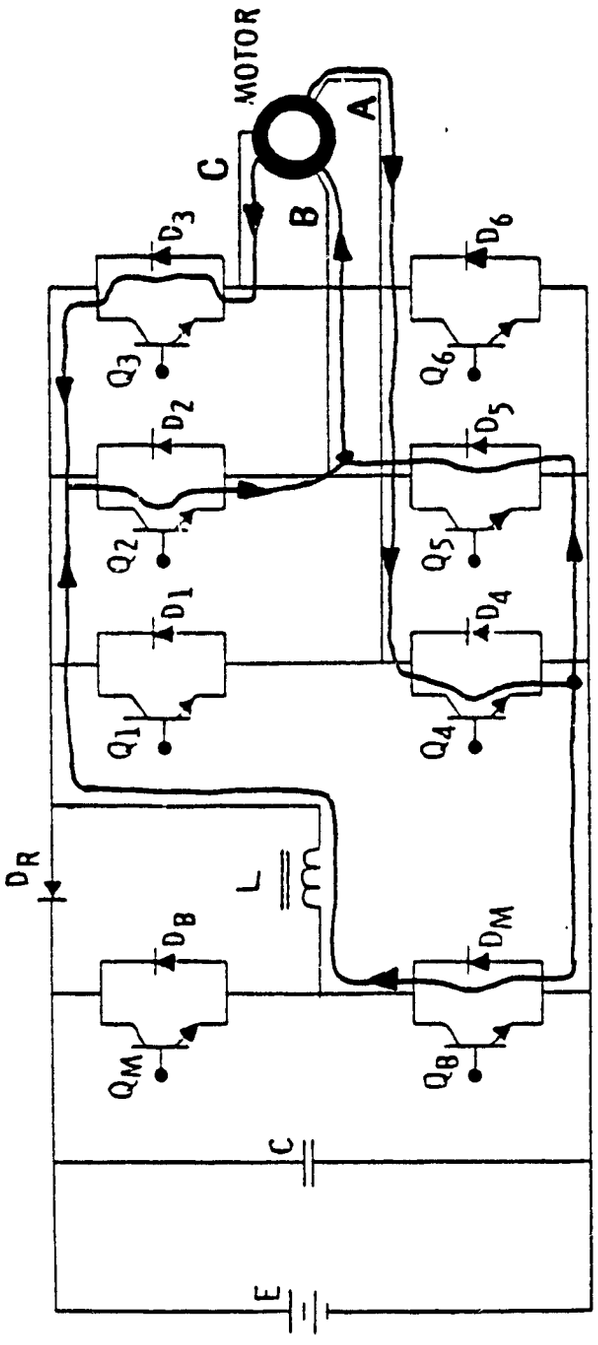

Figure 2.2-9. Current Paths during Plugging with QM OFF

mode, on the other hand, the battery voltage aids the machine back emf's, Figure (2.2-10), which means that the battery supplies energy to slow down the rotating masses.

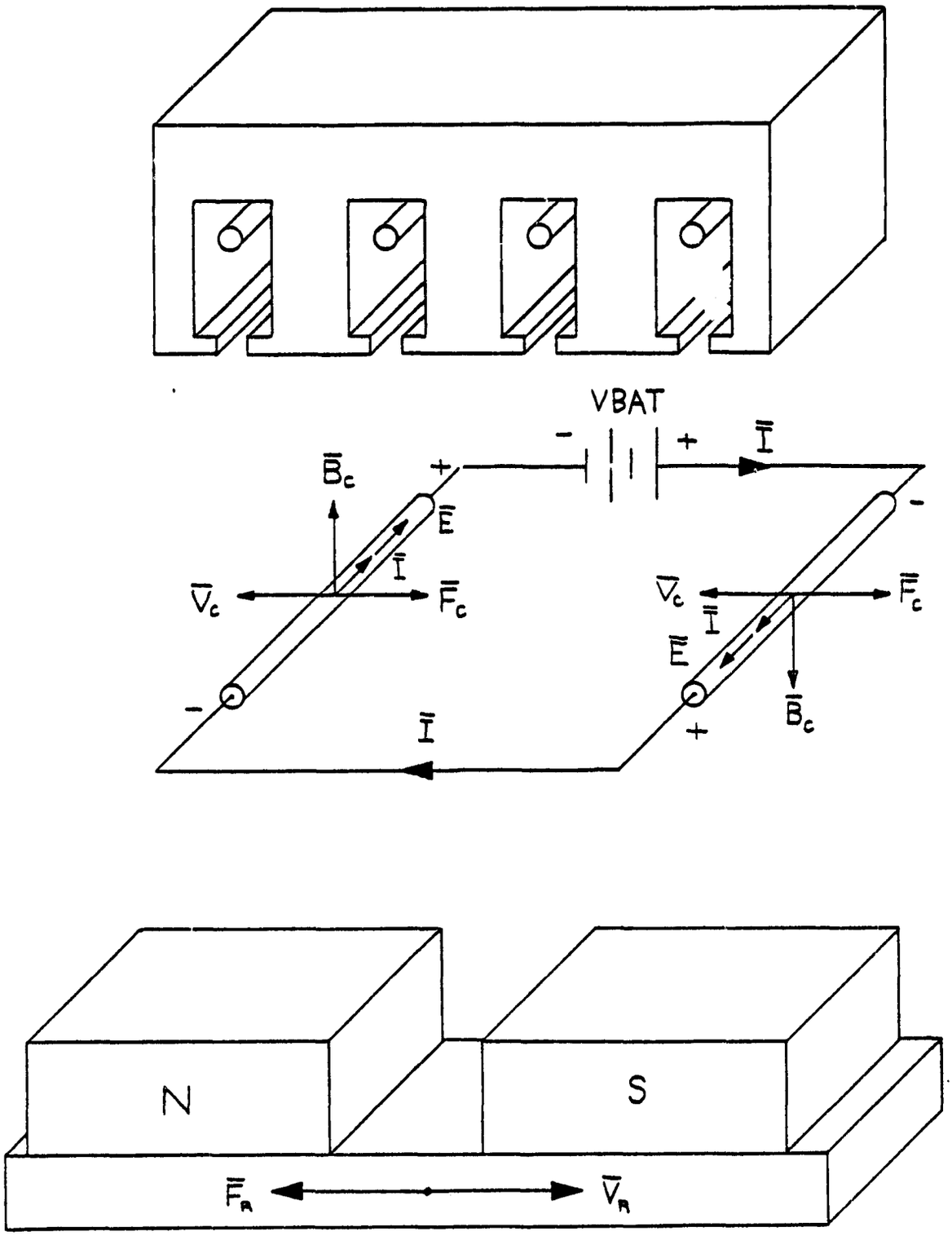

PLUGGING MODE

Figure 2.2-10. Electromagnetic Interactions Inside the Delco Machine during Plugging

2.3 ELECTRICAL MODELS OF THE PERMANENT MAGNET MACHINE

Two different electrical models of the permanent magnet brushless d.c. motor have been considered as possible candidates for the computer model developed under this contract. The first model consists of the standard six winding machine model commonly used to analyze conventional synchronous machines while the second model is based upon a back emf behind a leakage inductance. The back emf behind a leakage inductance machine model was chosen because of computational considerations and because the parameters of such a model (i.e. back emfs and leadage inductances) can be obtained readily from a nonlinear finite element field solution. These models are described in greater detail in Sections 2.3.1 and 2.3.2 which follow.

2.3.1 Six Winding Machine Model

As stated earlier, the structure of these permanent magnet brushless d.c. motors is very similar to the structure of conventional salient pole synchronous machines. Consequently, one can apply existing state space models of conventional synchronous machines to this new class of permanent magnet machines. The only difference between these machines and conventional salient pole synchronous machines is the lack of the field and damper windings on the rotor. The field winding function is performed by the permanent magnet pole pieces.

The six winding machine model developed in this section is based upon the lumped circuit model of a conventional two pole salient-pole type synchronous machine as shown in Figure (2.3-1). This lumped circuit model consists of three stator phase windings (a, b, c), two damper windings (kd, kq), and a field winding (f). A schematic representation of these windings is given in Figure (2.3-2).

The field winding shown in these figures does not actually exist in the machines at hand since permanent magnets are used to provide the necessary magnetic field. However, a "fictitious" field winding is retained in this model as an artifice to represent the magnetomotive force produced by these magnets. In order to obtain a value for this "fictitious" field current, i_F, one uses the demagnetization curve of the permanent magnet, Figure (2.3-3). Multiplying the coercivity, H_c (Amperes/Meter), by the height of a magnet, ℓ_m (Meters), one obtains the field mmf, F_{field}. That is,

$$F_{field} = H_c \cdot \ell_m \text{ (Ampere-Turns)} \qquad (2.3\text{-}1)$$

This is equivalent to a fixed value of field current for a given number of fictitious turns.

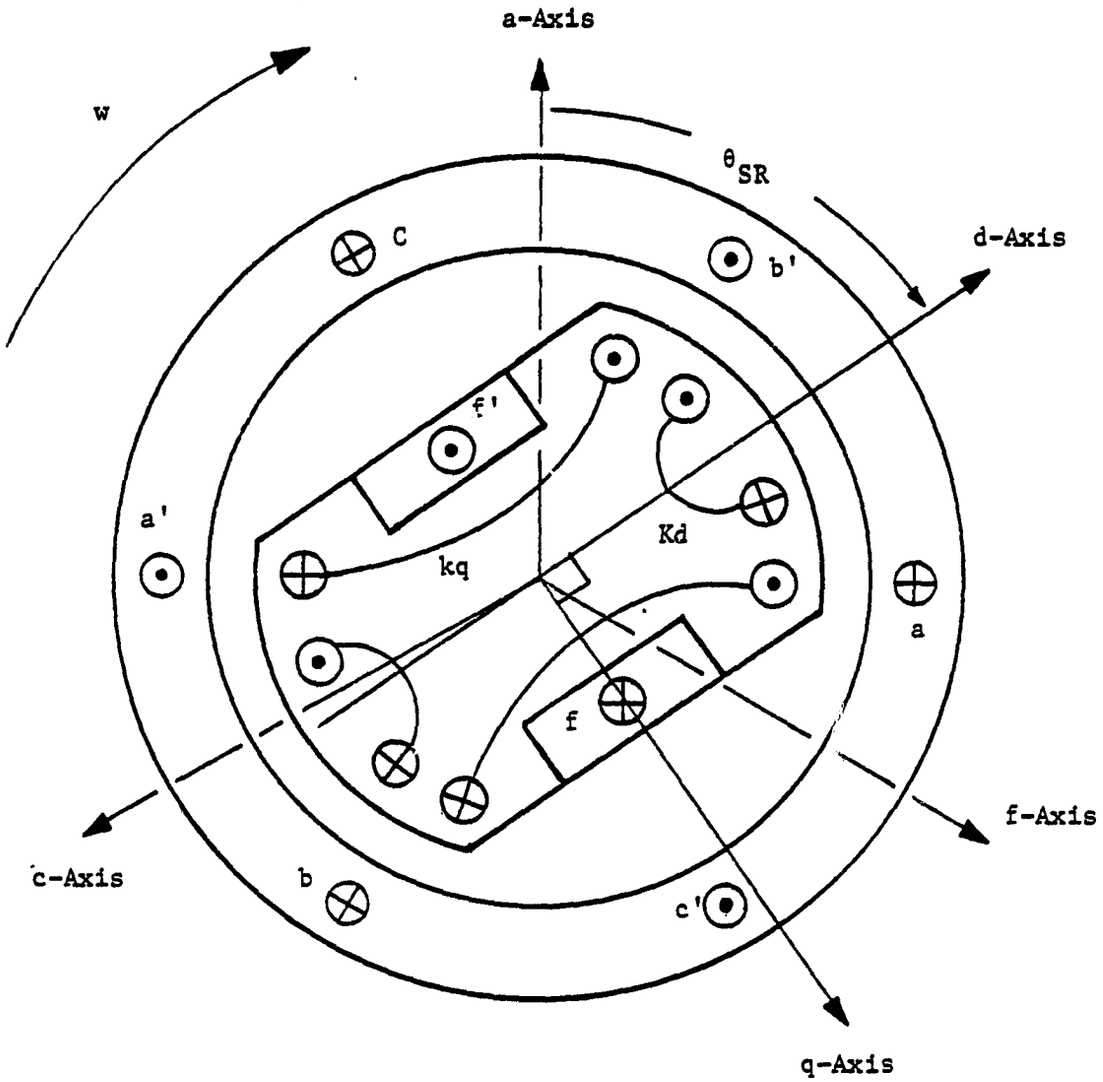

Figure 2.3-1. Lumped Circuit Model of a Salient Pole Synchronous Machine

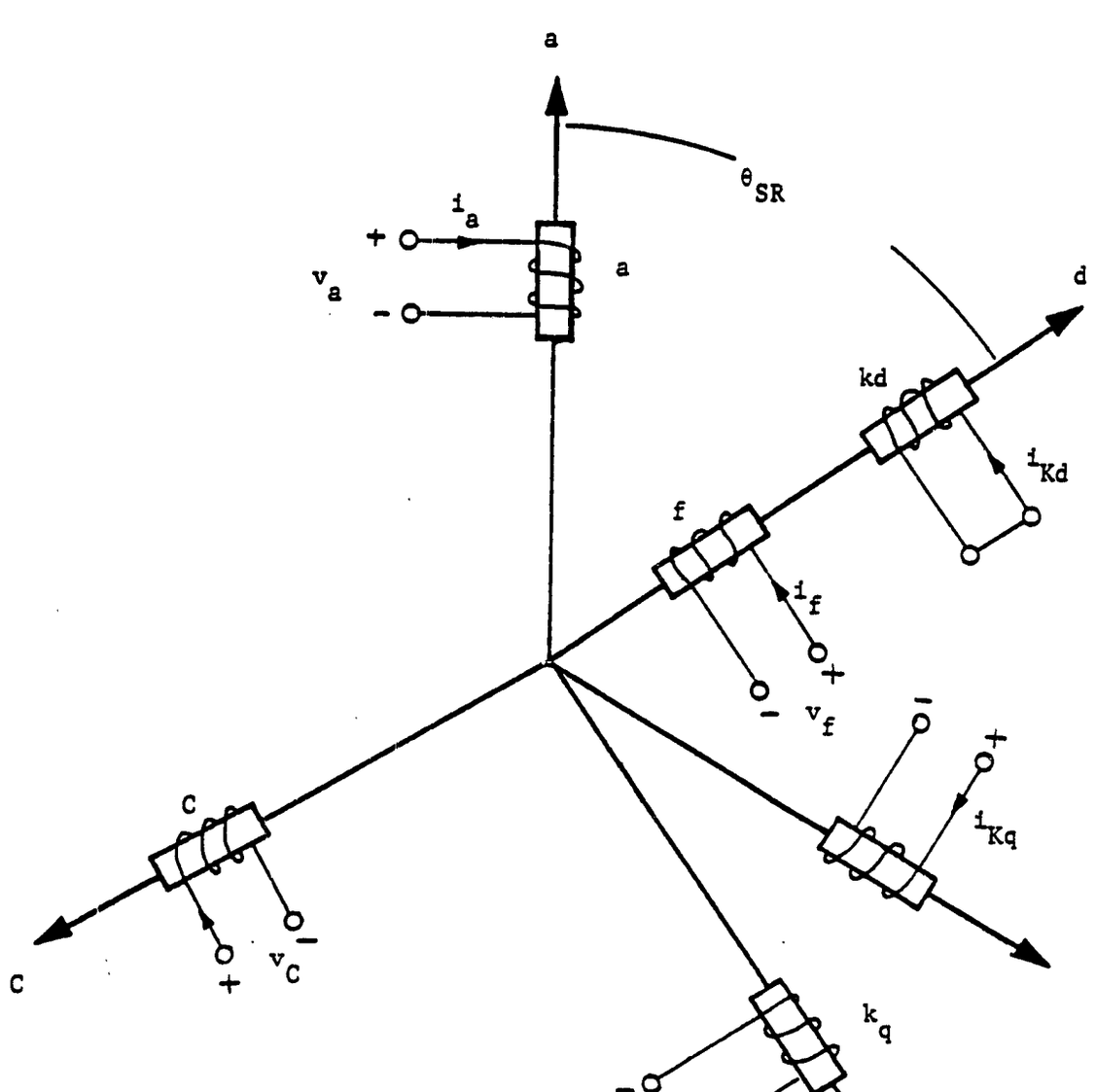

Figure 2.3-2. Schematic of the Lumped Circuit Machine Model

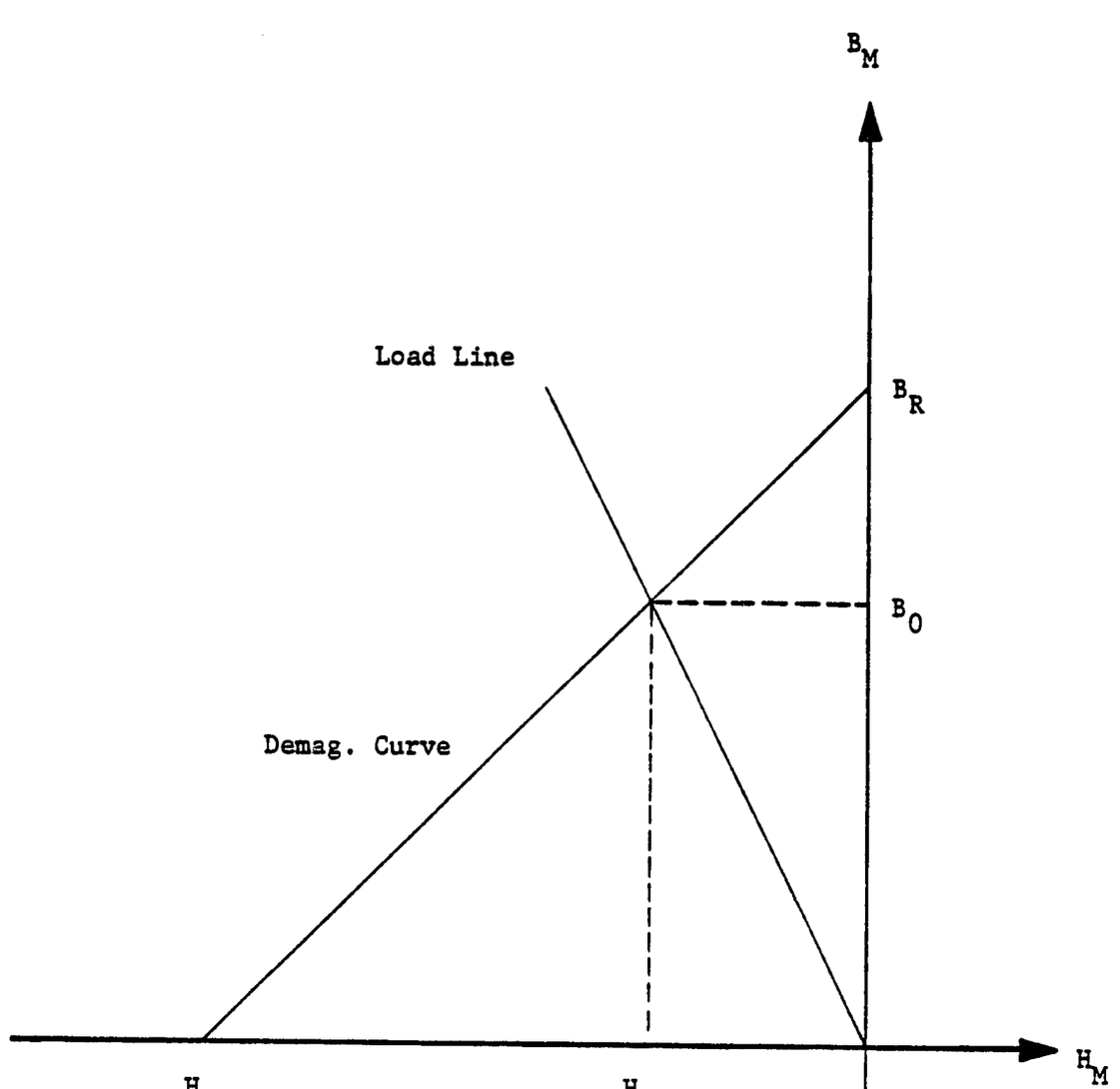

Figure 2.3-3. Magnet Demagnetization Curve
And a Typical Low Line

The six winding machine model can now be derived by writing the differential equations corresponding to these windings. Consider, for example, winding (a) in Figure (2.3-2) which is the stator phase winding corresponding to phase (a). Assuming that this winding has a resistance of R_a (Ohms) the phase voltage, v_a, can be written as

$$v_a = R_a i_a + \frac{d}{dt} \lambda_a$$

$$v_a = R_a i_a + \frac{d}{dt} (L_{aa} i_a + L_{ab} i_b + L_{ac} i_c + L_{af} i_f + L_{akd} i_{kd} + L_{akq} i_{kq}) \qquad (2.3\text{-}2)$$

where

λ_a = Total flux linkage of coil (a) (Weber-Turns/Ampere)

L_{aa} = Self inductance of coil (a) (Henries)

and

L_{ab}, L_{ac}, L_{af}, L_{akd} and L_{akq} are the mutuals between coil (a) and coils b, c, f, kd and kq respectively. (Henries)

For phases (b) and (c) similar expressions are written as follows:

$$v_b = R_b i_b + \frac{d}{dt} \lambda_b$$

$$v_b = R_b i_b + \frac{d}{dt} (L_{ab} i_a + L_{bb} i_b + L_{bc} i_c + L_{bf} i_f + L_{bkd} i_{kd} + L_{bkq} i_{kq}) \qquad (2.3\text{-}3)$$

and

$$v_c = R_c i_c + \frac{d}{dt} \lambda_c$$

$$v_c = R_c i_c + \frac{d}{dt} (L_{ac} i_a + L_{bc} i_b + L_{cc} i_c + L_{cf} i_f + L_{ckd} i_{kd} + L_{ckq} i_{kq}) \qquad (2.3\text{-}4)$$

Similar expressions are written for the coils of the field and damper windings f, kd, and kq respectively. The resulting system of six coupled first order differential equations constitutes the six winding lumped

circuit parameter model of a synchronous machine. In matrix form these equations are written as follows:

$$\begin{bmatrix} v_a \\ v_b \\ v_c \\ \hline v_f \\ 0 \\ 0 \end{bmatrix} = \left[\begin{array}{ccc:ccc} R_a & 0 & 0 & & & \\ 0 & R_b & 0 & & \underline{0} & \\ 0 & 0 & R_c & & & \\ \hdashline & & & R_f & 0 & 0 \\ & \underline{0} & & 0 & R_{kd} & 0 \\ & & & 0 & 0 & R_{kq} \end{array}\right] \begin{bmatrix} i_a \\ i_b \\ i_c \\ \hline i_f \\ i_{kd} \\ i_{kq} \end{bmatrix} +$$

$$\frac{d}{dt}\left\{\left[\begin{array}{ccc:ccc} L_{aa} & L_{ab} & L_{ac} & L_{af} & L_{akd} & L_{akq} \\ L_{ab} & L_{bb} & L_{bc} & L_{bf} & L_{bkd} & L_{bkq} \\ L_{ac} & L_{bc} & L_{cc} & L_{cf} & L_{ckd} & L_{ckq} \\ \hdashline L_{af} & L_{bf} & L_{cf} & L_{ff} & L_{fkd} & L_{fkq} \\ L_{akd} & L_{bkd} & L_{ckd} & L_{fkd} & L_{kdkd} & L_{kdkq} \\ L_{akq} & L_{bkq} & L_{ckq} & L_{fkd} & L_{kdkq} & L_{kqkq} \end{array}\right] \begin{bmatrix} i_a \\ i_b \\ i_c \\ \hline i_f \\ i_{kd} \\ i_{kq} \end{bmatrix}\right\} \qquad (2.3\text{-}5)$$

All of the inductance coefficients in equation (2.3-5) above are dependent upon the angular position of the rotor and upon the magnetic saturation picture which is a function of the currents. Hence all the inductance coefficients are functions of time. Therefore the inductance matrix cannot be taken outside the derivative operator $(\frac{d}{dt})$.

The samarium-cobalt permanent magnet pole pieces offer a high resistance to the flow of eddy currents because of their low electrical conductivity (0.2×10^7 ℧/m versus 5.8×10^7 ℧/m for copper). Consequently the currents i_{kd} and i_{kq} which flow in the fictitious (d) and (q) axis damper windings kd and kq are negligible. Applying these simplifications to Equation (2.3-5) reduces the order of this machine model from sixth to fourth order as follows:

$$\begin{bmatrix} v_a \\ v_b \\ v_c \\ \hdashline v_f \end{bmatrix} = \left[\begin{array}{ccc:c} R_a & 0 & 0 & 0 \\ 0 & R_b & 0 & 0 \\ 0 & 0 & R_c & 0 \\ \hdashline 0 & 0 & 0 & R_f \end{array}\right] \cdot \begin{bmatrix} i_a \\ i_b \\ i_c \\ \hdashline i_f \end{bmatrix} + \frac{d}{dt} \left\{ \left[\begin{array}{ccc:c} L_{aa} & L_{ab} & L_{ac} & L_{af} \\ L_{ab} & L_{bb} & L_{bc} & L_{bf} \\ L_{ac} & L_{bc} & L_{cc} & L_{cf} \\ \hdashline L_{af} & L_{bf} & L_{cf} & L_{ff} \end{array}\right] \begin{bmatrix} i_a \\ i_b \\ i_c \\ \hdashline i_f \end{bmatrix} \right. \tag{2.3-6}$$

Equation (2.3-6) represents a lumped parameter model of the permanent magnet brushless d.c. motor at hand. Unfortunately this model is rather combersome because of the fact that the inductances are all functions of time. There are techniques for determining the values of these inductances, Reference (2.3-1). However, a simpler but quite adequate approach to modeling this machine was adopted and is the topic of the next section. This adopted approach has proven itself, after comparing its numerical results with experimental test data, to be very accurate and reliable in the prediction of the dynamic performances of the machine. Proof of this is given in later chapters of this report.

2.3.2 Transient Back Emf - Leakage Inductance (Transient Inductance) Machine Model

The back emf-leakage inductance machine model per phase consists of a series connection of three elements; the d.c. winding resistance, the winding leakage (transient) inductance, and the induced winding (transient) back emf. A schematic diagram of this model is shown in Figure (2.3-4) for the three phase machine under study. This model will be derived from the reduced six winding machine model of equation (2.3-6) in the development which follows.

The stator phase inductances L_{aa}, L_{bb} and L_{cc} of equation (2.3-6) can be expressed as the sum of two inductances:

$$L_{aa} = L_{\ell a} + L_{ga} \tag{2.3-7}$$

$$L_{bb} = L_{\ell b} + L_{gb} \tag{2.3-8}$$

$$L_{cc} = L_{\ell c} + L_{gc} \tag{2.3-9}$$

That is, a leakage inductance associated with the leakage flux and an inductance associated with that portion of the total flux which crosses the airgap, see Figure (2.3-5). These inductances are symbolized by ($L_{\ell a}$, $L_{\ell b}$, $L_{\ell c}$) and (L_{ga}, L_{gb}, L_{gc}) respectively and they are defined as follows:

$$L_{\ell a} = \lambda_{\ell a}/i_a = N\phi_{\ell a}/i_a$$
$$L_{\ell b} = \lambda_{\ell b}/i_b = N\phi_{\ell b}/i_b$$
$$L_{\ell c} = \lambda_{\ell c}/i_c = N\phi_{\ell c}/i_c$$
$$L_{ga} = \lambda_{ga}/i_a = N\phi_{ga}/i_a$$
$$L_{gb} = \lambda_{gb}/i_b = N\phi_{gb}/i_b$$
$$L_{gc} = \lambda_{gc}/i_c = N\phi_{gc}/i_c$$

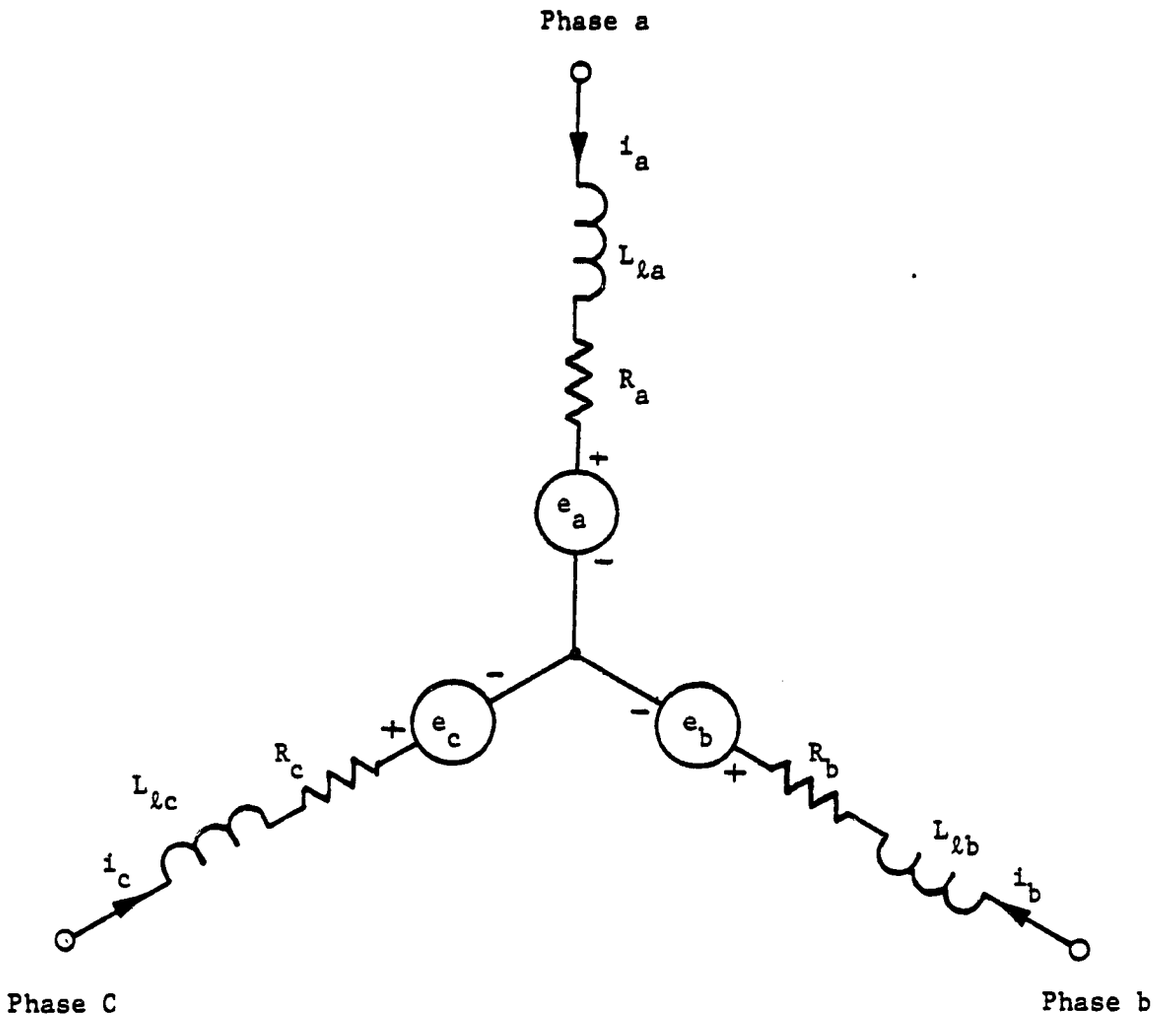

Figure 2.3-4. The Back Emf-Winding Resistance-Leakage Inductance Machine Model

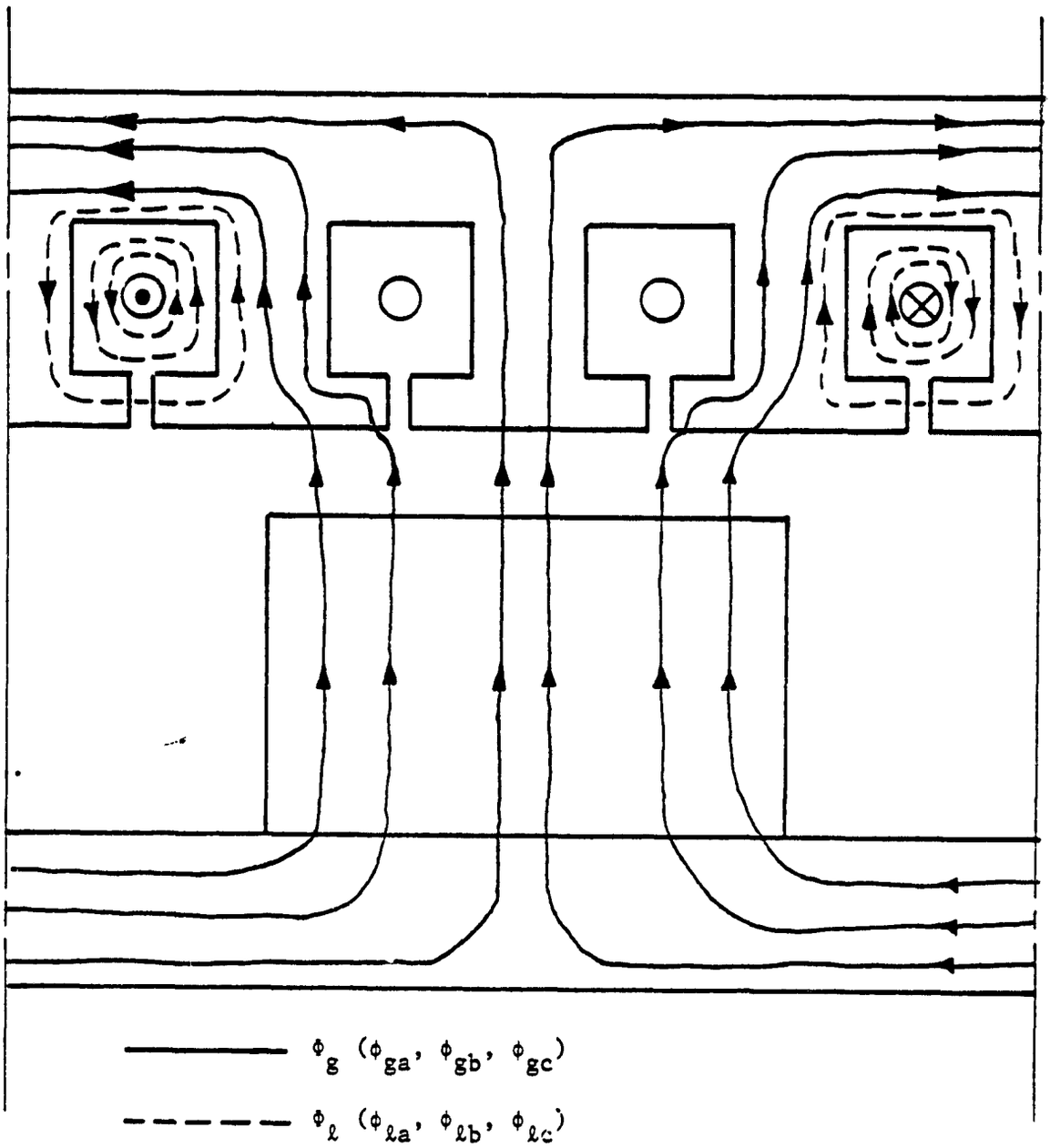

Figure 2.3-5. Leakage and Air Gap Flux Paths

where

$\lambda_{\ell a}$, $\lambda_{\ell b}$, and $\lambda_{\ell c}$ are the leakage flux linkages of phases (a), (b) and (c) respectively;

λ_{ga}, λ_{gb}, and λ_{gc} are the flux linkages of phases (a), (b) and (c) respectively, corresponding to that portion of the flux which crosses the airgap;

$\phi_{\ell a}$, $\phi_{\ell b}$, and $\phi_{\ell c}$ are the leakage fluxes of phases (a), (b) (c) respectively;

ϕ_{ga}, ϕ_{gb}, and ϕ_{gc} are the air gap fluxes of phases (a), (b) and (c) respectively;

and

N equals the number of turns of the abc phase windings.

Substituting equations (2.3-7), (2.3-8) and (2.3-9) into equation (2.3-6) results in:

$$\begin{bmatrix} v_a \\ v_b \\ v_c \\ v_f \end{bmatrix} = \left[\begin{array}{ccc:c} R_a & 0 & 0 & 0 \\ 0 & R_b & 0 & 0 \\ 0 & 0 & R_c & 0 \\ \hdashline 0 & 0 & 0 & R_f \end{array}\right] \begin{bmatrix} i_a \\ i_b \\ i_c \\ i_f \end{bmatrix} + \tag{2.3-10}$$

$$\frac{d}{dt}\left\{\left[\begin{array}{ccc:c} L_{\ell a} & 0 & 0 & 0 \\ 0 & L_{\ell b} & 0 & 0 \\ 0 & 0 & L_{\ell c} & 0 \\ \hdashline 0 & 0 & 0 & 0 \end{array}\right] \begin{bmatrix} i_a \\ i_b \\ i_c \\ i_f \end{bmatrix} + \left[\begin{array}{ccc:c} L_{ga} & L_{ab} & L_{ac} & L_{af} \\ L_{ab} & L_{gb} & L_{bc} & L_{bf} \\ L_{ac} & L_{bc} & L_{gc} & L_{cf} \\ \hdashline L_{af} & L_{bf} & L_{cf} & L_{ff} \end{array}\right] \begin{bmatrix} i_a \\ i_b \\ i_c \\ i_f \end{bmatrix}\right\}$$

or in symbolic matrix notation one can rewrite equation (2.3-10) as follows:

$$\underline{v}_{abcf} = \underline{R}_{abcf}\underline{i}_{abcf} + \frac{d}{dt}\left[\underline{L}_{abc\ell}\ \underline{i}_{abcf}\right] + \frac{d}{dt}\left[\underline{L}_{abcfg}\ \underline{i}_{abcf}\right] \tag{2.3-11}$$

The slot leakage shown in Figure (2.3-5) is mainly confined to an area immediately surrounding the slot conductor, therefore much of the leakage

flux passes through nonmagnetic materials such as copper, air, and insulation which do not experience saturation. In addition, the operating air gap flux densities at hand, namely, 0.64 wb/m^2 (41000 Lines/in^2) are relatively low, which reduces the levels of saturation in this machine. Consequently, the leakage inductance depends mainly upon the slot geometry and to a lesser degree upon the state of the machine currents. For these reasons, the leakage inductance matrix, $\underline{L}_{abc\ell}$, is essentially time invariant and can therefore be moved outside of the derivative operator, $(\frac{d}{dt})$. equation (2.3-11) then becomes:

$$\underline{v}_{abcf} = \underline{R}_{abcf}\underline{i}_{abcf} + L_{abc\ell}\frac{d}{dt}(\underline{i}_{abcf}) + \frac{d}{dt}[\underline{L}_{abcfg}\underline{i}_{abcf}] \qquad (2.3\text{-}12)$$

The calculation of the "ficticious" field winding voltage, v_f, in equation (2.3-10) is unnecessary in the case of the permanent magnet machine at hand because it has no physical existance. Consequently, the fourth row of equation (2.3-10) can be eliminated as follows:

$$\begin{bmatrix} v_a \\ v_b \\ v_c \end{bmatrix} = \begin{bmatrix} R_a & 0 & 0 \\ 0 & R_b & 0 \\ 0 & 0 & R_c \end{bmatrix} \cdot \begin{bmatrix} i_a \\ i_b \\ i_c \end{bmatrix} +$$

$$\begin{bmatrix} L_{\ell a} & 0 & 0 \\ 0 & L_{\ell b} & 0 \\ 0 & 0 & L_{\ell c} \end{bmatrix} \cdot \frac{d}{dt}\begin{bmatrix} i_a \\ i_b \\ i_c \end{bmatrix} +$$

$$\frac{d}{dt}\left\{\begin{bmatrix} L_{ga} & L_{ab} & L_{ac} & L_{af} \\ L_{ab} & L_{gb} & L_{bc} & L_{bf} \\ L_{ac} & L_{bc} & L_{gc} & L_{cf} \end{bmatrix} \cdot \begin{bmatrix} i_a \\ i_b \\ i_c \\ \hdashline i_f \end{bmatrix}\right\} \qquad (2.3\text{-}13)$$

or in compact notation

$$\underline{v}_{abc} = \underline{R}_{abc} \cdot \underline{i}_{abc} + \underline{L}_{abc\ell} \frac{d}{dt} \underline{i}_{abc} + \frac{d}{dt} \{\underline{L}_{abcfg} \underline{i}_{abcf}\}. \quad (2.3\text{-}14)$$

The three right hand terms of equation (2.3-14) are nothing more than the components of the back emf - leakage inductance machine model shown earlier in Figure (2.3-4), where

$$\underline{R}_{abc} = \begin{bmatrix} R_a & 0 & 0 \\ 0 & R_b & 0 \\ 0 & 0 & R_c \end{bmatrix} \quad (2.3\text{-}15)$$

represents the stator phase winding resistances,

$$\underline{L}_{abc\ell} = \begin{bmatrix} L_{\ell a} & 0 & 0 \\ 0 & L_{\ell b} & 0 \\ 0 & 0 & L_{\ell c} \end{bmatrix} \quad (2.3\text{-}16)$$

represents the stator leakage inductances, and

$$\underline{e}_{abc} = \frac{d}{dt} \{\underline{L}_{abcfg} \underline{i}_{abcf}\} \quad (2.3\text{-}17)$$

represents the phase back emfs, where $\underline{e}_{abc}$ is the vector containing the phase back emfs; e_a, e_b, and e_c.

Examination of equations (2.3-14) and (2.3-17) reveals that for the case where $\underline{i}_{abc} = \underline{0}$, the terminal voltage vector, $\underline{v}_{abc}$, becomes:

$$\underline{v}_{abc} = \underline{e}_{abc} = \begin{bmatrix} L_{af} \\ L_{bf} \\ L_{cf} \end{bmatrix} i_f \quad (2.3\text{-}17)$$

In other words the no load or open circuit terminal (phase to neutral) voltages are equivalent to the no load or open circuit back emfs. The open circuit back emfs can be obtained either through an open circuit

test as is the case in Figure (2.1-11) or by means of a finite element solution. Regardless of how the open circuit emf waveform is determined, it must be modified whenever stator currents are present. This can be accomplished by calculating the resultant air gap MMF distribution due to the nonzero stator currents and then magnetizing or demagnetizing the magnetic pole pieces of the rotor accordingly. These back emf calculations are the topic of the next section.

2.4 CALCULATION OF MACHINE BACK EMFS AND TORQUE

The machine model derived in the previous section requires the knowledge of the air gap phase back emfs on an instantaneous basis. The back emfs are functions of: (a) rotor position, (b) rotor speed, (c) the stator phase currents, and (d) the magnet properties.

A procedure to approximate the back emfs as a function of these parameters is presented in this section. In addition, the instantaneous machine torque is calculated from the values of the instantaneous phase back emfs, phase currents, and machine velocity. The calculated machine torque later becomes an input (or forcing function) to the dynamic model of the rotating masses which is developed in Chapter 4 of this volume.

2.4.1 Calculation of Machine Back Emfs

The determination of the machine back emfs requires detailed knowledge of the flux density distribution in the air gap at any given instant of time. Such distributions are obtainable from an instantaneous finite element solution of the nonlinear Poisson's equation which governs the machine behavior, References (7) and (8). The problem with this approach is the computational effort required to solve the large systems of nonlinear algebraic equations which are produced by the finite element discretization at each instant of time. For this reason, a lumped parameter model of the machine magnetic circuit was adopted. The lumped parameter approach approximates the distributed nature of the magnetic fields by a lumped parameter network consisting of equivalent flux path reluctances and magnetomotive forces or mmfs.

For purposes of discussion, a developed cross sectional view of the magnetic circuit spanned by two pole pairs (180° mechanical, 720° electrical) is given in Figure (2.4-1). This figure displays the electromagnetic interactions between two pole pairs of the stator and rotor circuits under maximum torque conditions. Maximum machine torque is developed when the stator and rotor mmf's are displayed by 90 electrical or 22.5 mechanical degrees, References (13) and (14). The stator phase winding which produces the stator mmf is represented by equivalent current filaments located at the centroids of the stator slots. These conductors are identified by the letters A, B, and C corresponding to phases, and by a superscript of (+) or (-) depending upon the orientation (+ or - z) of the induced back emf, for a positive phase current during motoring in the positive direction.

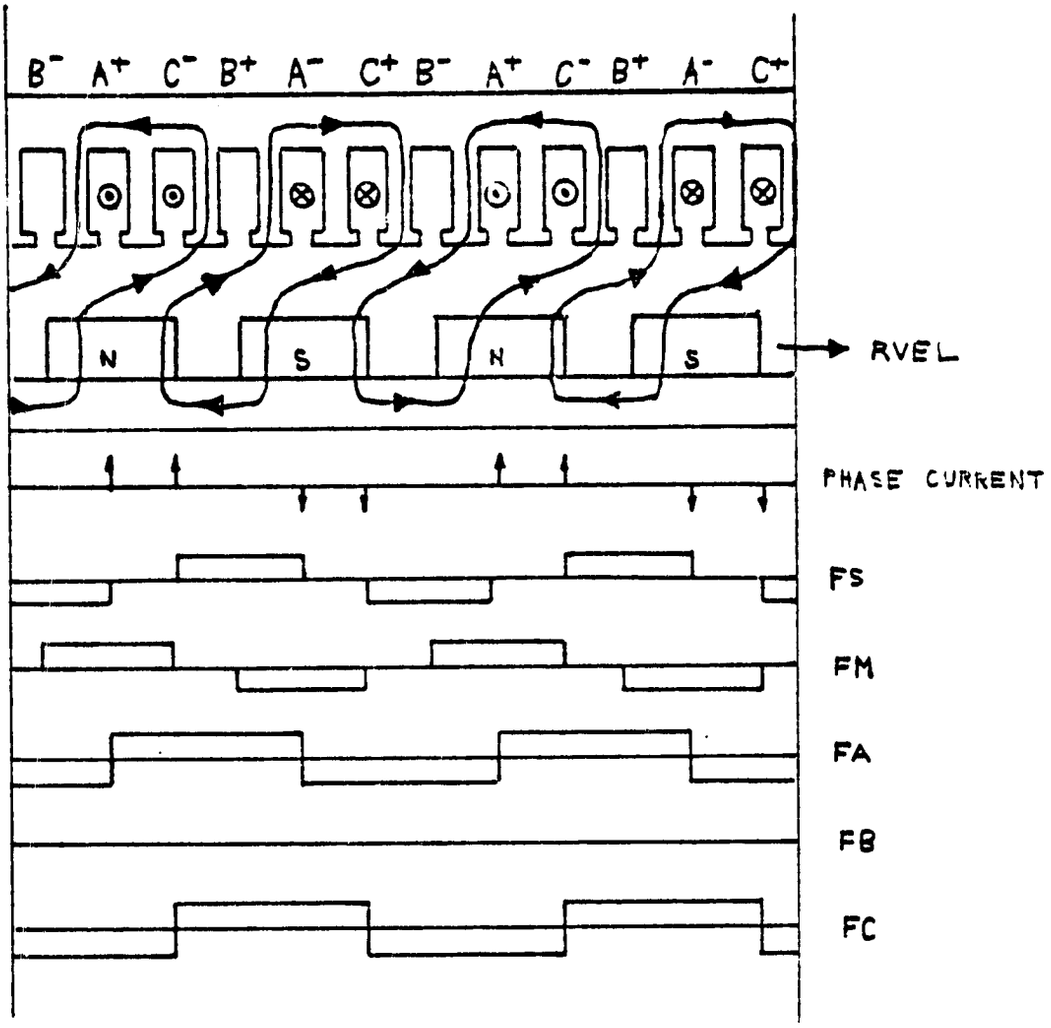

Figure 2.4-1. Machine Cross Section at Maximum Torque

The mmfs FA, FB, and FC produced by the above mentioned phase currents are displayed below the developed machine cross-section, Figure (2.4-1). The resultant stator mmf, FS, is obtained by summing these phase mmfs. The idealized mmf waveform, FM, of the permanent magnet pole pieces is given directly below the phase mmfs. These mmfs establish magnetic flux which follows closed paths similar to the ones shown in the machine cross-section.

The electromechanical interactions between the stator and rotor can be approximated by a lumped magnetic circuit consisting of reluctances in series with sources of mmf. Applying this model to any one of the eight symmetrical closed flux paths between the stator and rotor circuits yields the magnetic network of Figure (2.4-2). The permeability of the iron rotor and stator cores can be assumed to be infinite because of the dominance of the air gap and magnet reluctances at the low levels of flux densities in these cores. This model of the machine forms the basis from which the phase back emfs are calculated.

As was shown earlier in Section 2.2, one can determine the induced emf in a phase conductor by means of equation (2.2-2), once the flux density, $\overline{B}_c$, at the conductor and the velocity, $\overline{V}_c$, of the conductor with respect to the field, $\overline{B}_c$, are known. In the air gap, $\overline{B}_c$ is essentially radially oriented, and therefore perpendicular to $\overline{V}_c$. Consequently, the magnitude of the induced emf per unit conductor length, $\overline{E}$, as defined by equation (2.2-2) becomes

$$|\overline{E}| = |\overline{V}_c| \cdot |\overline{B}_c| \qquad (2.4\text{-}1)$$

Before the back emfs can be calculated, the total number of effective series conductors per phase must be determined. Each phase

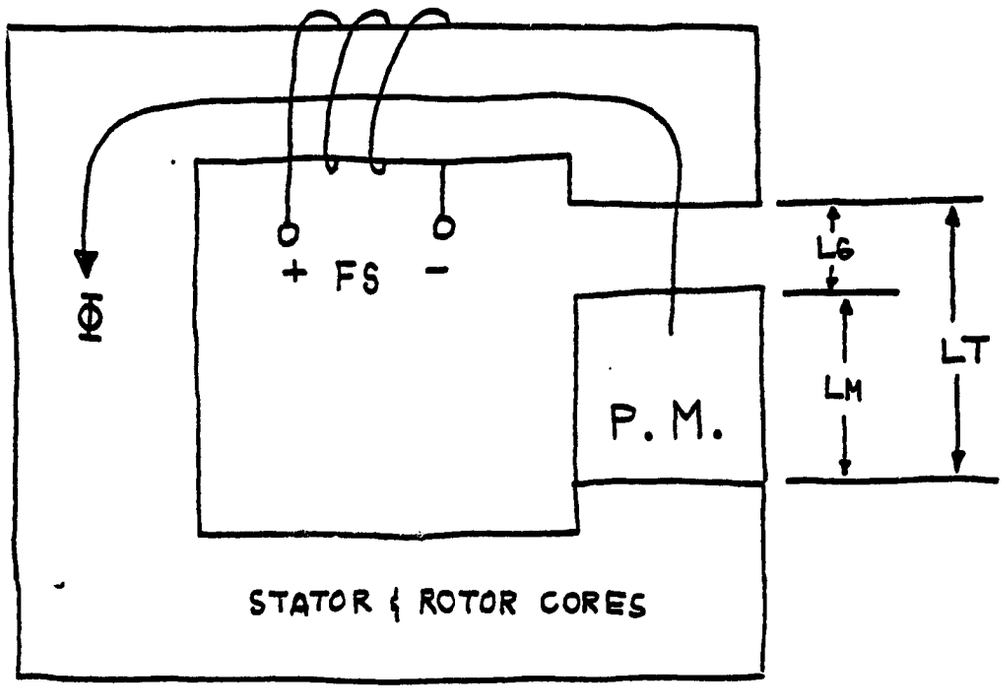

Figure 2.4-2. Equivalent Magnetic Circuit of the PM Machine.

winding per pole pair consists of 11 effective turns. Since there are four pole pairs, the total number of turns per phase winding equals 44. Each of these turns is composed of two conductors which experience equal but oppositely oriented flux densities, see Figure (2.2-4). Therefore, the magnitude of the emf per unit length, $|\bar{E}|$, which is induced in each of the 88 conductors is equal. The total phase back emfs induced in the phase windings therefore become:

$$e_A = [88\ell_C\bar{a}_Z] \cdot [\bar{V}_C \times \bar{B}_C(\Theta_{SA})] \quad \text{Volts} \qquad (2.4\text{-}2)$$

$$e_B = [88\ell_C\bar{a}_Z] \cdot [\bar{V}_C \times \bar{B}_C(\Theta_{SB})] \quad \text{Volts} \qquad (2.4\text{-}3)$$

$$e_C = [88\ell_C\bar{a}_Z] \cdot [\bar{V}_C \times \bar{B}_C(\Theta_{SC})] \quad \text{Volts} \qquad (2.4\text{-}4)$$

All parameters in equations (2.4-2), (2.4-3), and (2.4-4) are known, except for the flux densities $\bar{B}_C(\Theta_{SA})$, $\bar{B}_C(\Theta_{SB})$, and $\bar{B}_C(\Theta_{SC})$. These flux densities are functions of the rotor position, stator currents, and of the magnet demagnetization characteristics. In order to keep the computational costs within manageable bounds, the just mentioned lumped parameter approach will be used. In this approach, the flux path around the phase conductors is replaced by an equivalent lumped parameter circuit as shown in Figure (2.4-2). This circuit consists of an iron core, representing the flux paths in the stator and rotor bodies connected in series with an air gap and permanent magnet. Notice that only one half of the total flux path shown in the developed diagram of Figure (2.4-1) needs to be considered because of symmetry.

The behavior of the magnet is modeled by the magnet demagnetization (B-H) curve. The B-H characteristic of the permanent magnets used for the rotor pole pieces is given in Figure (2.4-3). The upper

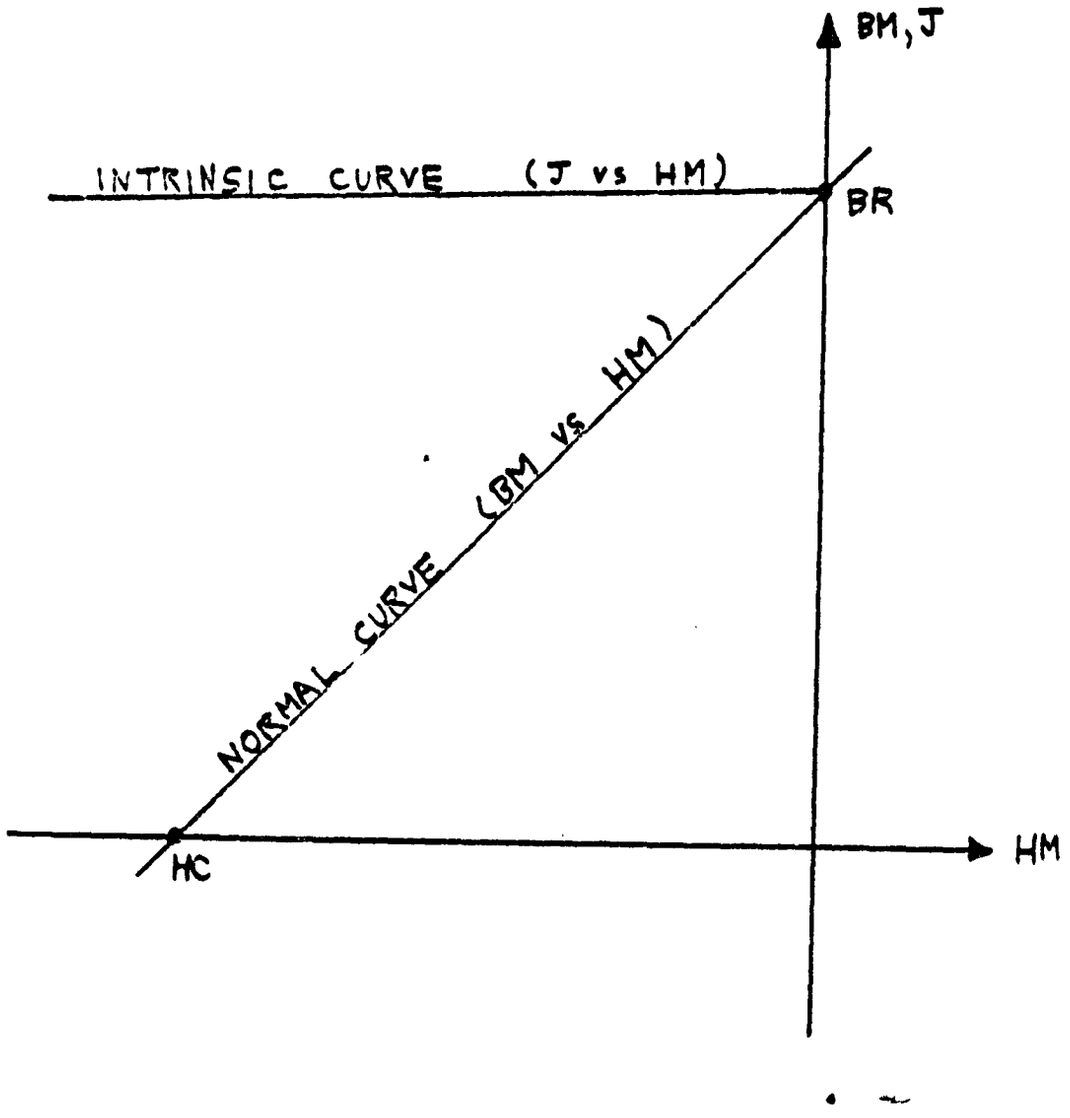

Figure 2.4-3 Permanent Magnet Demagnetization Characteristic

line represents the INTRINSIC demagnetization curve of the permanent magnet and in the linear region is described by the equation:

$$J = -(\mu_o + B_R/H_C)H_M + B_R \qquad (2.4\text{-}5)$$

The lower line is called the NORMAL demagnetization curve and in the linear region can be approximated by the line:

$$B_M = -(B_R/H_C)H_M + B_R \qquad (2.4\text{-}6)$$

These two curves obey a linear interrelationship given by

$$B_M = J + \mu_o H_M \qquad (2.4\text{-}7)$$

As mentioned before, the flux paths in the stator and rotor iron are assumed to be ideal ($\mu = \infty$) because of the relatively low operating flux densities encountered in this machine.

At the present time, the air gap plus magnet length, ℓ_T, is held fixed for all levels of machine torque. However, a finite element analysis would allow the calculation of an effective air gap length based upon different levels of machine torque. As the torque increases, the flux is twisted, thus increasing the effective air gap length, see Figure (2.4-1).

The procedure used to calculate the flux densities of the stator conductors is as follows:

Step 1: Determine the open circuit (stator phase currents zero) flux densities from a Fourier analysis of the open circuit voltage (back emf) waveform given in Figure (2.1-11). A normalized series representation of this waveform is given by:

$$\begin{aligned} & 1.111111 \cos \Theta_{RR} \\ & - .0819017 \cos 3\Theta_{RR} \\ & - .0807241 \cos 5\Theta_{RR} \\ & + .0405518 \cos 7\Theta_{RR} \end{aligned} \qquad (2.4\text{-}8)$$

This series is multiplied by the flux density, BPEAK, such that substitution into equation (2.4-2), (2.4-3), and (2.4-4) results in the measured open circuit voltage waveform given in Figure (2.1-11). The above series therefore becomes:

$$\begin{aligned} BGAP = BPEAK & [1.111111 \cos \Theta_{RR} \\ & - .0819017 \cos 3\Theta_{RR} \\ & - .0807241 \cos 5\Theta_{RR} \\ & + .0405518 \cos 7\Theta_{RR} \end{aligned} \qquad (2.4\text{-}9)$$

The spatial flux density distribution represented by this series is produced entirely by the rotor permanent magnets. Rewriting this series in terms of a stator reference angle Θ_{SS} and the angle Θ_{SR} between the phase A mmf axis and the closest rotor north pole, Figure (2.1-9), yields

$$\begin{aligned} BGAP = BPEAK & [1.111111 \cos [4(\Theta_{SS} - \Theta_{SR})] \\ & - .0819017 \cos 3[4(\Theta_{SS} - \Theta_{SR})] \\ & - .0807241 \cos 5[4(\Theta_{SS} - \Theta_{SR})] \\ & + .0405518 \cos 7[4(\Theta_{SS} - \Theta_{SR})] \end{aligned} \qquad (2.4\text{-}10)$$

This equation enables one to determine the air gap flux density at any stator angle Θ_{SS} given a rotor-stator displacement of Θ_{SR}. The open circuit conductor flux densities can now be calculated simply by substituting for Θ_{SS} the angular displacements Θ_{SA}, Θ_{SB}, and Θ_{SC} of the conductors.

Step 2. Determine the equivalent magnet and air gap lengths ℓ_m and ℓ_g necessary to produce the flux densities given in STEP 1.

These calculations make use of the magnetic lumped circuit machine model of Figure (2.4-2) and the magnet demagnetization curve of Figure (2.4-3). In the open circuit case the stator mmf, FS, equals zero, therefore by Ampere's Law one obtains:

$$\int H \cdot d\ell = H_m \ell_m + H_g \ell_g = 0 \qquad (2.4\text{-}11)$$

Since fringing is neglected

$$B_m = B_g = B = \mu_o H_g \qquad (2.4\text{-}12)$$

Substituting equation (2.4-12) into (2.4-11) and solving for H_m results in:

$$H_m = -B\ell_g/\mu_o \ell_m \qquad (2.4\text{-}13)$$

Substituting equation (2.4-13) into equation (2.4-6) yields

$$B = (B_R \ell_g/\mu_o \ell_m H_C)B + B_r \qquad (2.4\text{-}14)$$

The ratio ℓ_g/ℓ_m can now be written as

$$\ell_g/\ell_m = \mu_o H_C/B_R - \mu_o H_C/B \qquad (2.4\text{-}15)$$

Now

$$\ell_T = \ell_g + \ell_m \qquad (2.4\text{-}16)$$

Substituting for ℓ_m in equation (2.4-15) and solving for ℓ_g results in:

$$\ell_g = \frac{\ell_T \mu_o H_C [B - B_R]}{\mu_o H_C [B - B_R] + B_R B} \qquad (2.4\text{-}17)$$

Step 3. Determine the resultant stator mmf, F_S, at conductor locations. The stator mmf at any arbitrary stator angle, θ_{SS}, can be approximated as shown in Figure (2.4-1).

Step 4. Given ℓ_m, ℓ_g and F_S determine the new operating flux density B′. From $\oint H \cdot d\ell = I$ one obtains:

$$H_m \ell_m + H_g \ell_g = F_S \tag{2.4-18}$$

Solving for H_m results in:

$$H_m = F_S/\ell_m - B'\ell_g/\mu_o\ell_m \tag{2.4-19}$$

Substituting equation (2.4-19) into equation (2.4-5) yields the intrinsic flux density J as follows:

$$J = -(\mu_o + B_R/H_C)[F_S - B'\ell_g/\mu_o]/\ell_m + B_R \tag{2.4-20}$$

The new operating flux density B′ of the magnet is given by Equation (2.4-7). Substituting for H_m and J into equation (2.4-7) and solving for B′ yields:

$$B' = \frac{B_R[H_C\ell_m - F_S]}{H_C\ell_m - B_R\ell_g/\mu_o} \tag{2.4-21}$$

This flux density is then used to calculate the induced back emf as described earlier. In the subsection which follows, these emfs are used to determine the developed electromagnetic machine torque.

2.4.2 Machine Torque Calculation

The developed machine torque is required as an input for the model of the dynamics of the rotating masses which is developed later in Chapter 4. The developed air gap electromagnetic torque is calculated as follows:

$$TEM = (e_A i_A + e_B i_B + e_C i_C)/RVEL \qquad (2.4\text{-}22)$$

where TEM is the developed air gap electromechanical torque;

e_A, e_B, and e_C are the phase back emfs;

i_A, i_B, and i_C are the phase currents;

and RVEL is the rotor velocity.

3. STATE SPACE MODEL OF THE POWER CONDITIONER AND MACHINE NETWORK

The utilization of the permanent magnet machine, described in the pervious chapter, for servo applications requires a current or power conditioner network capable of controlling the machine phase currents so as to produce actuation torques of specified orientations and magnitudes. This function is performed by four power conditioner networks, one for each of the four machines which together constitute a single four channel EM actuator.

The nonlinear differential equations and their related output equations which characterize the electromagnetic dynamics of a single power conditioner and machine unit are derived in this chapter. The differential equations are subsequently integrated forward in time using the exponential series method. This projection of the system state variables forward in time makes it possible to calculate the developed machine torques as well as the power conditioner voltages, currents, and powers instantaneously. This time sequence of machine torques couples the electromagnetic model of the machine and power conditioner developed in this chapter with the mechanical model developed in the next chapter. The calculated, instantaneous values of voltages, currents, and powers are used to quantify the stresses experienced by the power conditioner components under various operating regimes. The knowledge of the magnitude and nature of these stresses is of great concern in aerospace applications where system reliability and margins of safety are of paramount importance.

3.1 DESCRIPTION OF THE POWER CONDITIONER

The function of the power conditioner as stated earlier in the introduction to this chapter is to modulate the d.c. current of the supply battery into a three phase current which will produce a specified average machine torque in response to a torque (current) command from the servo controller. Figure (3.1-1) shows a schematic diagram of the power conditioner along with the associated three phase permanent magnet machine. The principal components or elements of the power conditioner can be categorized as follows:

a) A DC Power Supply

b) A Filter Capacitor

c) A Pulse Width Modulator or Chopper

d) A Coupling or Chopper Inductor

e) A Six Leg Power Inverter Bridge

These power conditioner elements are indicated in Figure (3.1-1).

The d.c. power supply, in the present system, consists of a bank of 24 conventional lead acid batteries connected together to produce a nominal potential of 270 volts. This is roughly equal to the d.c. voltages which presently exist on the space shuttle. The battery output is connected across a large filter capacitor which helps to suppress voltage transients which might otherwise result in damage to the switching transistors QM and QB as well as suppressing possible supply transients.

The d.c. power available at the terminals of this capacitor is then pulse width modulated or chopped into a series of current pulses. The width of these pulses is controlled by logic described in the next chapter. This chopper or pulse width modulator is made up of two

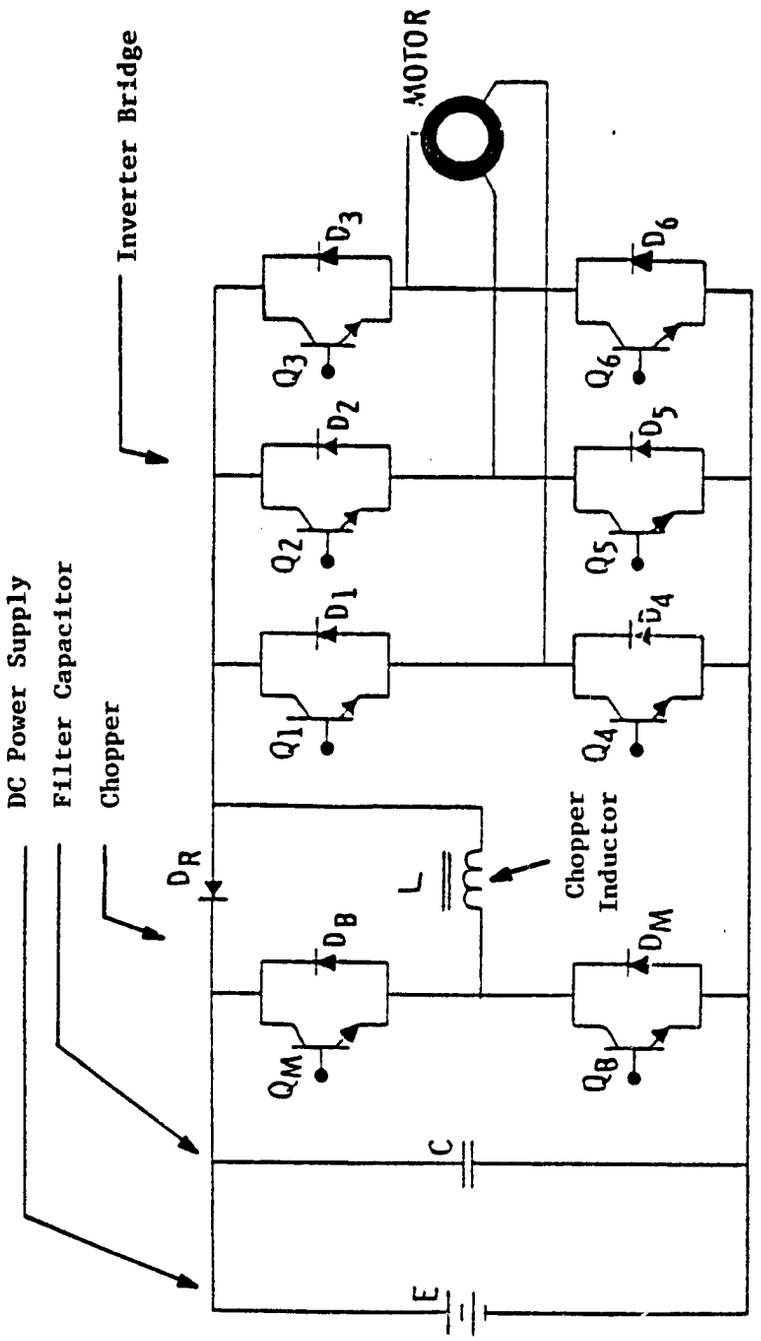

Figure 3.1-1. Machine and Power Conditioner Schematic

transistor switches QM and QB as well as the two antiparallel diodes DB and DM respectively.

The chopping action of these transistors (QM and QB) maintains an average d.c. current level in the attached coupling or chopper inductor. The time averaged valued of this current approximately equals the commanded machine current, IMC. This current command is directly proportional to the machine torque command because of the linear relationship between machine current and torque. The actual chopper inductor current does not track the command, IMC, exactly since this would require a chopper switching frequency of infinity. Instead, the chopper current oscillates in a sawtooth fashion of magnitude $\pm$ ITOL amperes about the commanded current IMC. The antiparallel diodes, DB and DM provide paths for the decaying inductor current which results from the cut off of transistors QM or QB respectively.

The modulated inductor current is then injected into the proper machine phase windings by a six leg transistor inverter bridge. Each of the three machine phase windings is serviced by two oppositely oriented transistor switches which allow control of the current entering or leaving a particular phase. In addition, each inverter transistor is spanned by a diode with a current orientation opposite to that of the attached transistor. These antiparallel diodes provide a path for the decaying phase currents which result when a phase is commutated (or disconnected) from the source. This greatly reduces the magnitudes of the voltage transients across the inverter transistors because of the lower time rate of change of the inductor current. The phase assignment of these switches is given below:

Phase A: Q1-D1 and Q4-D4

Phase B: Q2-D2 and Q5-D5

Phase C: Q3-D3 and Q6-D6

Notice that the upper inverter transistors Q1, Q2, and Q3 control positive phase currents (i.e. currents entering the machine), while the lower inverter switches Q4, Q5, and Q6 control negative phase currents.

The above mentioned commutation process results in a current unbalance at the node which connects the chopper inductor and the top of the inverter bridge. The commutation recovery diode, DR, provides a path for this excess current and at the same time clamps the maximum potential at this node to a level slightly above the supply potential. There would be a large voltage transient across the inverter bridge if such a path did not exist. This is a direct consequence of the large (L di/dt) which results from the high resistance path.

The logic which controls the switching of the chopper transistors QM and QB, and the logic which controls the six inverter transistors Q1-Q6 is described in detail in the chapter which follows. Mathematical representations of these components for the power conditioner and machine network model are developed in the next section.

3.2 MODELS OF THE VARIOUS POWER CONDITIONER COMPONENTS

This section deals with the derivation of equivalent electrical models of the various components of the power conditioner network. These components can all be classified as one of the five basic component types listed below:

a) Battery

b) Inductor

c) Capacitor

d) Switching Transistor

e) Switching Diode

The development of mathematical representations for these components is the objective of this section.

The first component listed above is a battery which in the present case consists of a bank of 24 standard lead acid batteries connected together to provide a potential of approximately 270 volts. The actual discharge characteristics of such batteries are extremely difficult to model analytically. However at the present time such a detailed battery model is not warranted for two reasons. First the battery bank is usually operated at energy levels which are well below the levels where these discharge nonlinearities are apparent. And secondly this battery bank is of a temporary nature and therefore bears little resemblance to the actual d.c. supply present in the space shuttle. Based upon these assumptions the supply battery can be represented by a constant voltage source, v_{BAT}, in series with a resistance R_{BAT}. The constant voltage source, v_{BAT}, is assigned the value of the open circuit or no load battery voltage. The series resistance accounts for the internal battery resistance plus the resistance associated with the interconnec-

tion between the battery and the power conditioner. A symbolic representation of this battery model is given below:

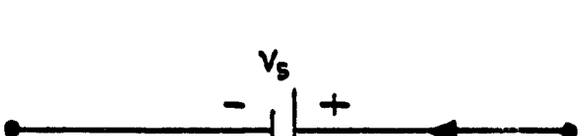

IDEAL BATTERY

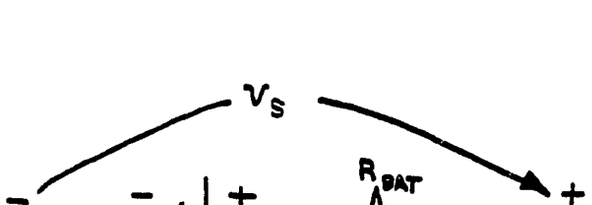

LOSSY BATTERY

The relationship between i_{BAT}, v_{BAT}, v_S, and R_{BAT} is given by ohms law as follows:

$$v_S = R_{BAT} i_{BAT} + v_{BAT} \tag{3.2-1}$$

Notice that the relationship between the assigned branch voltage and branch current obeys the consumer system of notation. Consequently, the battery receives or consumes power when the product $v_{BAT} \cdot i_{BAT}$ is positive, and likewise it supplies power to the load when $v_{BAT} \cdot i_{BAT}$ is negative. Henceforth, all branch current and voltage orientations will follow this convention.

The power conditioner and machine model developed in this chapter contains a total of four inductances. The power conditioner network contains one of these four inductances, namely the inductance associated with the chopper inductor. This inductance is heavily influenced by

the magnitude of the chopper current. Figure (3.2-1) displays this nonlinear relationship between the chopper current and the chopper inductance. The computer program developed under this contract utilizes a cubic spline curve fitting algorithm to represent this nonlinearlity numerically. The remaining three inductances are from the electrical model of the machine derived earlier in Chapter 2. These three leakage inductances account for the flux leakage of the stator phase windings. The volt-ampere relationship for the inductors is given by

$$v = L\frac{di}{dt} \tag{3.2-2}$$

where

v is the voltage across the inductor in volts,

i is the current through the inductor in amperes,

L is the inductance in henries and

t is the time in seconds.

A schematic representation of such an inductor branch is given below:

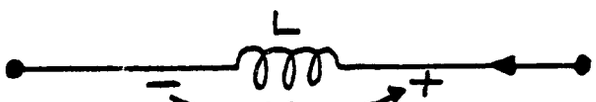

A proper representation of the chopper and leakage inductors must include the voltage drop due to the non zero resistances associated with their windings. The addition of this resistive voltage drop results in the following:

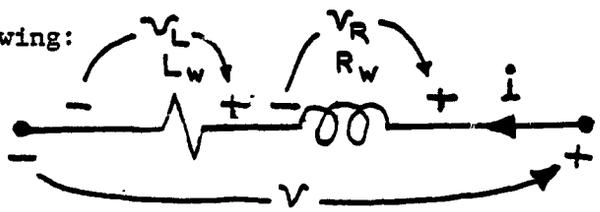

where

R_w is the winding resistance in ohms.

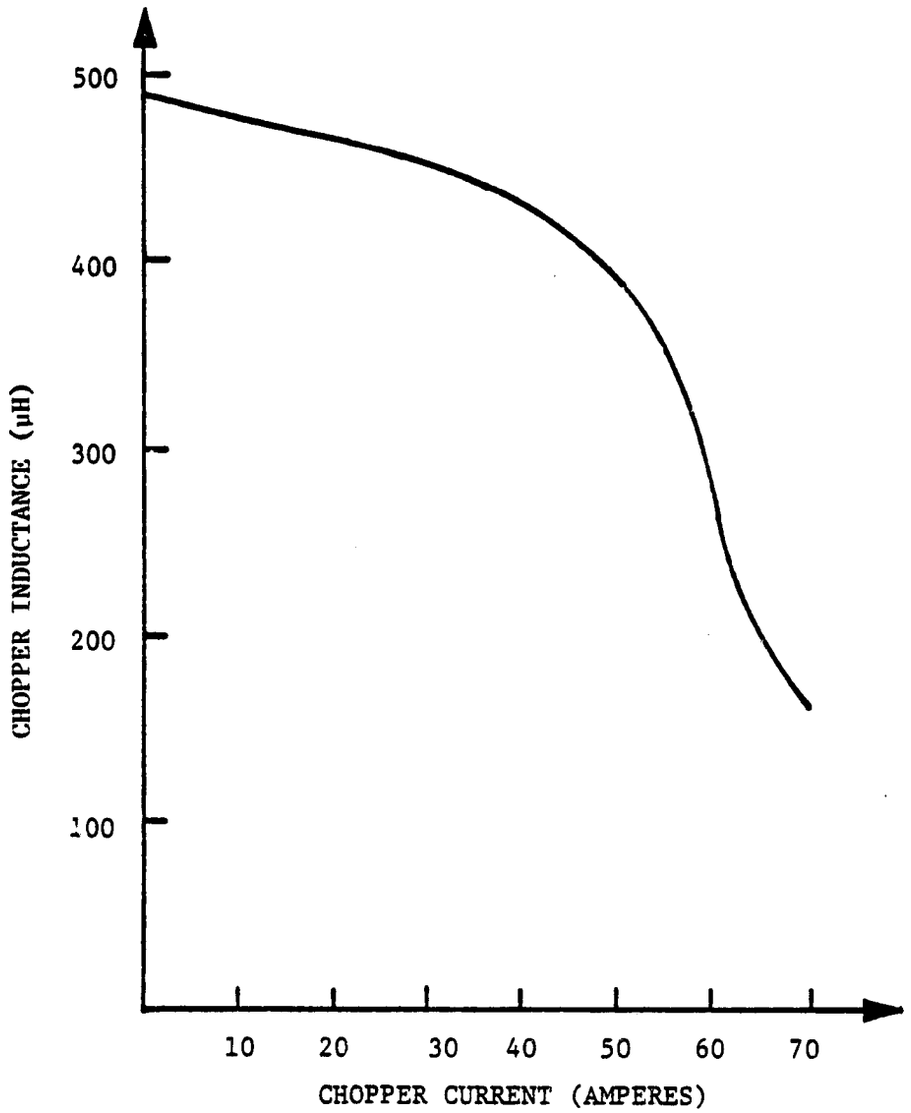

Figure 3.2-1. Chopper Saturation Curve

L_w is the winding resistance in henries,

v_L is the voltage drop in volts due to the winding inductance L_w,

v_R is the voltage drop in volts due to the winding resistance R_w,

and v is the total voltage drop across the inductor terminals in volts.

This schematic can be expressed analytically as

$$v = v_L + v_R$$

or

$$v = L_w \frac{di}{dt} + R_w i \tag{3.2-3}$$

The power conditioner network as represented in this report contains only one capacitor. The functional relationship between the voltage and current of this capacitor is given by:

$$i = C \frac{dv}{dt} \tag{3.2-4}$$

where i is the current in amperes through the capacitor,

C is the capacitance in Farads,

and v is the voltage in volts across the capacitor terminals.

Schematically this equation is represented by

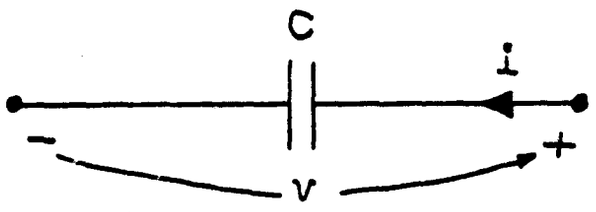

The transistors and diodes which make up the power conditioner basically function as simple ON/OFF switches. Consequently, their

behavior can be approximated with relative accuracy by logical variables which take on values of either 1 (TRUE or ON) or 0 (FALSE or OFF). The transistors are able to switch in very little time; typically in less than 1 μs. For this reason the transistor and diode switches are represented by an ideal switch in series with a resistor to represent the voltage drop. The steps in the determination of the switch status and resistance are outlined below:

STEP 1. Determine the status of all power conditioner transistors. The transistor switching commands are generated by the pulse width modulator (chopper controller) and by the inverter controller (see chapter 4.0). The commands are defined as follows:

QMON Logical Switching Command for QM

QBON Logical Switching Command for QB

Q(1) Logical Switching Command for Q1

Q(2) Logical Switching Command for Q2

Q(3) Logical Switching Command for Q3

Q(4) Logical Switching Command for Q4

Q(5) Logical Switching Command for Q5

Q(6) Logical Switching Command for Q6

Each of these logical variables is either 1 (TRUE) or 0 (FALSE) corresponding to an ON or OFF switching command.

STEP 2. From the transistor switching commands generated in STEP 1, assign the proper resistance to each switch. Transistors commanded to be ON are assigned a low resistance based upon the voltage drop at rated current. Transistors commanded to be OFF are assigned resistances which are 10,000 times larger than the ON resistance.

The procedure for the determination of the status of the switching diodes is analogous to the one used for the transistors. This procedure can be summarized as follows:

STEP 1. Determine the diode switching commands D(1), . . . , D(9) from the signs of the diode branch voltages. These commands are defined as follows:

D(1) Logical Switching Command for D1

D(2) Logical Switching Command for D2

D(3) Logical Siwtching Command for D3

D(4) Logical Switching Command for D4

D(5) Logical Switching Command for D5

D(6) Logical Switching Command for D6

D(7) Logical Switching Command for D8

D(8) Logical Switching Command for DM

D(9) Logical Switching Command for DR

Each of these logical variables is either 1 (TRUE) or 0 (FALSE) corresponding to the ON or OFF diode states.

STEP 2. Assign the proper branch resistance to each diode based upon the diode switching commands D(1), . . . , D(9) described in STEP 1. Diodes commanded to be ON are assigned a low resistance based upon the voltage drop at rated current. Diodes commanded to be OFF are assigned resistances 10,000 times larger than the corresponding ON resistance.

The diodes which are connected across transistors (D1, . . . , D6, DB, and DM) are always OFF when the transistor is on because of their antiparallel connection. Consequently the transistor switching commands

take precedence over the corresponding antiparallel diode switching commands.

The incorporation of these component models into a unified state space representation of the power conditioner and machine network is accomplished in the next section.

3.3 DERIVATION OF THE STATE EQUATIONS FOR THE POWER CONDITIONER AND MACHINE NETWORK

3.3.1 Introduction and Modeling Approach

The state equations of the combined power conditioner and machine network are derived in this section. These equations will be derived in standard state space form as symbolized by:

$$\dot{\underline{x}}_n = \underline{A}_n \cdot \underline{x}_n + \underline{B}_n \cdot \underline{u}_n \tag{3.3-1}$$

where

$\underline{x}_n$ is the vector of the network state variables,

$\underline{u}_n$ is the vector of the network input or forcing functions,

$\dot{\underline{x}}_n$ is the vector of the first derivatives of the elements of $\underline{x}_n$ with respect to time,

$\underline{A}_n$ is the nonlinear coefficient matrix of the vector $\underline{x}_n$,

and

$\underline{B}_n$ is the coefficient matrix of the vector $\underline{u}_n$.

The procedure selected for the derivation of these state equations is described in detail in References (1) and (5). This procedure can be summarized briefly as follows:

STEP 1. Select a tree and cotree to represent the network topology. The rules for the selection of these is given in References (1) and (5).

STEP 2. Derive the state equations in the intermediate form

$$\underline{F}_n \dot{\underline{x}}_n = \underline{G}_n \underline{x}_n + \underline{H}_n \underline{u}_n \tag{3.3-2}$$

where

$\underline{F}_n$ is the non singular coefficient matrix of $\dot{\underline{x}}_n$,

C-2

$\underline{G}_n$ is the nonlinear coefficient matrix of $\underline{x}_n$,

and

$\underline{H}_n$ is the coefficient matrix of $\underline{u}_n$.

STEP 3. Convert the intermediate form of the state equations given in STEP 2 into the standard state space form of equation (3.3-1). This is accomplished by premultiplying both sides of equation (3.3-2) by $\underline{F}_n^{-1}$, which results in

$$\dot{\underline{x}}_n = [\underline{F}_n^{-1} \cdot \underline{G}_n]\, \underline{x}_n + [\underline{F}_n^{-1} \cdot \underline{H}_n]\, \underline{u}_n \qquad (3.3\text{-}3)$$

The matrices $\underline{A}_n$ and $\underline{B}_n$ of equation (3.3-1) can now be defined as

$$\underline{A}_n = \underline{F}_n^{-1} \cdot \underline{G}_n \qquad (3.3\text{-}4)$$

$$\underline{B}_n = \underline{F}_n^{-1} \cdot \underline{H}_n \qquad (3.3\text{-}5)$$

All derivations performed in these steps are kept in symbolic form, so as to reduce the time required for the numerical calculation of these equations.

3.3.2 Derivation of the Nonlinear Network State Equations

Substitution of the component models developed in Section 3.2 into the power conditioner and machine schematic given in Figure (3.1-1) results in the network shown in Figure (3.3-1). The heavy lined branches in this figure represent the twigs of the chosen tree. The thin lined branches belong to the cotree, see References (1) and (5). The assumed direction of the current in each of these branches is indicated by a solid arrow for the twigs, and by the outline of an arrow for the links. The sense of the branch voltages with respect to the assumed current orientations is determined by employing the consumer (load) system of notation.

For purposes of identification, each branch is characterized by two different labels; a branch label and a branch component label. The branch label identifies the branch number and is denoted by the prefix B and the branch number. For example, B1 denotes branch one. The component labels are identified by the prefixes C, E, L, and R (capacitor, emf, inductor, and resistor) and the component number. In addition to the branch labels, each node is identified by the prefix N and the chosen node number. Node N0 is taken to be at ground or zero volts potential and is therefore used as the reference for the other node voltages.

Branch currents are denoted by the prefix IB followed by the appropriate branch number. For example, IB16 represents the current through branch 16. Similarly, the branch voltage is symbolized by VB16.

The state variables for this network are the branch voltages of the twig capacitors and the currents through the link inductors. This corresponds to VB5, IB21, IB22, and IB23, see Reference (1).

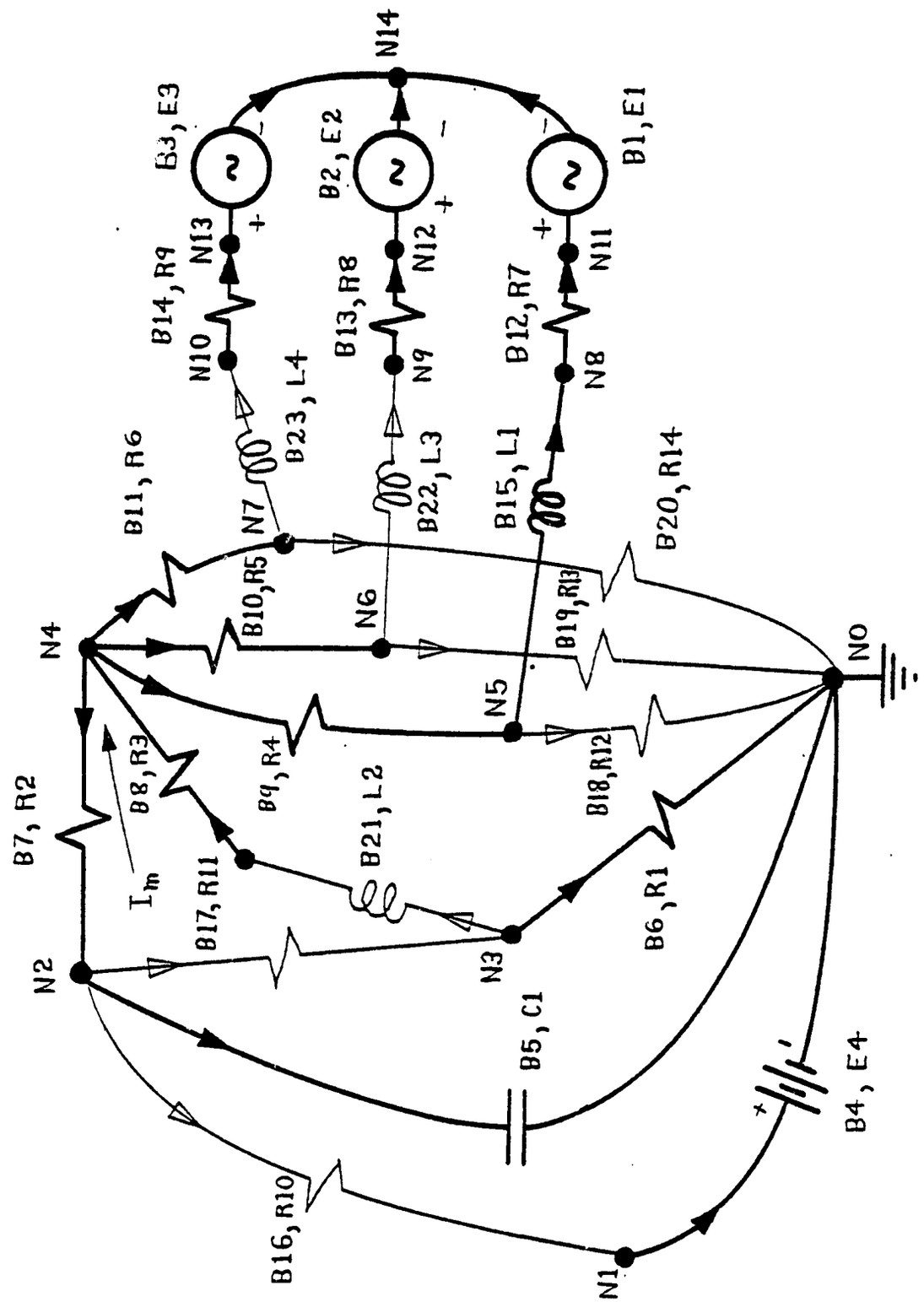

Figure 3.3-1. The Machine and Power Conditioner Network Model

The steps in the derivation of the power conditioner and machine state equations are listed below.

STEP 1. Determine the fundamental current loops for the given tree. The fundamental current loops are formed by taking one link at a time and tracing out the unique loop which would be formed by that particular link and the tree with all other links removed from the network. There are eight links in this network, consequently the number of fundamental current loops equals eight, see Figures (3.3-2), . . . , (3.3-9).

STEP 2. Determine the resistive link currents, IB16, . . . , IB20, in terms of the state variables, VB5, IB21, IB22, and IB23, and the sources, E1, E2, E3, and E4. The link current, IB16, corresponding to link 1 (branch 16) is obtained by applying Kirchoffs voltage law around the loop through the tree formed by link 1. Solving for IB16 yields:

$$IB16 = (VB5-E4)/R10 \qquad (3.3\text{-}6)$$

Similarily one obtains for link 2:

$$IB17 = (VB5 + IB21R1)/(R1 + R11) \qquad (3.3\text{-}7)$$

The loop equations for links 3, 4, and 5 yield a set of coupled simultaneous equations which relate the link currents IB18, IB19, and IB20 to the state variables as follows:

$$\underline{\underline{K}}_n \cdot \text{col}\{IB18, IB19, IB20\} = \underline{\underline{L}}_n \cdot \text{col}\{VB5, IB21, IB22, IB23\}$$

or in expanded form:

$$\begin{bmatrix} R2 + R4 + R12 & R2 & R2 \\ R2 & R2 + R5 + R13 & R2 \\ R2 & R2 & R2 + R6 + R14 \end{bmatrix} \cdot \begin{bmatrix} IB18 \\ IB19 \\ IB20 \end{bmatrix} =$$

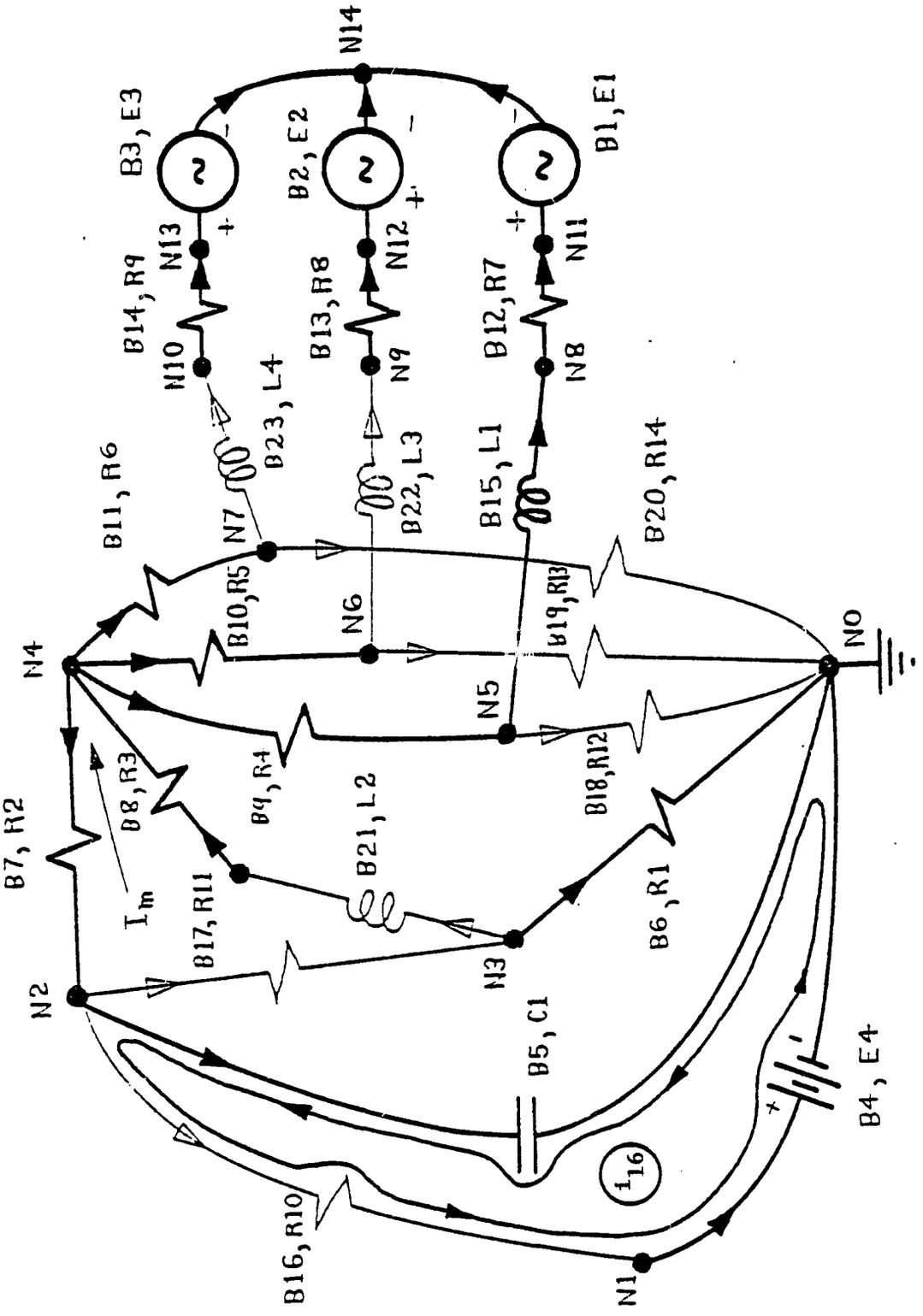

Figure 3.3-2. Fundamental Current Loop Due to Link 1 (B16)

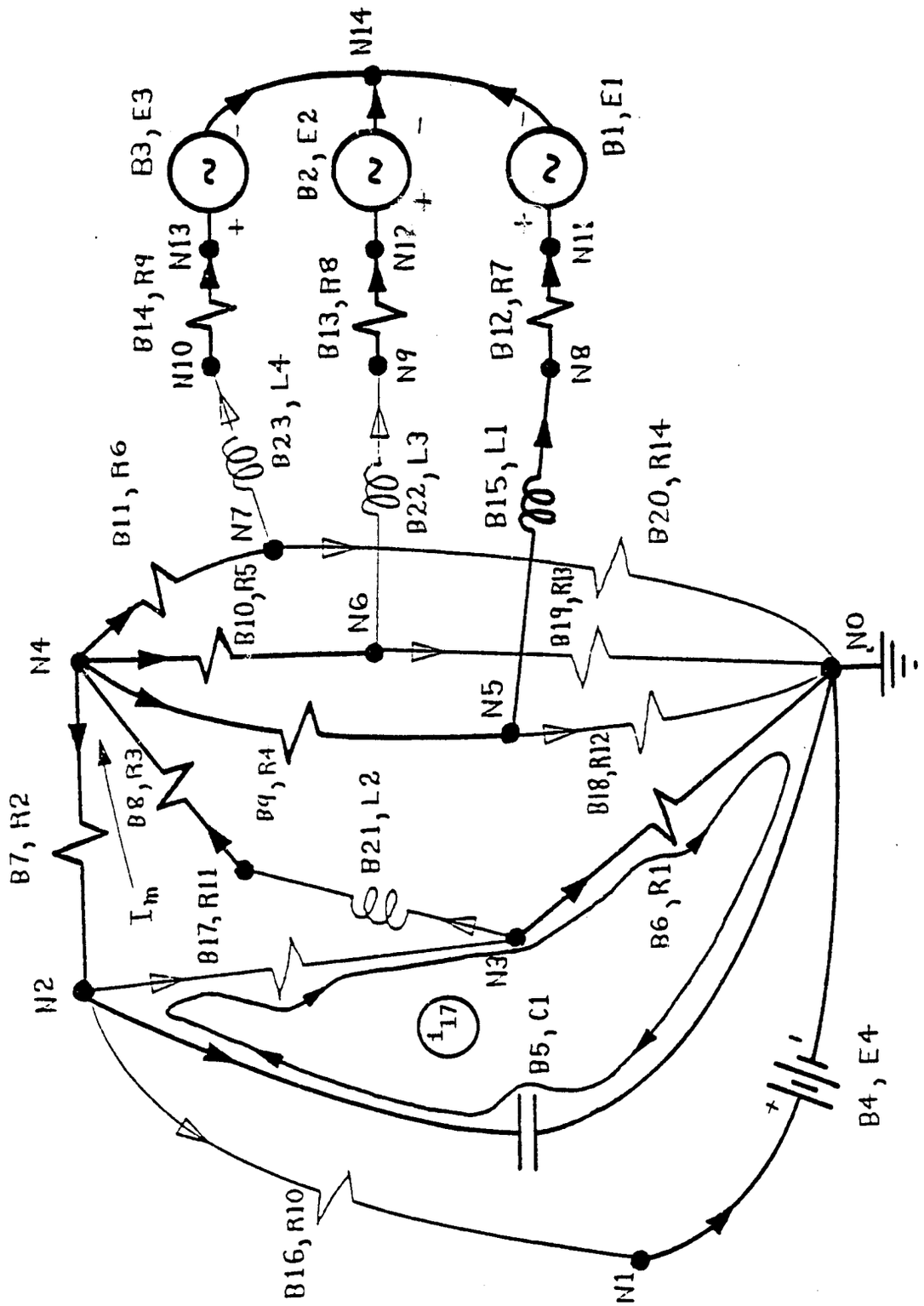

Figure 3.3-3. Fundamental Current Loop Due to Link 2 (B17)

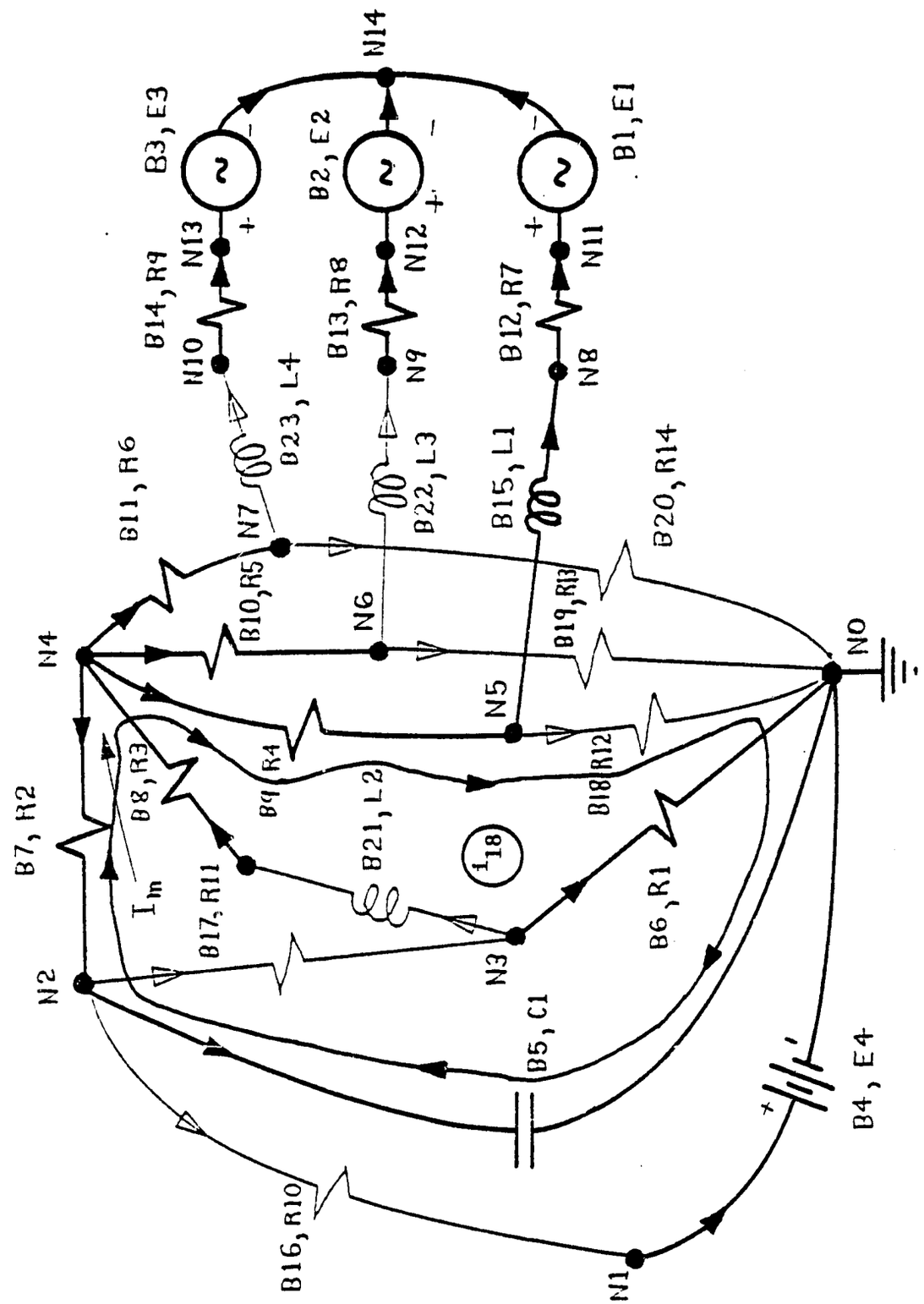

Figure 3.3-4. Fundamental Current Loop Due to Link 3 (B18)

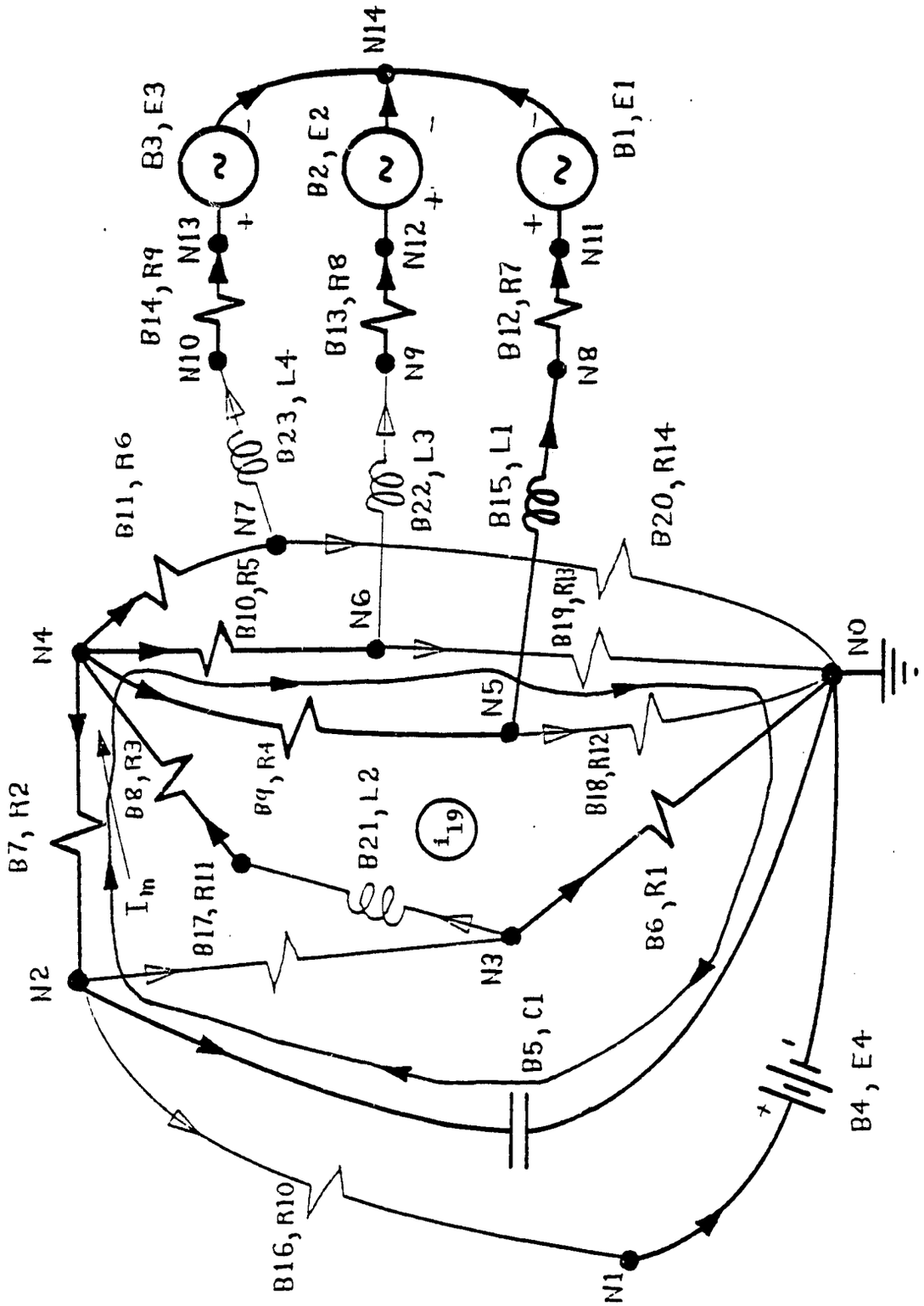

Figure 3.3-5. Fundamental Current Loop Due to Link 4 (B19)

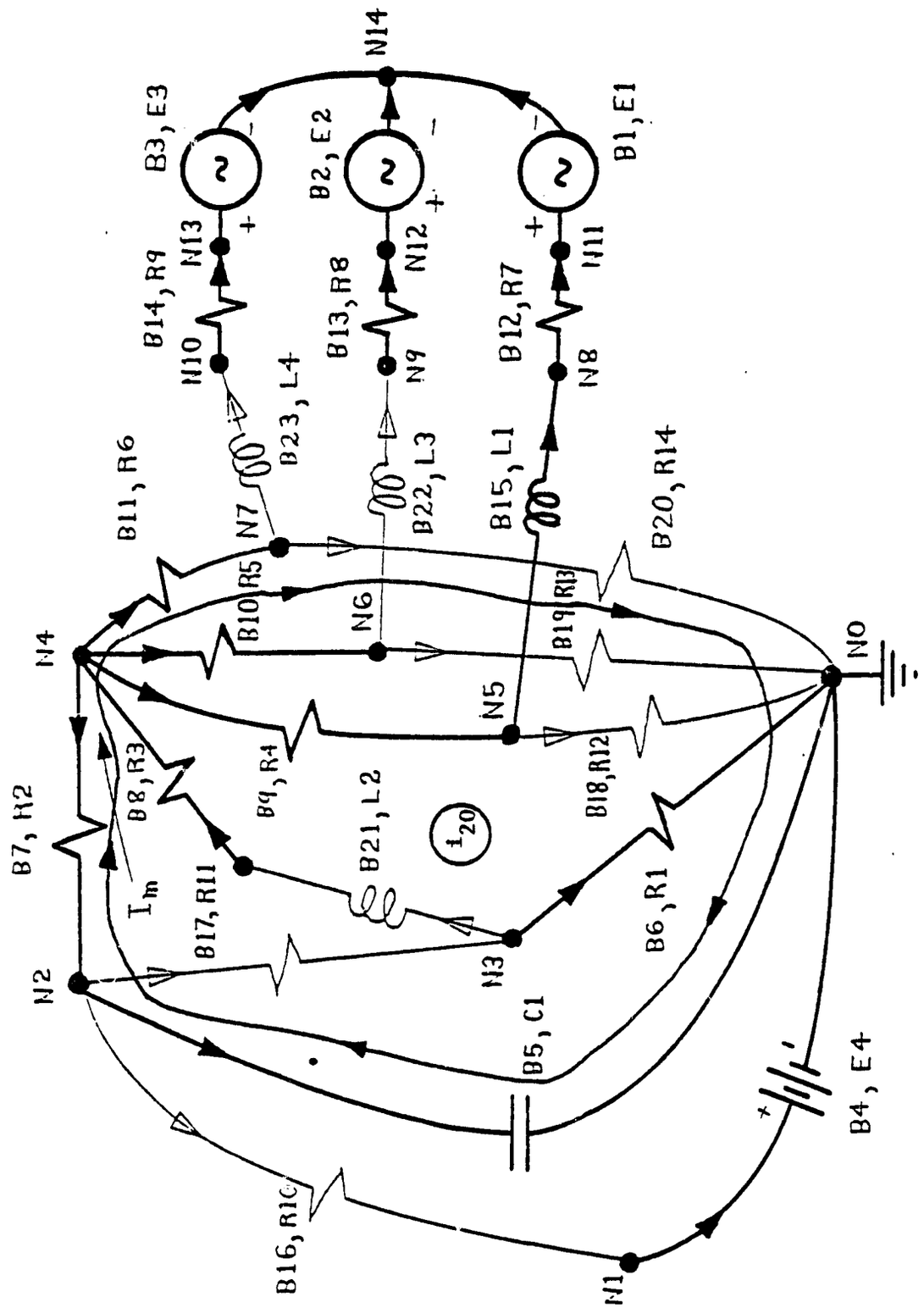

Figure 3.3-6. Fundamental Current Loop Due to Link 5 (B20)

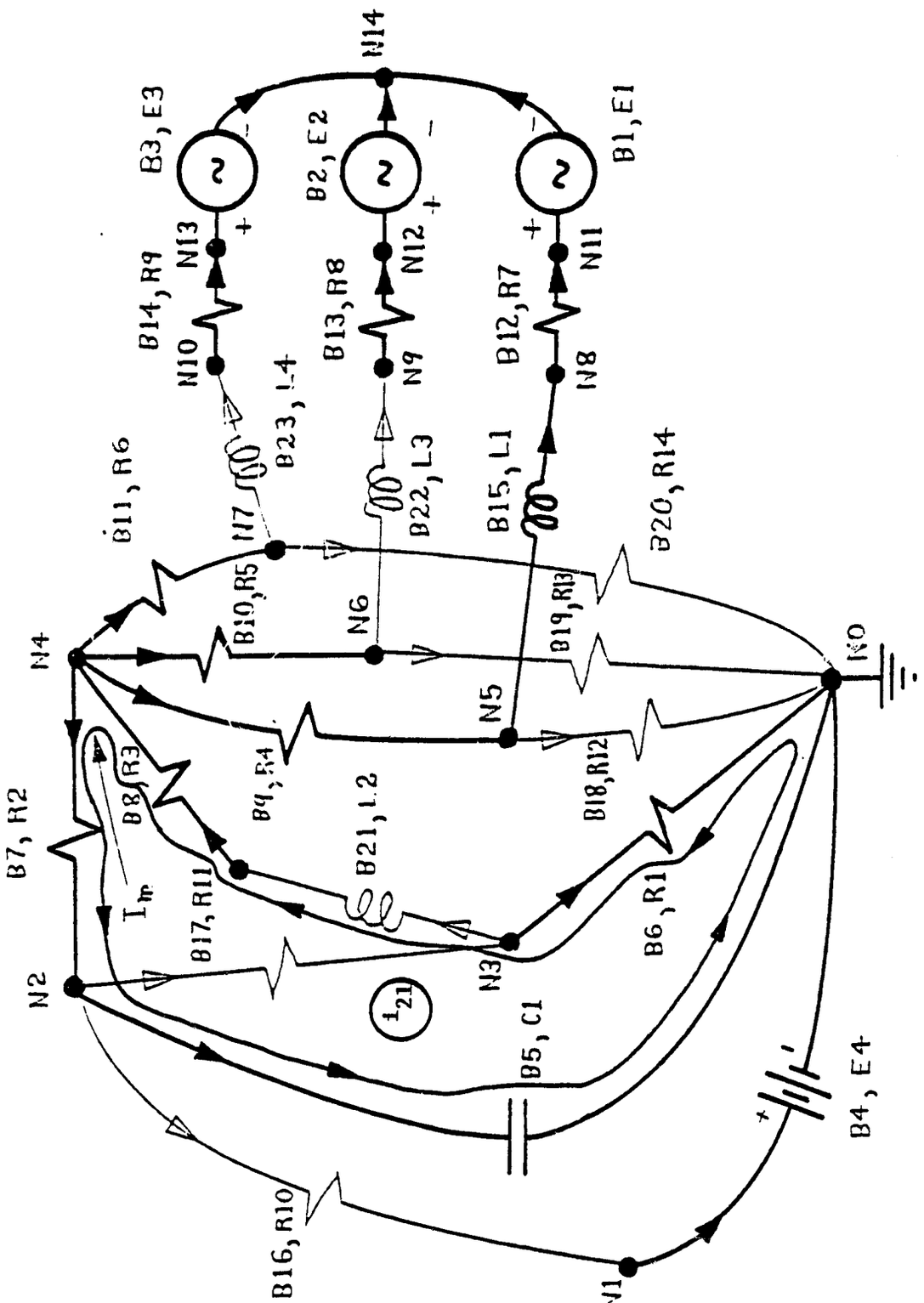

Figure 3.3-7. Fundamental Current Loop Due to Link 6 (B21)

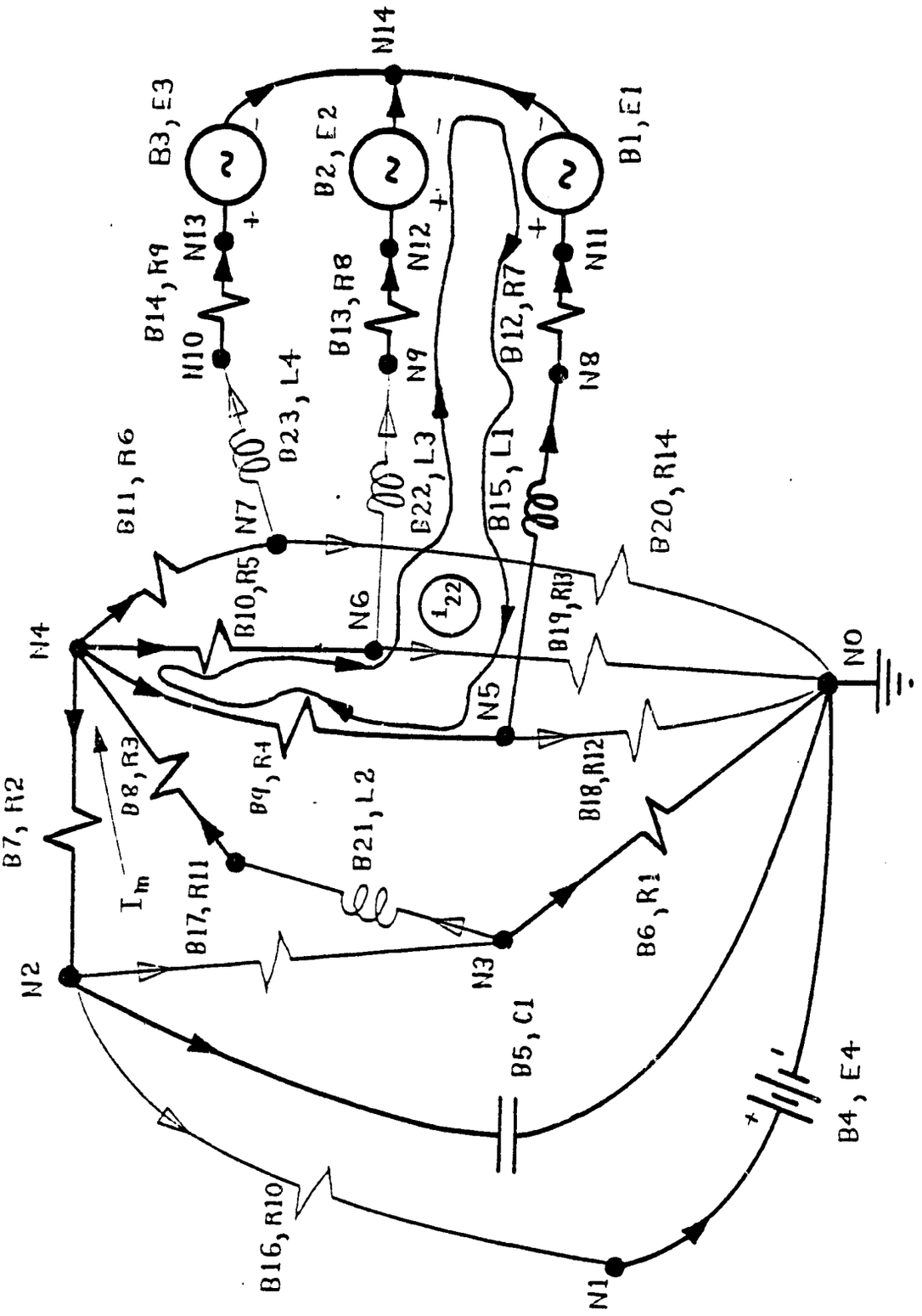

Figure 3.3-8. Fundamental Current Loop Due to Link 7 (B22)

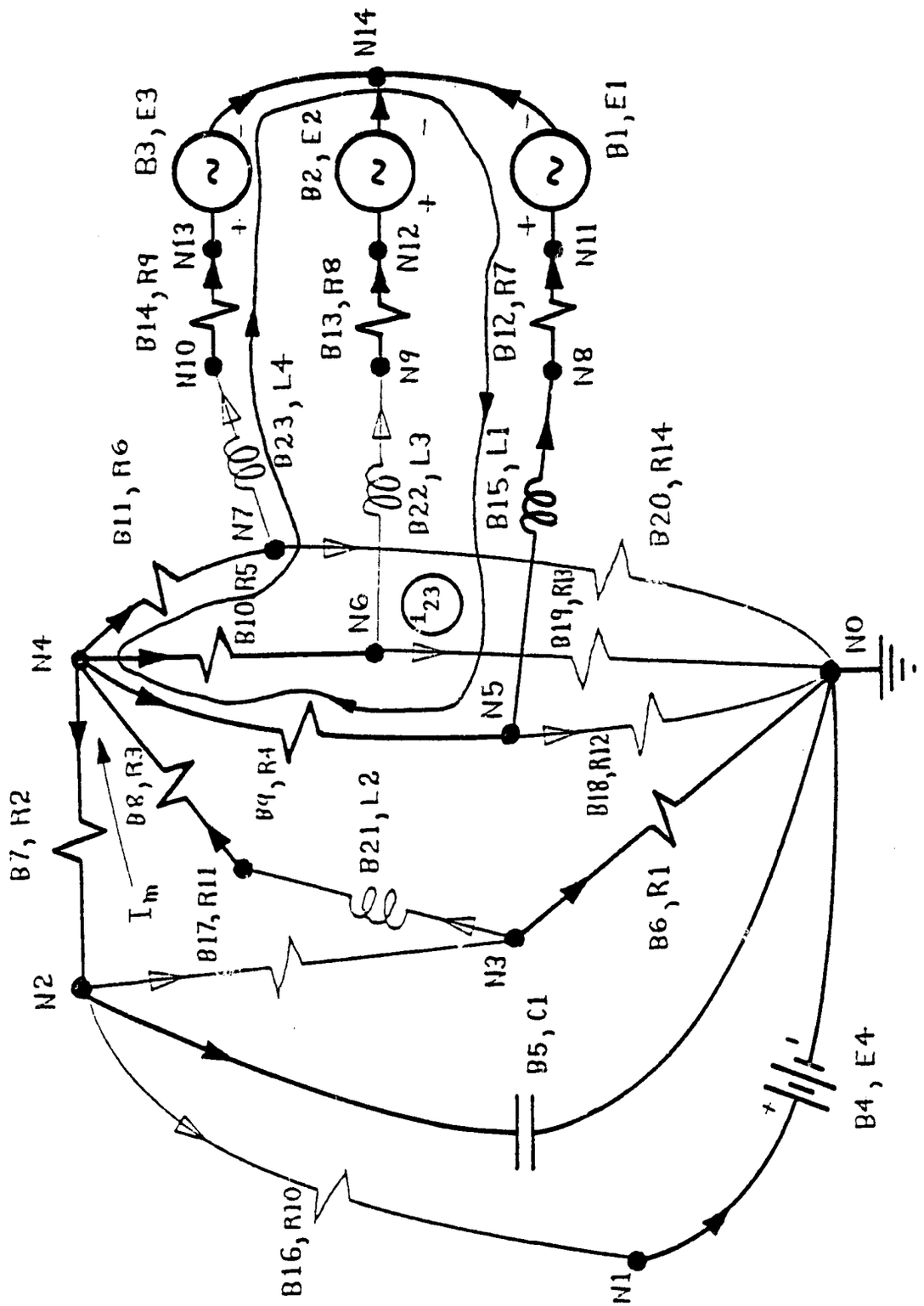

Figure 3.3-9. Fundamental Current Loop Due to Link 8 (B23)

$$\begin{bmatrix} 1 & R2 & R4 & R4 \\ 1 & R2 & -R5 & 0 \\ 1 & R2 & 0 & -R6 \end{bmatrix} \cdot \begin{bmatrix} VB5 \\ IB21 \\ IB22 \\ IB23 \end{bmatrix} \qquad (3.3\text{-}8)$$

Premultiplying both sides of equation (3.3-8) by $\underline{K}_n^{-1}$ yields:

$$\text{col } \{IB18, IB19, IB20\} = \underline{C}_n \text{ col } \{VB5, IB21, IB22, IB23\}$$

where $\underline{C}_n = \underline{K}_n^{-1} \cdot \underline{L}_n$

or in matrix form

$$\begin{bmatrix} IB18 \\ IB19 \\ IB20 \end{bmatrix} = \begin{bmatrix} C11 & C12 & C13 & C14 \\ C21 & C22 & C23 & C24 \\ C31 & C32 & C33 & C34 \end{bmatrix} \cdot \begin{bmatrix} VB5 \\ IB21 \\ IB22 \\ IB23 \end{bmatrix} \qquad (3.3\text{-}9)$$

STEP 3. Form the loop equations corresponding to the link inductors. These loop equations will involve the resistive link currents, IB16, . . ., IB21. These currents have already been expressed as a linear combination of the state variables and the independent voltage sources; consequently, the loop equations for the link inductors can be written entirely in terms of these state variables and voltage sources.

The loop equations corresponding to links 6, 7, and 8 (branches 21, 22, and 23) become:

Link 6

$$L2 \frac{dIB21}{dt} = VB5 \cdot \left[\frac{R1}{R1 + R11} + R2(C11 + C21 + C31) - 1\right]$$

$$+ IB21\ [-(R1 + R2 + R3) + \frac{R1\ R1}{R1 + R11} + R2(C12 + C22 + C32)]$$

$$+ IB22\ [R2(C13 + C23 + C33)]$$

$$+ IB23[R2(C14 + C24 + C34)] \qquad (3.3\text{-}10)$$

Link 7

$$(L1 + L3)\ \frac{dIB22}{dt} + L1\ \frac{dIB23}{dt} =$$

$$VB5\ [C11\ R4 - C21R5] + IB21\ [C21\ R4 - C22R5]$$

$$+ IB22\ [C13\ R4 - C23\ R5 - (R4 + R5 + R7 + R8)]$$

$$+ IB23\ [-(R4 + R7) + C14\ R4 - C24\ R5]$$

$$+ E1 - E2 \qquad (3.3\text{-}11)$$

Link 8

$$L1\ \frac{dIB22}{dt} + (L1 + L4)\ \frac{dIB23}{dt} =$$

$$VB5\ [C11\ R4 - C31\ R6] + IB21\ [C12\ R4 - C32\ R6]$$

$$+ IB22\ [C13\ R4 - C33\ R6 - (R4 + R7)]$$

$$+ IB23\ [C14\ R4 - C34\ R6 - (R4 + R6 + R7 + R9)]$$

$$+ E1 - E3 \qquad (3.3\text{-}12)$$

STEP 4. Write the capacitor current in terms of the state variables and independent voltage sources. Applying Kirchoff's Current Law (KCL) at node 2 yields:

$$C1\ \frac{dVB5}{dt} + IB18 + IB19 + IB20$$

$$- IB21 + IB17 + IB16 = 0 \qquad (3.3\text{-}13)$$

Substituting for IB16, . . . , IB21 in equation (3.3-12) results in:

$$C1\,\frac{dVB5}{dt} = -VB5\,\left[\frac{1}{R10} + \frac{1}{R1 + R11} + C11 + C21 + C31\right]$$

$$-IB21\,\left[\frac{R1}{R1 + R11} + C12 + C22 + C32 - 1\right]$$

$$-IB22\,[C13 + C23 + C33]$$

$$-IB23\,[C14 + C24 + C34]$$

$$+ E4/R10 \qquad (3.3\text{-}14)$$

Rewriting equations (3.3-10), (3.3-11), (3.3-12), and (3.3-14) in matrix form results in:

C1	0	0	0
0	L2	0	0
0	0	L1+L3	L1
0	0	L1	L1+L4

$\frac{d}{dt}$

VB5
IB21
IB22
IB23

=

$-1/R10 - 1/(R1 + R10)$ $-(C11 + C21 + C31)$	$1 - R1/(R1 + R11)$ $-(C12 + C22 + C32)$	$-(C13 + C23 + C33)$	$-(C14 + C24 + C34)$		VB5
$-1 + R1/(R1 + R11)$ $+R2\ (C11 + C21 + C31)$	$R1\ R1/(R1 + R11)$ $-(R1 + R2 + R3)$ $+R2\ (C12 + C22 + C32)$	$R2(C13 + C23 + C33)$	$R2(C14 + C24 + C34)$		IB21
$C11\ R4 - C21\ R5$	$C12\ R4 - C22\ R5$	$C13\ R4 - C23\ R5$ $-(R4 + R5 + R7 + R8)$	$-(R4 + R7) +$ $C14\ R4 - C24\ R5$		IB22
$C11\ R4 - C31\ R6$	$C12\ R4 - C32\ R6$	$-(R4 + R7)$ $+ C13\ R4 - C33\ R6$	$C14\ R4 - C34\ R6$ $-(R4 + R6 + R7 + R9)$		IB23

$$\begin{bmatrix} 0 & 0 & 0 & \frac{1}{R10} \\ 0 & 0 & 0 & 0 \\ 1 & -1 & 0 & 0 \\ 1 & 0 & -1 & 0 \end{bmatrix} \cdot \begin{bmatrix} E1 \\ E2 \\ E3 \\ E4 \end{bmatrix} \qquad (3.3\text{-}15)$$

STEP 5. The matrix equation given in equation (3.3-15) can be written symbolically as in equation (3.3-2) which is

$$\underline{F}_n \dot{\underline{x}}_n = \underline{G}_n \underline{x}_n + \underline{H}_n \underline{u}_n$$

This intermediate form of the network state equations can be transformed into the standard form given in equation (3.3-1) by premultiplying both sides of equation (3.3-15) by $\underline{F}_n^{-1}$, where $\underline{F}_n^{-1}$ is defined below.

$$\underline{F}_n^{-1} =$$

$\frac{1}{C1}$	0	0	0
0	$\frac{1}{L1}$	0	0
0	0	$\frac{(L1 + L4)}{L1\ L4 + L3\ L1 + L3\ L4}$	$\frac{-L1}{L1\ L4 + L3L1 + L3\ L4}$
0	0	$\frac{-L1}{L1\ L4 + L3\ L1 + L3\ L4}$	$\frac{(L1 + L3)}{L1\ L4 + L3\ L1 + L3\ L4}$

(3.3-16)

3.4 DERIVATION OF THE NETWORK OUTPUT EQUATIONS

The network output equations relate the states and inputs of the system to the branch voltages and currents. Knowledge of the four state variables and inputs is sufficient to uniquely determine the twenty-three branch currents and voltages. The algorithm for the calculation of these branch voltages and currents from the vectors $\underline{x}_n$ and $\underline{u}_n$ is outlined in the steps listed below.

STEP 1. Determine the first derivatives with respect to time of the state variables. These derivatives, $\dot{\underline{x}}_n$, are evaluated by means of equation (3.3-1). The vector $\dot{\underline{x}}_n$ in matrix form can be written as:

$$\dot{\underline{x}}_n = \frac{d}{dt} \begin{bmatrix} VB5 \\ IB21 \\ IB22 \\ IB23 \end{bmatrix} \tag{3.4-1}$$

STEP 2. Determine the current IB5 which flows through the twig capacitor C1 and the voltages VB21, VB22, and VB23 across the link inductors L2, L3, and L4 respectively, using $\dot{\underline{x}}_n$ defined above as follows:

$$\begin{bmatrix} IB5 \\ VB21 \\ VB22 \\ VB23 \end{bmatrix} = \begin{bmatrix} C1 & 0 & 0 & 0 \\ 0 & L2 & 0 & 0 \\ 0 & 0 & L3 & 0 \\ 0 & 0 & 0 & L4 \end{bmatrix} \cdot \frac{d}{dt} \begin{bmatrix} VB5 \\ IB21 \\ IB22 \\ IB23 \end{bmatrix} \tag{3.4-2}$$

STEP 3. Calculate the voltage, VB15, across the twig inductor L1 as follows:

$$VB15 = -L1 \cdot \frac{d}{dt} (IB22 + IB23) \tag{3.4-3}$$

STEP 4. Calculate the currents through the resistive links (IB16, . . . , IB20). From equations (3.3-6), (3.3-7), and (3.3-8), one obtains

the following matrix equation:

$$\begin{bmatrix} IB16 \\ IB17 \\ IB18 \\ IB19 \\ IB20 \end{bmatrix} = \begin{bmatrix} \frac{1}{R10} & 0 & 0 & 0 \\ \frac{1}{R1+R11} & \frac{R1}{R1+R11} & 0 & 0 \\ C11 & C12 & C13 & C14 \\ C21 & C22 & C23 & C24 \\ C31 & C32 & C33 & C34 \end{bmatrix} \cdot \begin{bmatrix} VB5 \\ IB21 \\ IB22 \\ IB23 \end{bmatrix} + \begin{bmatrix} 0 & 0 & 0 & -\frac{1}{R10} \\ 0 & 0 & 0 & 0 \\ 0 & 0 & 0 & 0 \\ 0 & 0 & 0 & 0 \\ 0 & 0 & 0 & 0 \end{bmatrix} \cdot \begin{bmatrix} E1 \\ E2 \\ E3 \\ E4 \end{bmatrix} \quad (3.4\text{-}4)$$

STEP 5. Calculate the twig currents IB1, . . . , IB15 from the link currents IB16, . . . , IB23 which were determined in the previous steps. These calculations make use of the network cut set matrix $\underline{Q}$ which is described in detail in References (1) and (5). The cut set matrix relates the twig current vector, $\underline{i}_t$, and the link current vector, $\underline{i}_\ell$, at the cut sets formed from the twigs. The twig current vector $\underline{i}_t$ consists of the twig currents IB1, . . . , IB15. The link current vector $\underline{i}_\ell$ is composed of the link currents IB16, . . . , IB23. The cut set matrix, $\underline{Q}$, can be partitioned as follows:

$$[\underline{Q}_{tt} \quad \underline{Q}_{t\ell}] \cdot \begin{bmatrix} \underline{i}_t \\ \hline \underline{i}_\ell \end{bmatrix} = \underline{0} \tag{3.4-5}$$

where $\underline{Q}_{tt}$ equals the identity matrix, $\underline{I}$, of dimension 15, and $\underline{Q}_{t\ell}$ is a 15 × 8 matrix as defined in Figure (3.4-1), Reference (5). Since $\underline{Q}_{tt} = \underline{I}$, equation (3.4-5) becomes:

$$\underline{i}_t + \underline{Q}_{t\ell} \cdot \underline{i}_\ell = \underline{0} \tag{3.4-6}$$

The twig currents $\underline{i}_t$ can now be written as

$$\underline{i}_t = -\underline{Q}_{t\ell} \cdot \underline{i}_\ell \tag{3.4-7}$$

STEP 6. Calculate the branch voltages across all branch resistances using the twig and link currents determined in the previous steps. The voltages VB6, . . . , VB14 across the twig resistors; R1, . . . , R9, are given by

Twigs \ Links	16	17	18	19	20	21	22	23
1	0	0	0	0	0	0	1	1
2	0	0	0	0	0	0	-1	0
3	0	0	0	0	0	0	0	-1
4	-1	0	0	0	0	0	0	0
5	1	1	1	1	1	-1	0	0
6	0	-1	0	0	0	1	0	0
7	0	0	1	1	1	-1	0	0
8	0	0	0	0	0	-1	0	0
9	0	0	-1	0	0	0	1	1
10	0	0	0	-1	0	0	-1	0
11	0	0	0	0	-1	0	0	-1
12	0	0	0	0	0	0	1	1
13	0	0	0	0	0	0	-1	0
14	0	0	0	0	0	0	0	-1
15	0	0	0	0	0	0	1	1

$= \underline{Q}_{tl}$

Figure (3.4-1). Network Cut Set Matrix $\underline{Q}_{tl}$

$$\begin{bmatrix} VB6 \\ VB7 \\ VB8 \\ VB9 \\ VB10 \\ VB11 \\ VB12 \\ VB13 \\ VB14 \end{bmatrix} = \begin{bmatrix} R1 & 0 & 0 & 0 & 0 & 0 & 0 & 0 & 0 \\ 0 & R2 & 0 & 0 & 0 & 0 & 0 & 0 & 0 \\ 0 & 0 & R3 & 0 & 0 & 0 & 0 & 0 & 0 \\ 0 & 0 & 0 & R4 & 0 & 0 & 0 & 0 & 0 \\ 0 & 0 & 0 & 0 & R5 & 0 & 0 & 0 & 0 \\ 0 & 0 & 0 & 0 & 0 & R6 & 0 & 0 & 0 \\ 0 & 0 & 0 & 0 & 0 & 0 & R7 & 0 & 0 \\ 0 & 0 & 0 & 0 & 0 & 0 & 0 & R8 & 0 \\ 0 & 0 & 0 & 0 & 0 & 0 & 0 & 0 & R9 \end{bmatrix} \cdot \begin{bmatrix} IB6 \\ IB7 \\ IB8 \\ IB9 \\ IB10 \\ IB11 \\ IB12 \\ IB13 \\ IB14 \end{bmatrix} \quad (3.4\text{-}8)$$

The voltages VB16, . . . , VB20 across the link resistors R10, . . . , R14 are related to the link currents as follows:

$$\begin{bmatrix} VB16 \\ VB17 \\ VB18 \\ VB19 \\ VB20 \end{bmatrix} = \begin{bmatrix} R10 & 0 & 0 & 0 & 0 \\ 0 & R11 & 0 & 0 & 0 \\ 0 & 0 & R12 & 0 & 0 \\ 0 & 0 & 0 & R13 & 0 \\ 0 & 0 & 0 & 0 & R14 \end{bmatrix} \cdot \begin{bmatrix} IB16 \\ IB17 \\ IB18 \\ IB19 \\ IB20 \end{bmatrix} \quad (3.4\text{-}9)$$

Once all of these branch currents and voltages have been determined, one can calculate the instantaneous power flowing through each of these branches by obtaining the product of the corresponding branch currents and voltages. The branch voltages are also used to update the status of the switching diodes. The next section deals with the instantaneous solution of the equations derived in this and the previous sections.

3.5 DISCRETIZATION AND SOLUTION OF THE CONTINUOUS TIME NONLINEAR NETWORK

The nonlinear system of differential equations for the power conditioner and machine model must be integrated forward in time to generate the time sequence of state vectors which characterize the dynamics of the EMA in time. The network equations are of the general form:

$$\dot{\underline{x}} = \underline{A}\underline{x} + \underline{B}\underline{u} \tag{3.5-1}$$

This class of matrix equations can be numerically integrated forward in time by considering time intervals or steps, T, which are sufficiently small so as to allow holding $\underline{A}$ and $\underline{B}$ constant over such intervals, Figure (3.5-1). Given $\underline{x}(k)$ and $\underline{u}(k)$ at a time $t = t_k = k\tau$, one can calculate the state transistion matrices $\underline{\Phi}(\tau_k)$ and $\Theta(\tau_k)$ which relate $\underline{x}(t_{k+1})$ to $\underline{x}(t_k)$ and $\underline{u}(k)$ as follows:

$$\underline{x}(t_{k+1}) = \underline{\Phi}(\tau_k)\underline{x}(t_k) + \underline{\Theta}(\tau_k)\underline{u}(t_k) \tag{3.5-2}$$

The transition matrices $\underline{\Phi}(\tau_k)$ and $\underline{\Theta}(\tau_k)$ are defined in terms of $\underline{A}(T_k)$ and $B(\tau_k)$ as follows:

$$\underline{\Phi}(\tau_k) = e^{\underline{A}(\tau_k)\tau_k} = \underline{I} + \tau_k\underline{A}(\tau) + \frac{T_k}{2!}\underline{A}(\tau_k)^2 + \text{ooo} \tag{3.5-3}$$

and

$$\underline{\Theta}(\tau_k) = \int_{t=t_k}^{t=t_{k+1}} e^{\underline{A}(\tau_k)t}\,\underline{B}\,dt$$

or

$$\underline{\Theta}(\tau_k) = (\tau_k\underline{I} + \frac{\tau_k}{2!}\underline{A}(\tau_k) + \frac{\tau_k^2}{3!}\underline{A}(\tau_k^2) + \text{ooo})\underline{B}(\tau_k) \tag{3.5-4}$$

where $\underline{I}$ is the identity matrix.

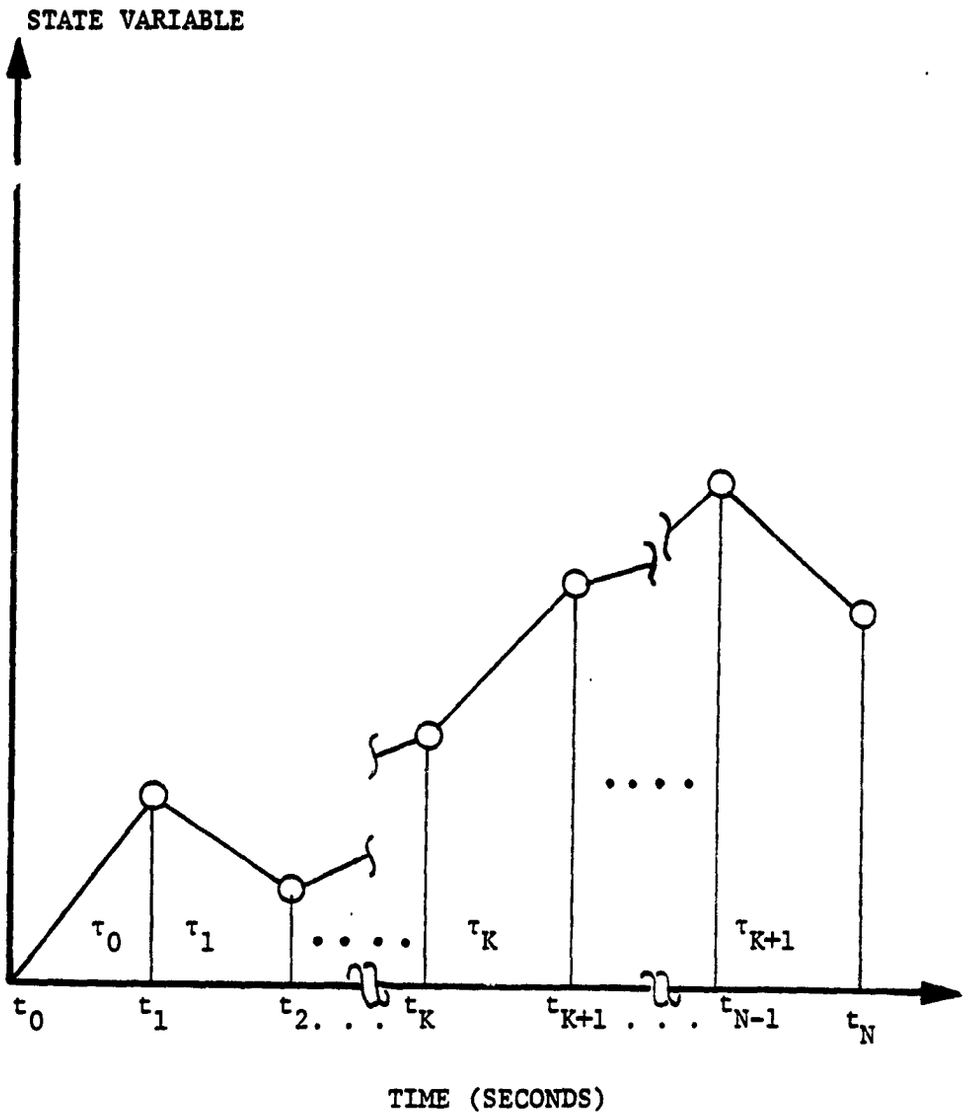

Figure 3.5-1. Discretization of the Continuous Time Power Conditioner and Machine Network State Variables

The time steps $\tau_0, \tau_1, \cdots \tau_N$ are all chosen to equal the constant, τ, in the EMA model. The steps followed by the computer program to integrate the network forward by the N time steps are shown in the flow chart, Figure (3.5-2). This algorithm proceeds as follows:

Step 1. Determine the initial system and transition matrices; $\underline{A}_n(\tau_o)$, $\underline{B}_n(\tau_o)$, $\underline{\Phi}_n(\tau_o)$, and $\underline{\Theta}_n(\tau_o)$ respectively.

Step 2. Set the network integration counter, k, to zero.

Step 3. Increment the integration counter, k, by one.

Step 4. Integrate the state variables forward in time from $\underline{x}_n(t_k)$ to $\underline{x}_n(t_{k+1})$ by means of Equation (3.5-2).

Step 5. Determine the network branch voltages, currents, and powers at time t_{k+1}, from the vectors $\underline{x}_n(t_{k+1})$ and $\underline{u}_n(t_{k+1})$.

Step 6. Determine if the network configuration has changed.

NO: GO TO STEP 7

YES: Update $\underline{A}_n$, $\underline{B}_n$, $\underline{\Phi}_n$, and $\underline{\Theta}_n$.

Step 7. Have there been N integrations?

NO: GO TO STEP 3

YES: STOP

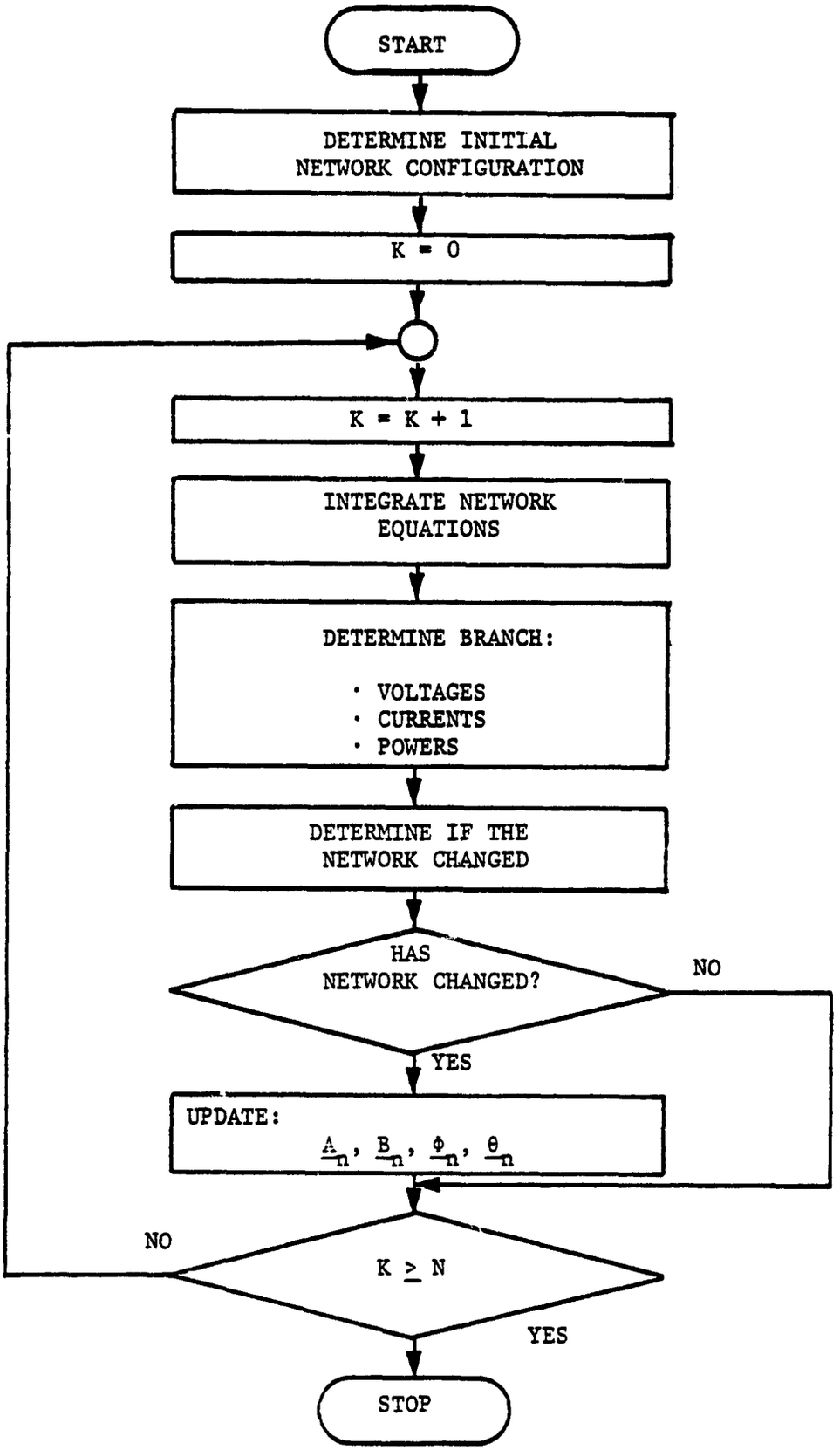

Figure 3.5-2. Solution Procedure for the Nonlinear Network Equations

4.0 STATE SPACE MODELS OF THE EMA SERVO LOOPS AND OF THE ROTATING MASSES

The power conditioner and machine networks described and modeled in the previous chapter are controlled by four independent servo loops. These loops generate the control signals to switch the appropriate power conditioner transistors on or off depending upon the position command, the state of the machine line current, and the states of the rotating masses.

The dynamics of this servo loop as well as the dynamics of the rotating masses are derived in this chapter. As before, these dynamics will be written in the standard state space form described earlier.

The EMA to be modeled here is usually run with two channels braked, Reference (2). For this reason, the model developed is limited to one or two channel operation. The servo loop equations are highly nonlinear due to the current magnitude and rate limiters which are used to control the magnitude and rate of the commanded machine torque.

The first section of this chapter describes the configurations of the servo loops under one and two channel operation as well as the configuration of the rotating masses.

4.1 DESCRIPTIONS OF THE CONTROL LOOPS AND OF THE ROTATING MASSES

A complete mechanization diagram of a single channel of the EMA is shown in Figure (4.1-1). Inspection of this diagram reveals the three basic feedback loops per channel. There is an outer position loop which feeds back the actuator position for comparison with the deflection command, DC. The time constant of the position error

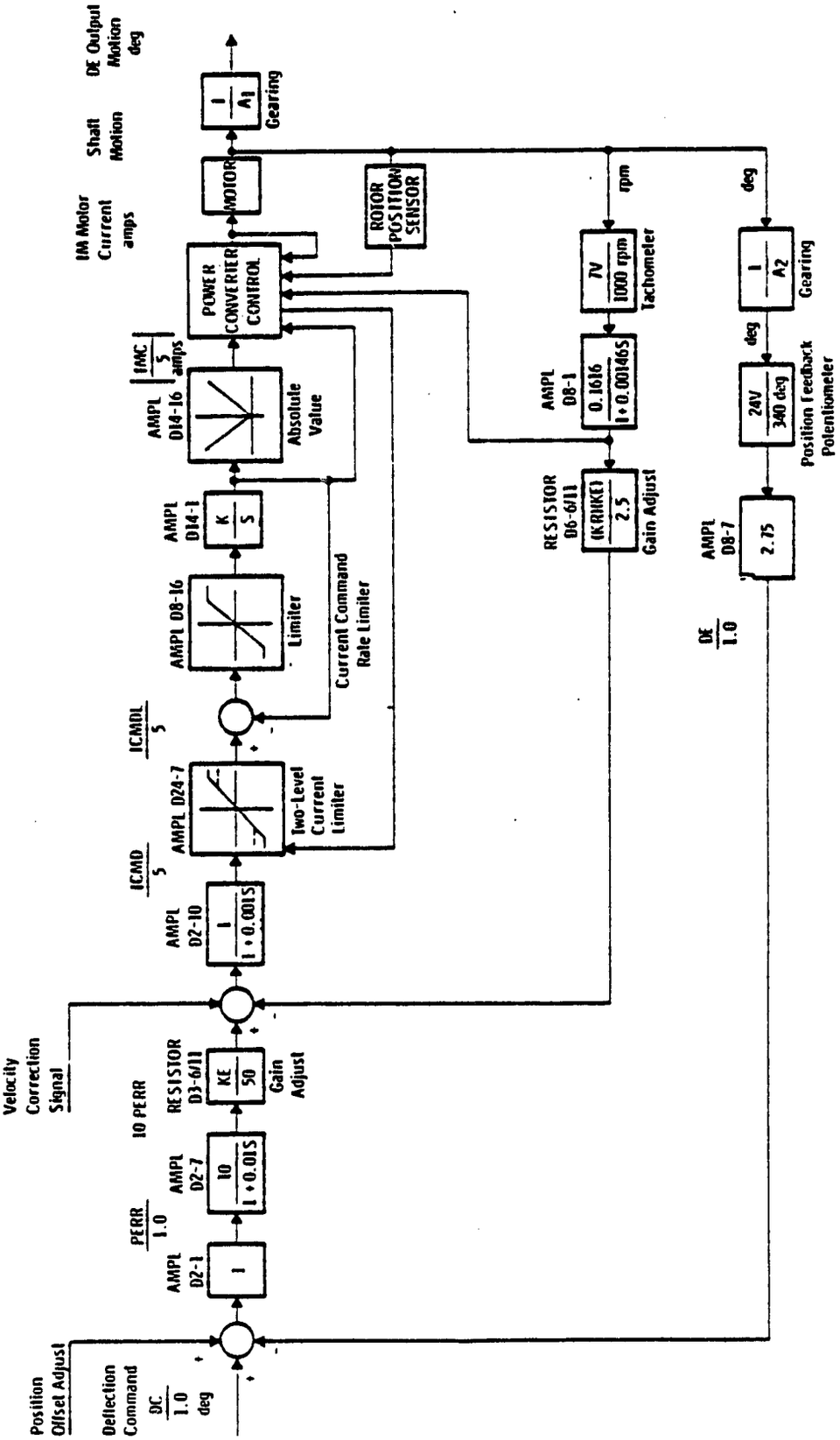

Figure 4.1-1. Mechanization of a Single EMA Channel

amplifier (AMPL D2-7) is approximately 10 milliseconds. Inside this loop lies an inner velocity feedback loop which contains two amplifiers, labeled AMPL D8-1 and AMPL D2-10. Notice that the time constants of this loop are approximately one order of magnitude faster than those of the position error loop. The innermost loop consists of the current command magnitude and rate limiters, the power conditioner controller, the power conditioner, and the permanent magnet machine. This loop contains all of the nonlinearities accounted for in this effort. The time constants for this loop are in the microsecond range because of the rapid power conditioner dynamics.

The wide variations in the time constants of these loops can lead to numerical instabilities if one tries to solve the entire system of coupled differential equations in terms of a single matrix equation such as equation (4.1-1). Instead, the EMA will be broken into the three sub systems;

$$\dot{\underline{x}}_n = \underline{A}_n\underline{x}_n + \underline{B}_n\underline{u}_n \qquad (4.1\text{-}2)$$

$$\dot{\underline{x}}_v = \underline{A}_v\underline{x}_v + \underline{B}_v\underline{u}_v \qquad (4.1\text{-}3)$$

and

$$\dot{\underline{x}}_p = \underline{A}_p\underline{x}_p + \underline{B}_p\underline{u}_p \qquad (4.1\text{-}4)$$

based upon the magnitudes of the time constants. Equation (4.1-2) represents the dynamics of the power conditioner and machine network described earlier in Chapter 3. This portion of the EMA is outlined by block #1 in Figure (4.1-2). Equation (4.1-3) represents the portion of the EMA servo loop enclosed by block #2. This portion includes the velocity feedback loop as well as the nonlinearities introduced by the current command magnitude and rate limiters. These equations

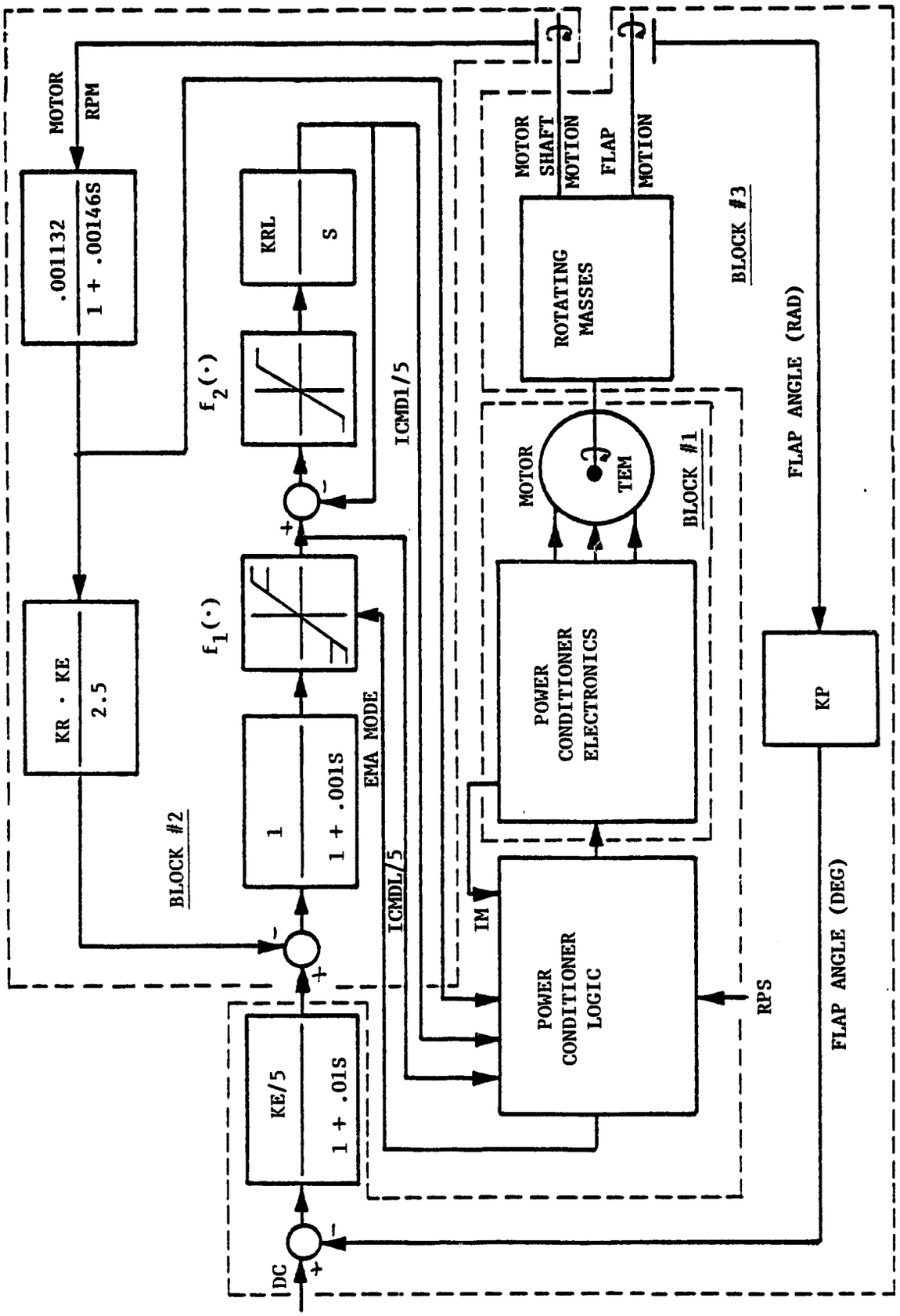

Figure 4.1-2. Classification of the EMA Components into Three Subsystems Based upon the Time Constants

are derived later in Section 4.3. The last system of differential equations symbolized by Equation (4.1-4) models the dynamics of the rotating mass and of the position feedback loop, see block #3 in Figure (4.1-2). These equations are derived later in Section 4.4.

The servo loop gain constants KE and KR shown in Figure (4.1-1) must be determined from tests performed upon the actual hardware at hand. This is accomplished by using the velocity gain and torque gain tests performed by Delco on the actual hardware, References (2), (3), (4). The results of these tests are presented in Figures (4.1-3) and (4.1-4) respectively.

These gain tests will be used to reformulate or consolidate the numerous gains of the velocity and position loops shown in Figure (4.1-2) into forms more suitable for the modeling process described later in this chapter. The proposed equivalent velocity and position loop structures are shown in Figure (4.1-5).

The gains KE and KV can be determined from the velocity gain test. Since the velocity loop can have only one gain, let KE = 1 (dimensionless) for convenience. The other gain, KV, can now be determined from the velocity gain test. The velocity gain test was performed with the EMA output blocked and the position loop opened. The measured gain in the linear region was 0.035 amperes per rotor rpm, see Figure (4.1-3). The input-output relationship of the velocity loop in the linear (unclamped) region is given by

$$\frac{ICMD1}{5} = [KV \cdot KE]RVEL \qquad (4.1\text{-}5)$$

From the gain test we have:

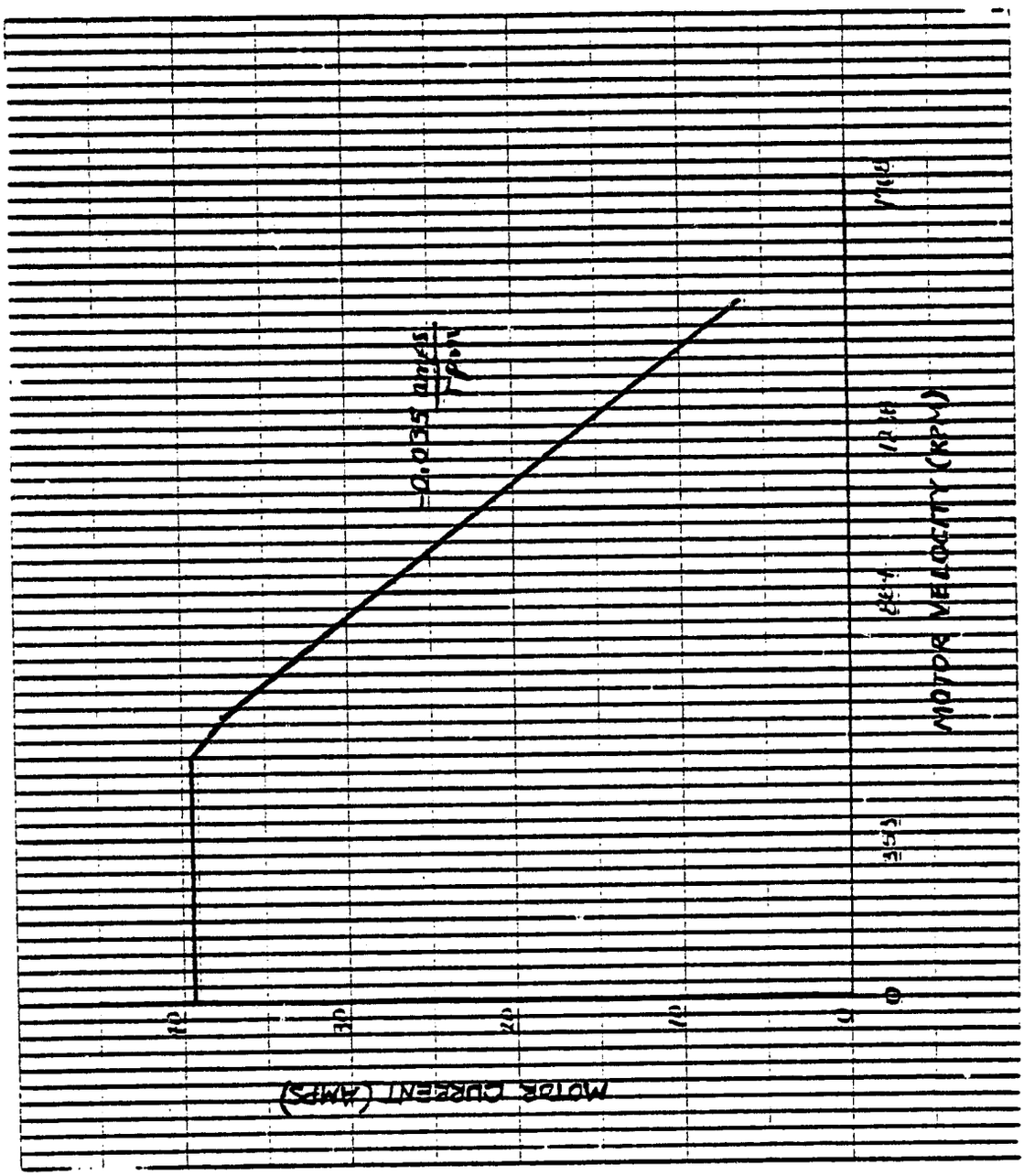

Figure 4.1-3. EMA Velocity Gain Test

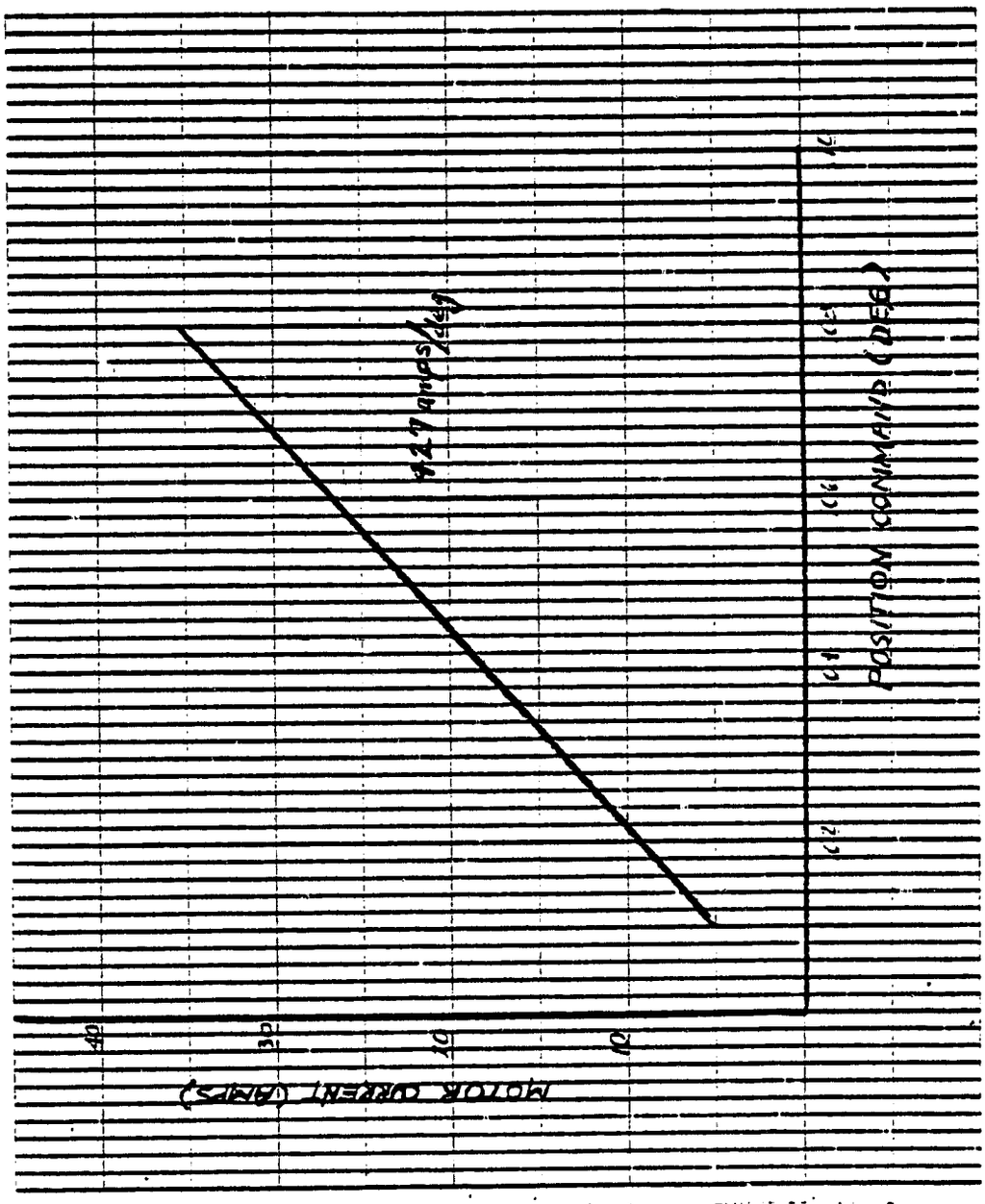

Figure 4.1-4. EMA Torque Gain Test

Velocity Loop

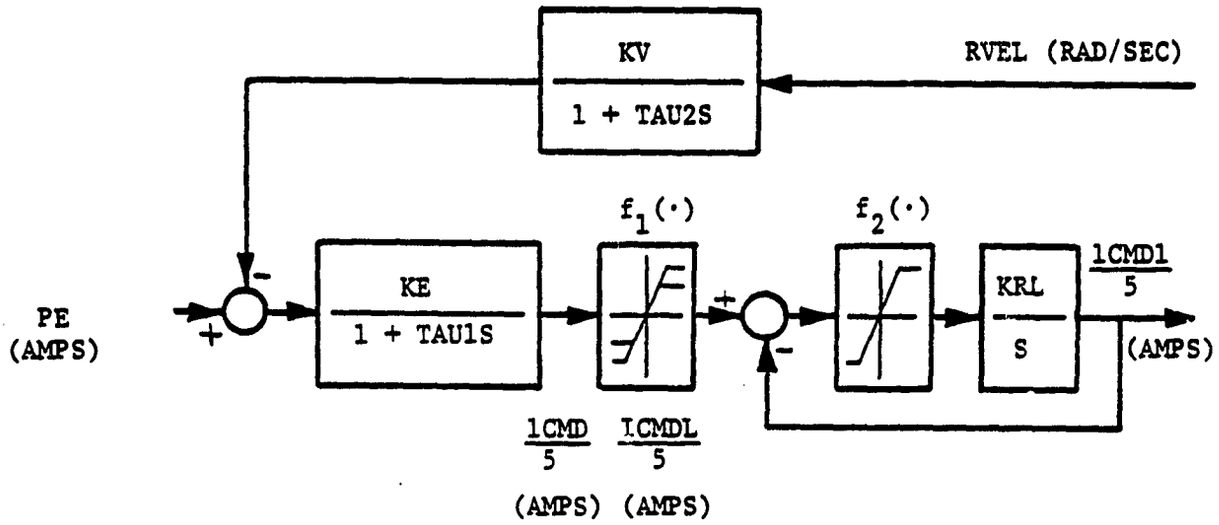

Position Loop

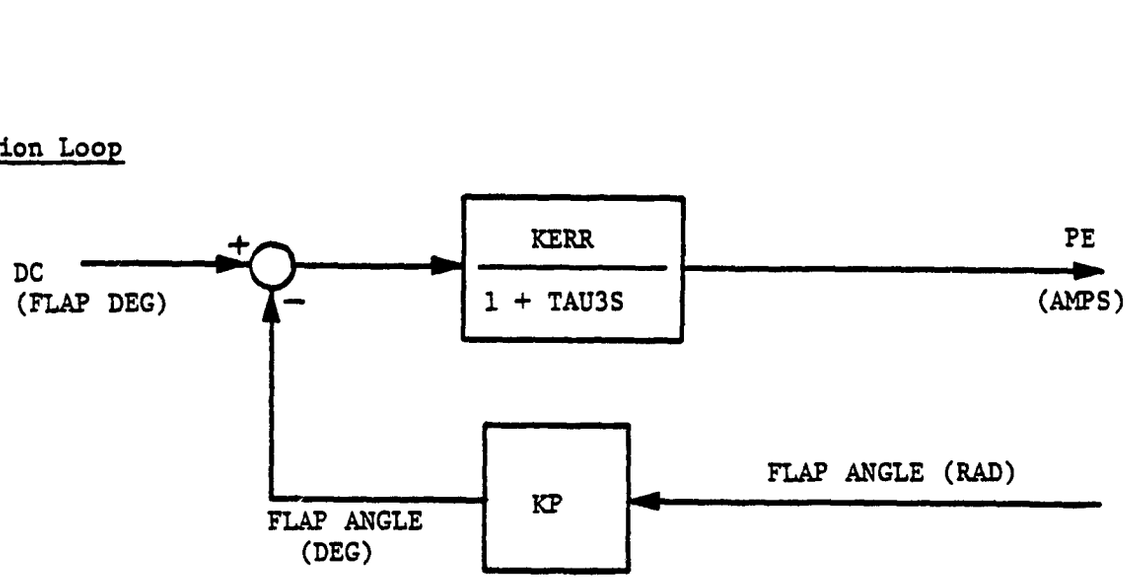

Figure 4.1-5. Velocity and Position Feedback Loops

$$\frac{ICMDL}{RVEL}\left(\frac{amps}{rad/sec}\right) = 0.035\left(\frac{amps}{rpm}\right) \cdot \frac{30}{\pi}\left(\frac{rpm}{rad/sec}\right)$$

$$= 0.33422538\ \left(\frac{amps}{rad/sec}\right) \qquad (4.1\text{-}6)$$

Therefore;

$$KV \cdot KE = 0.33422538/5$$

$$.066845076\ (amps/rad/sec) \qquad (4.1\text{-}7)$$

In a similar fashion, the gain, KERR, of the position error portion of the position feedback loop becomes:

$$KERR \cdot KE = 85.1(amps/deg\ flap) \qquad (4.1\text{-}8)$$

The position feedback loop described above is lumped together with the rotating elements of the EMA. These elements are depicted in Figure (4.1-6).

The next section describes and analyzes the EMA control logic.

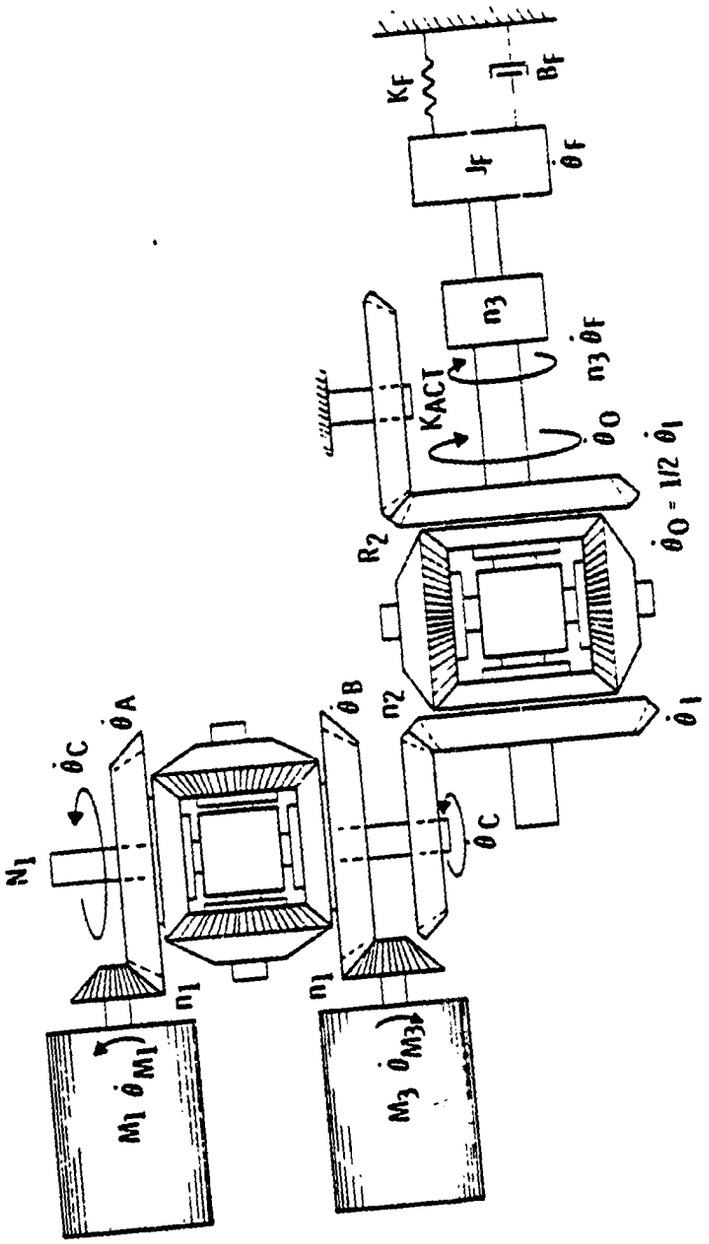

Figure 4.1-6. The Rotating Masses of the EMA

4.2 EMA CONTROL LOGIC

The EMA control logic which generates the switching commands: {QMON, QBON, Q(1), Q(2), Q(3), Q(4), Q(5), and Q(6)} for the power conditioner transistors is described in this section. The aforementioned control logic can be divided into four basic components:

a) The EMA Mode Decoding Logic

b) The Current Command Magnitude and Rate Limiters

c) The Pulse Width Modulator or Chopper Controller

d) The Inverter Controller

Figure (4.2-1) displays the functional interactions between these components. Descriptions and mathematical representations of these components follow immediately.

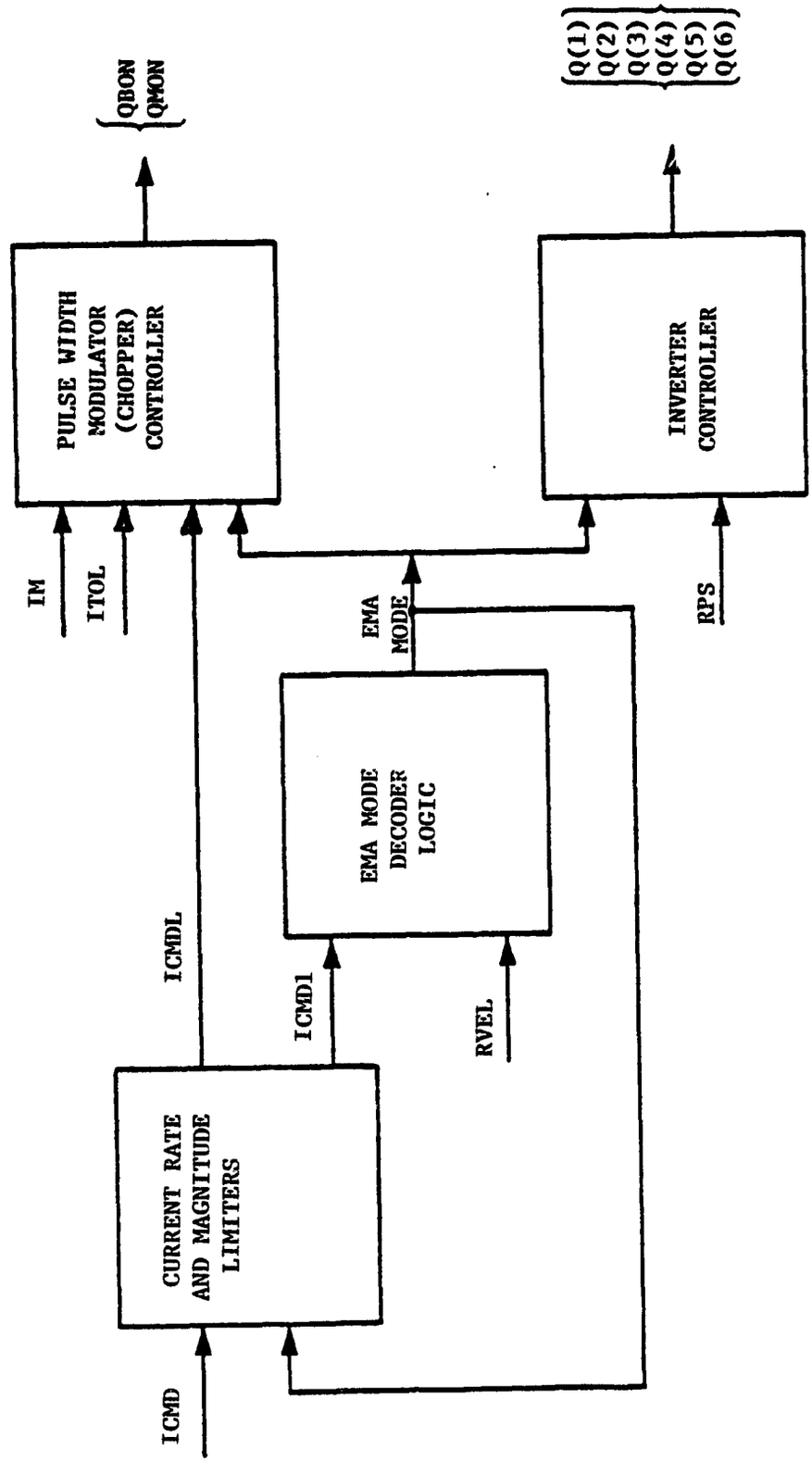

Figure 4.2-1. Black Diagram of the EMA Control Logic

4.2.1 EMA Mode Decoding Logic

As stated earlier the Delco EM Actuator can operate in any one of the following modes:

a) The Motoring Mode

b) The Regenerative Braking Mode

c) The Plugging Mode

These modes of operation effect the operating configurations of both the control and power electronics as will be shown later in this chapter.

The location of these modes in the torque-speed plane was given earlier in Figure (2.2-1). Each of the six modes shown in this figure is identified by a logical variable which is enclosed by a pair of parenthesis. These variables are defined as follows:

MTRG1: Motoring - Speed (+)

RGN4: Regenerative Braking - Speed (+)

PLUG4: Plugging - Speed (+)

MTRG3: Motoring - Speed (-)

RGN2: Regenerative Braking - Speed (-)

PLUG2: Plugging - Speed (-)

Each of these variables is either TRUE or FALSE depending upon the operating point in the torque-speed plane of Figure (2.2-1). Such a variable is TRUE when this point lies within a specified region and FALSE elsewhere. For example, MTRG 1 is TRUE whenever the motor torque and speed are both positive.

These logical variables are generated by a decoder network from the rotor velocity RVEL (radians/second) and the commanded machine current

(or torque), ICMD1 (amperes). The decoder network is composed of two basic parts: 1) a comparator network which generates the logical variables {SPDHI, SPDLO, SPDPOS, SPDNEG, TPOS, and TNEG} from the rotor velicity and the commanded current, and 2) a network of logic gates which operate on the outputs of the comparators to generate the mode variables {MTRG1, RGN4, PLUG4, MTRG3, RGN2, and PLUG 2}. Figure (4.2-2) shows the functional relationship between these two components of the EMA mode decoder network.

The comparisons performed upon the analog signals, RVEL and ICMD1, by the comparator network are listed in the left hand column of Table (4.2-1). The corresponding logical output signals are given in the right hand column.

The comparator output signals are then processed by the logic network shown in Figure (4.2-2). The outputs of this network are designated by the logical variables {MTRG1, RGN4, PLUG4, MTRG3, RGN2, and PLUG2} defined earlier. The boolean expressions, see Reference (2), which define this logic network are:

$$MTRG1 = TPOS \cdot SPDPOS \tag{4.2-1}$$

$$RGN4 = \overline{TPOS} \cdot SPDHI \tag{4.2-2}$$

$$PLUG4 = \overline{TPOS} \cdot SPDPOS \cdot \overline{SPDHI} \tag{4.2-3}$$

$$MTRG3 = TNEG \cdot SPDNEG \tag{4.2-4}$$

$$RGN2 = TPOS \cdot SPDLO \tag{4.2-5}$$

$$PLUG2 = TPOS \cdot SPDNEG \cdot \overline{SPDLO} \tag{4.2-6}$$

The dot ($\cdot$) operator which appears in these equations denotes the logical AND operator.

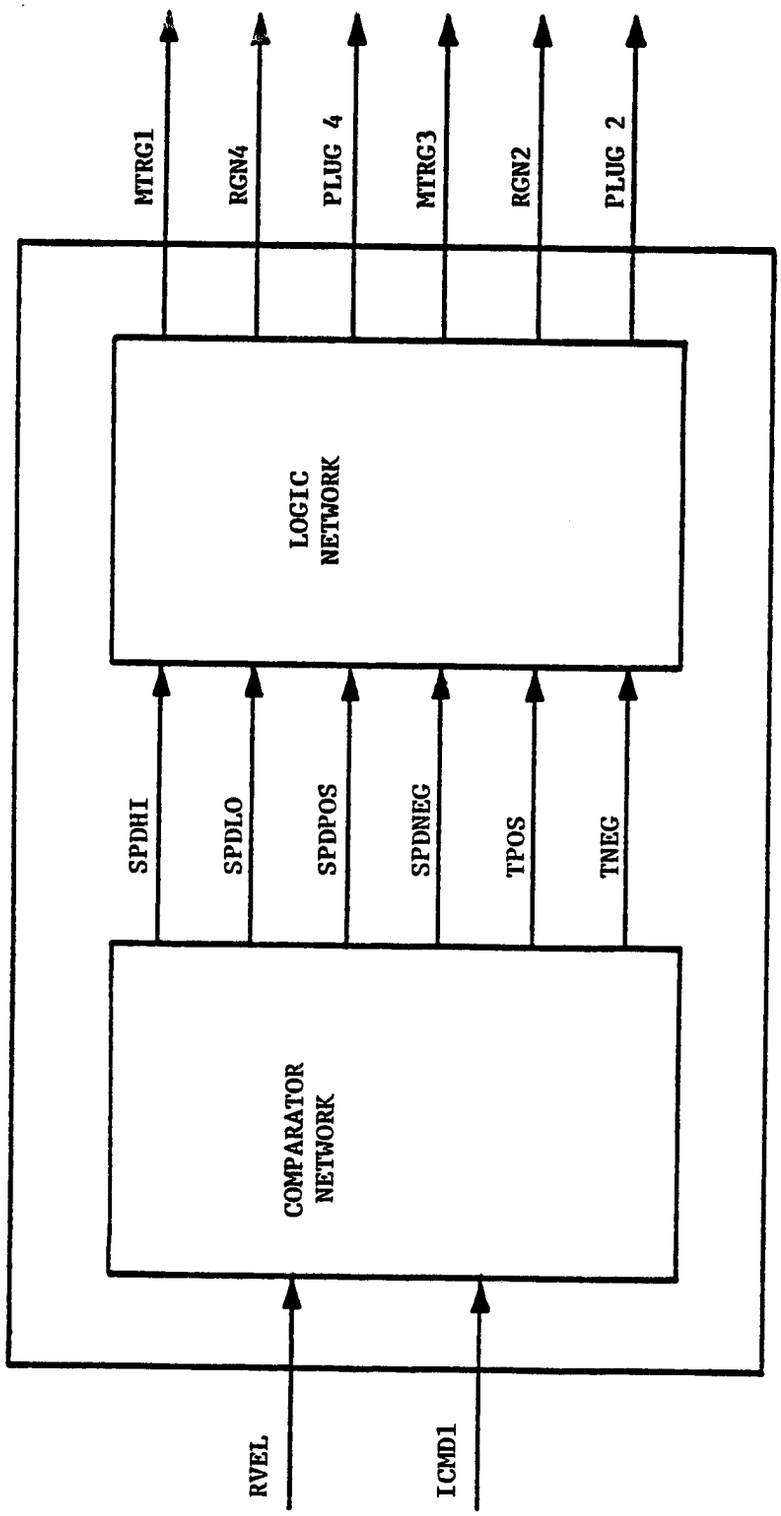

Figure 4.2-2. Functional Block Diagram of the EMA Mode Decoder

Table (4.2-1) Functional Description of the Comparator for the EMA Mode Decoder

COMPARATOR FUNCTION	COMPARATOR OUTPUT
RVEL $\geq$ VHI	YES: SPDHI = 1 or True NO: SPDHI = 0 or False
RVEL $\leq$ VLO	YES: SPDLO = 1 NO: SPDLO = 0
RVEL > 0	YES: SPDPOS = 1 NO: SPDPOS = 0
RVEL < 0	YES: SPDNEG = 1 NO: SPDNEG = 0
ICMD1 > 0	YES: TPOS = 1 NO: TPOS = 0
ICMD1 < 0	YES: TNEG = 1 NO: TNEG = 0

The six EMA mode status variables derived here later become inputs to the command current magnitude limiter, the chopper controller and the inverter controller which are covered in the remainder of this section.

4.2.2 Current Command Magnitude and Rate Limiter

The permanent magnet brushless d.c. machines were designed to deliver maximum shaft torques of up to 13.558 nt-m (120 in-lb) each. This level of output torque corresponds to a current command, ICMD1, of approximately 60 amperes. This, unfortunately, is equal to the current rating of the power conditioner switches. Consequently, at rated torque the switches are operating close to the maximum rated conditions, with the ever present danger of voltage and current transients of dangerous magnitudes. For this reason, the maximum machine torque during the motoring and regenerative braking modes has been limited to 9.0387 nt-m (80 in-lb). This torque limit is accomplished by clamping the current command, ICMDL, at $\pm$40 amperes. During plugging, ICMDL is limited to 25 amperes because of the circulating currents which exist in the machine windings (see Section 2.2.3). These relationships between the unclamped current command, ICMD, and the magnitude limited current command ICMDL, are illustrated in Figure (4.2-3).

Furthermore, to prevent rapid fluctuations in the torque or current command, the magnitude limited current command, ICMDL, is passed through the rate limiter shown in Figure (4.2-4). The output of the rate limiter is designated by the variable ICMD.

The rate limiter operates by integrating the difference between the input, ICMDL, and the output, ICMD1, Figure (4.2-4). Therefore, at steady state, the integrator input is zero which results in a clamped output, ICMD1, equal to ICMDL.

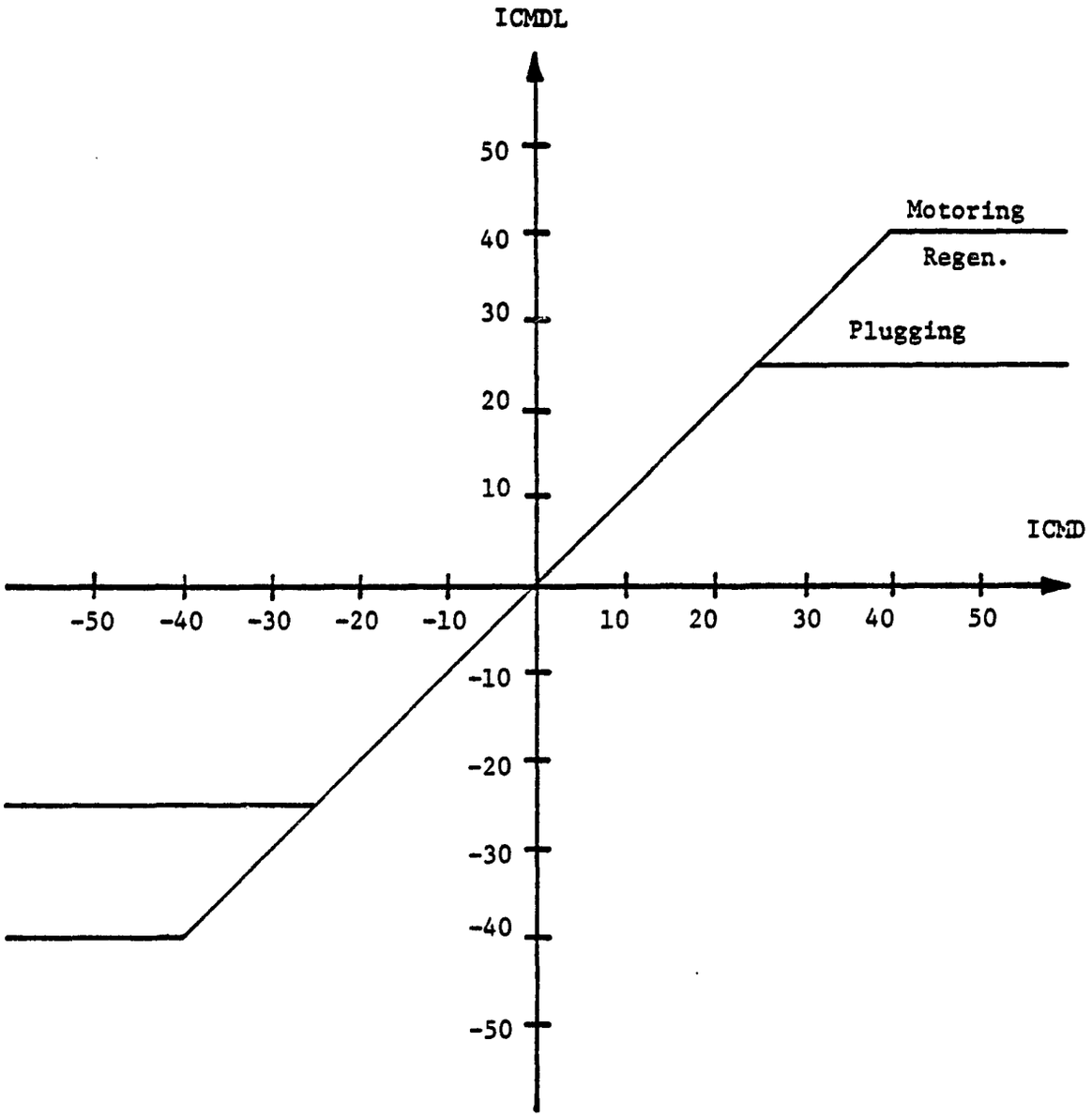

Figure 4.2-3. Magnitude Limiting of the Commanded Current ICMD

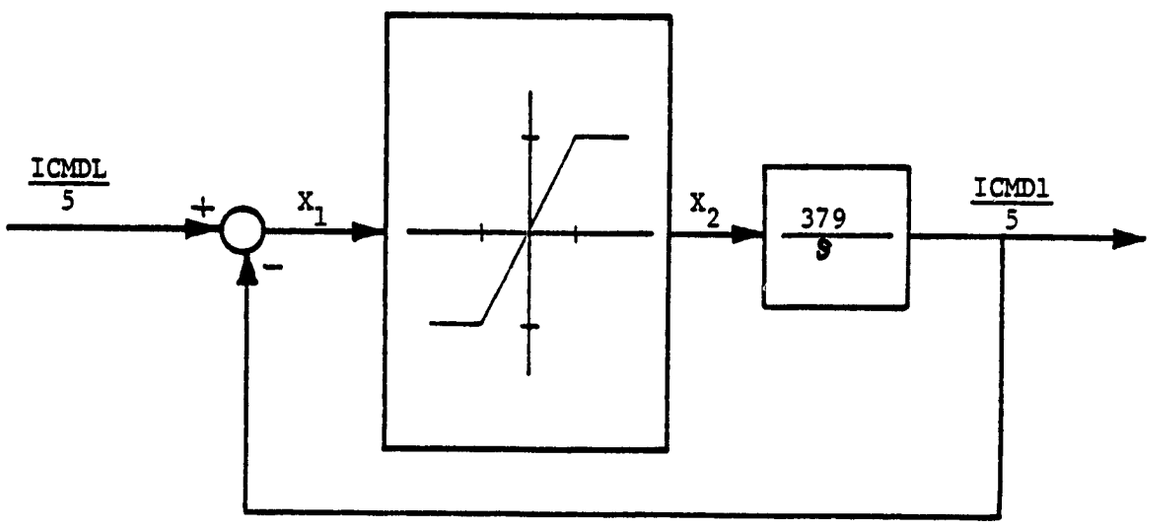

Figure 4.2-4. Current Command Rate Limiter

The maximum rate of change of the rate limited command current, ICMD1, can be calculated by letting the input, ICMDL, take on the maximum values during each of the three modes. During the motoring and regenerative braking modes ICMDL has a maximum value of 40 amperes. Assuming that ICMD1 is initially zero, the output of the clamp, x_2, (see Figure 4.2-4)) equals:

$$x_2 = \text{Clamp } (\frac{40}{5}) = 12$$

Therefore the maximum rate of change of ICMD1 during motoring and regeneration becomes:

$$\frac{d}{dt} (\text{ICMD1})_{MAX} = 379 \cdot 12 \cdot 5 = 22740 \text{ Amps/Sec}$$

or

$$\frac{d}{dt} (\text{ICMD1})_{MAX} = 22.74 \text{ Amps/ms} \qquad (4.2\text{-}7)$$

During the plugging mode ICMDL is limited to 25 amperes, therefore;

$$x_2 = \text{Clamp } (\frac{25}{5}) = 12$$

and

$$\frac{d}{dt} (\text{ICMD1}) = 22.74 \text{ Amps/ms.} \qquad (4.2\text{-}8)$$

The response envelope of the current command rate limiter is shown in Figure (4.2-5). The solid curves represent the maximum rate of change of ICMD1 as calculated above and assuming open loop operation. The dashed lines represent expected outputs under closed loop operation.

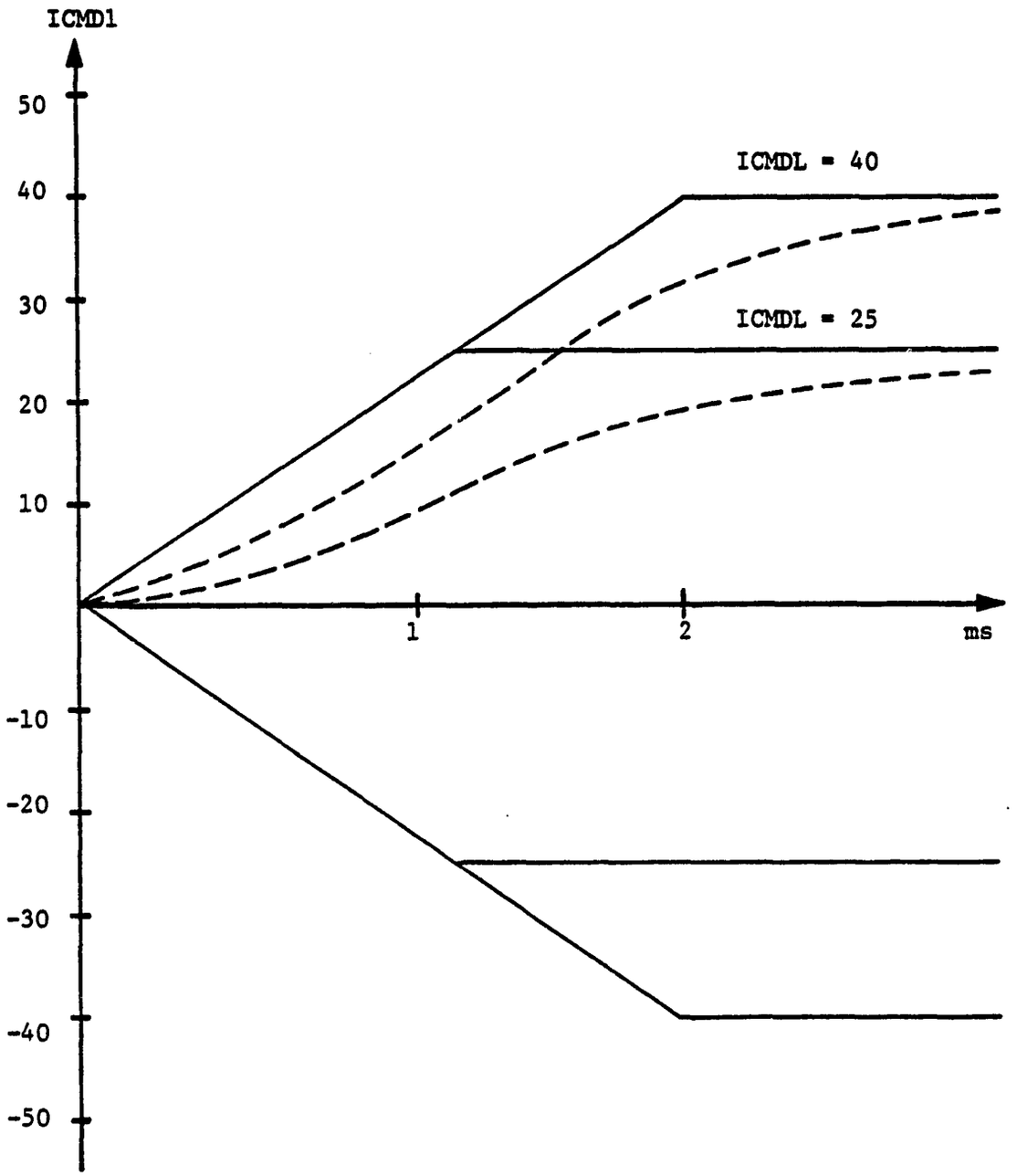

Figure 4.2-5. Current Rate Limiter Response Envelope

The magnitude limited command current, ICMDL, and the rate and magnitude limited command current, ICMD1, control the operation of the chopper controller which is presented next.

4.2.3 Current Chopper

The EMA control loops generate a torque command, TCMD, in response to the position error, motor speed and the mode of operation. This torque command can be translated into an equivalent current command, ICMD1, in a linear fashion as follows:

$$ICMD1 = TCMD/0.1129 \qquad (4.2\text{-}9)$$

This specified machine current is developed and maintained by a pulse width modulator or chopper network which is shown in Figure (4.2-6). The components of this network are:

a) Transistor QM

b) Transistor QB

c) Diode DB

d) Diode DM

e) Coupling or Chopper Inductor L2

Transistors QM and QB are used to maintain the line current, IM, within a specified tolerance of $\pm$ITOL (amperes) about the command current IMC. IMC is defined as:

$$IMC = |ICMD1| \ . \qquad (4.2\text{-}10)$$

The two diodes, DB and DM provide paths for the decaying chopper inductor current which results when QB or QM respectively are switched off.

The chopper network can take on two different operating configurations depending upon the EMA mode of operation. During the motoring and plugging modes, QM is switched on and off while QB is always off. This allows current from the battery to be pulsed into the coupling (chopper) inductor.

The dynamics of the active chopper elements during the motoring

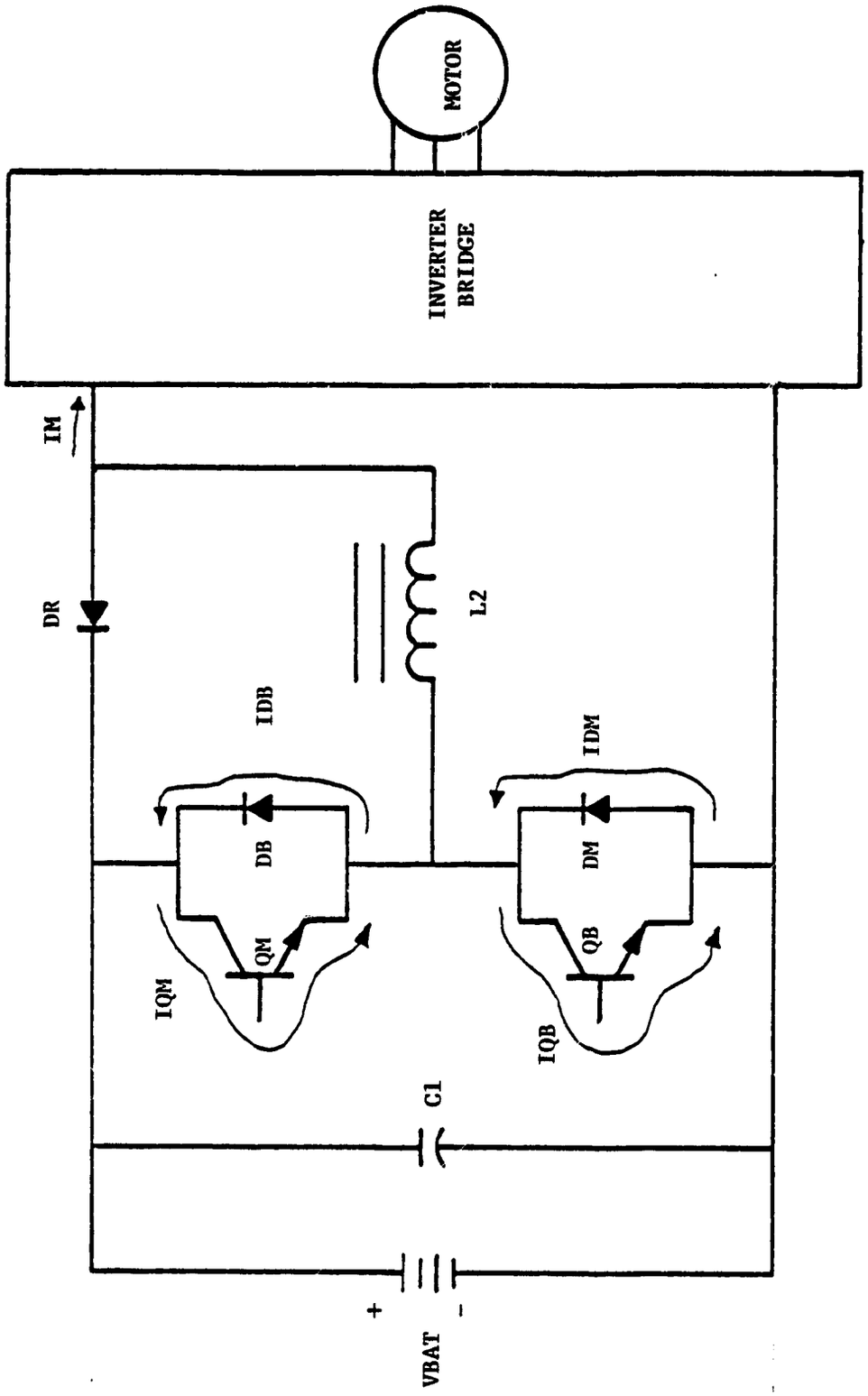

Figure 4.2-6. Pulse Width Modulator (Chopper) Schmatic

and plugging modes of operation are displayed graphically in Figure (4.2-7). During these modes, the magnitude of the d.c. line current, IM, flowing into the inverter is monitored and compared with the commanded current, IMC. If IM is below the commanded current, IMC, by a specified tolerance of ITOL amperes, QM is switched on. This causes a rise in IM as shown in Figure (4.2-7). As soon as IM reaches a values (IMC + ITOL) amperes, QM is switched off, which gives rise to a large voltage across the inductor terminals. This induced voltage is caused by the rapid time rate of change of the inductor current which is produced by switching QM off. The rapidly rising inductor voltage turns on diode DM; thereby providing a low resistance path for the decaying inductor current. When IM decays to a value below (IMC-ITOL) amperes, QM is switched on again, thereby repeating the cycle.

The regenerative braking case is different from the motoring and plugging cases described above because the d.c. line current, IM, is negative. In this case, transistor QB, instead of QM as before, becomes the active element. QB switches on and off to maintain IM within the specified tolerance about the commanded current, ICMDL, Figure (4.2-8). IM is not rate limited as is the case during motoring and plugging because ICMDL instead of ICMD1 is used as the current command. When QB is switched off, the decaying inductor current flows through diode DB and into the supply battery; consequently, the kinectic energy of the rotating masses is converted into electrical energy.

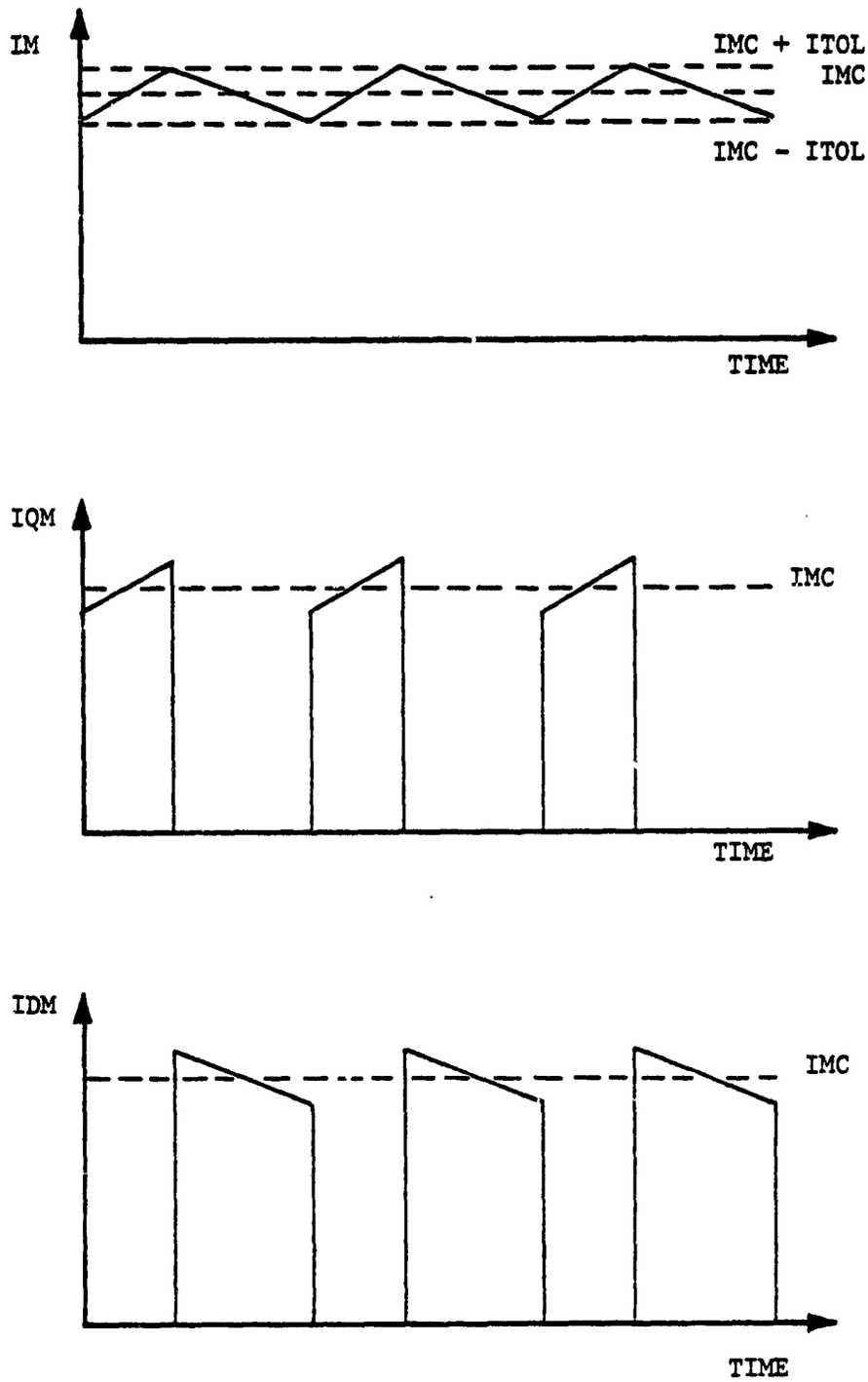

Figure 4.2-7. Chopper Dynamics During the Motoring and Plugging Modes

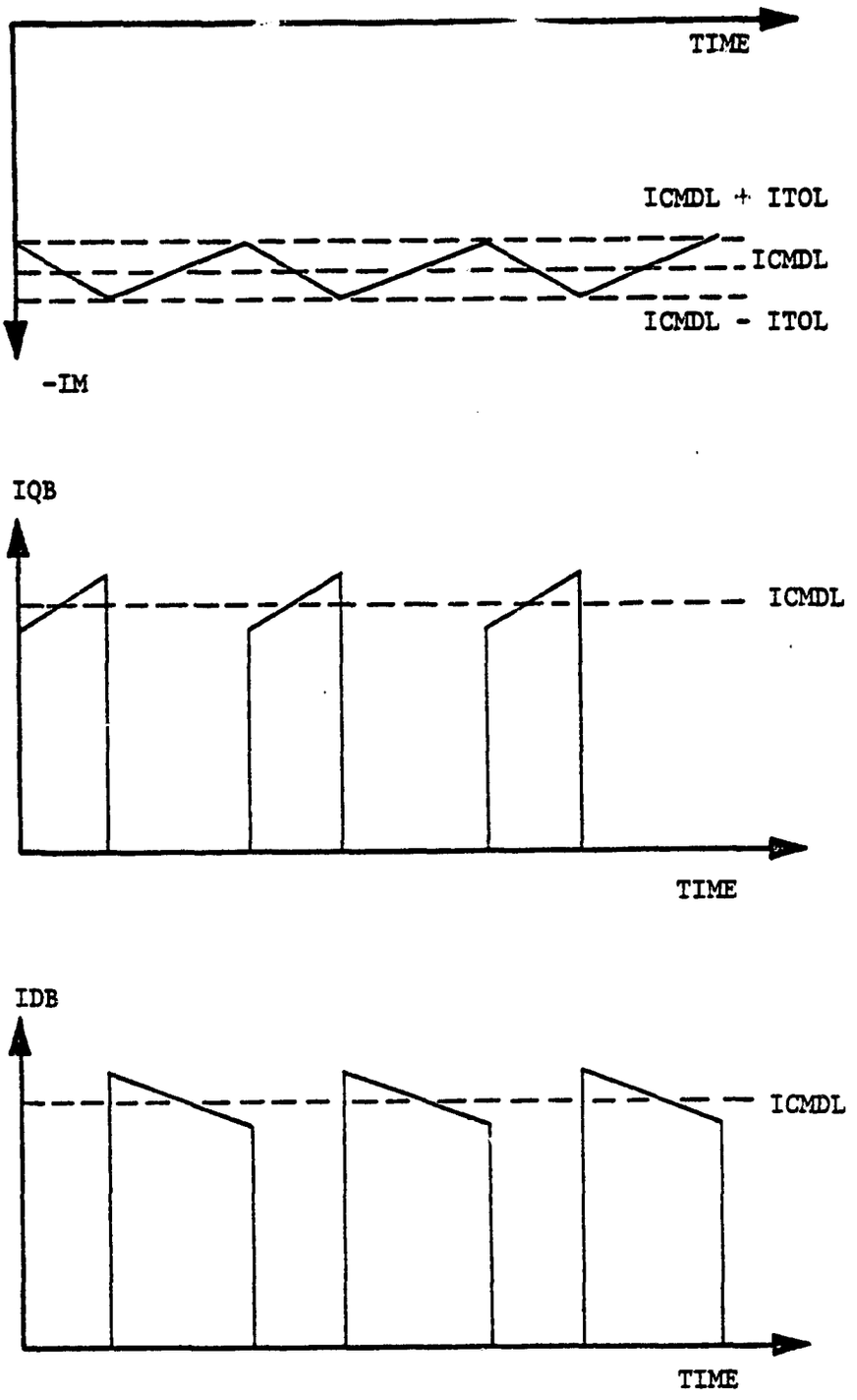

Figure 4.2-8. Chopper Dynamics during the Regenerative Braking Mode

Control of these transistors is accomplished by analog comparators and logic gates which are located in the low level electronics. A black box representation of this chopper controller is shown in Figure (4.2-9). The first set of controller inputs: {IM, IMC and ICMDL} are analyzed by two analog to digital comparators. The comparator outputs are designated by the logical variables QMC and QBC. The input-output relationships for these comparators are given in Figure (4.2-10). Notice that both comparators have a built in hysteresis to prevent toggling on input noise. The operating locus defined by such hysteresis loops is shown in Figure (4.2-11). The functional relationships between the comparator inputs and outputs are given by

$$QMC = \begin{cases} 1 & \text{IF IM} < \text{IMC} \\ 0 & \text{IF IM} \geq \text{IMC} \end{cases} \tag{4.2-10}$$

and

$$QBC = \begin{cases} 1 & \text{IF IM} > -\text{IMC} \\ 0 & \text{IF IM} \leq -\text{IMC}. \end{cases} \tag{4.2-11}$$

The second set of inputs {RGN2, RGN4} to the chopper control logic are processed together with QMC and QBC to generate the chopper switching commands, QMON and QBON, as follows:

$$RGN = RGN2 + RGN4 \tag{4.2-12}$$

$$QMON = QMC \cdot \overline{RGN} \tag{4.2-13}$$

$$QBON = QBC \cdot RGN \tag{4.3-14}$$

These commands control the switching of the chopper transistors QM and

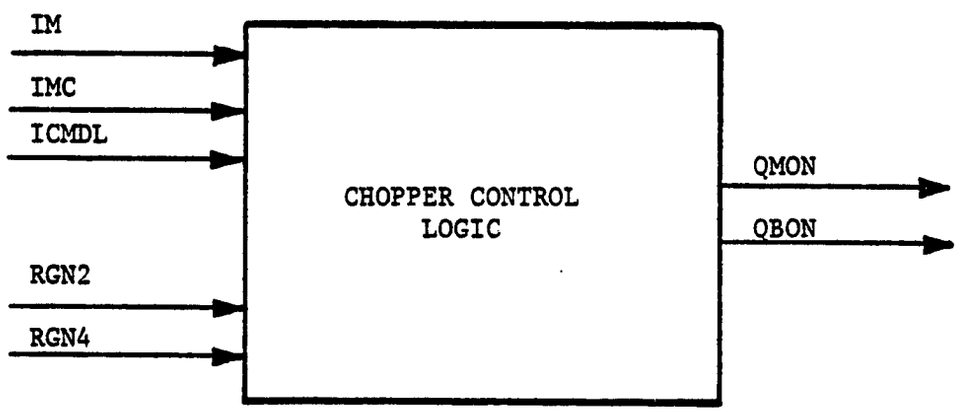

Figure 4.2-9. Block Diagram of the Chopper Controller

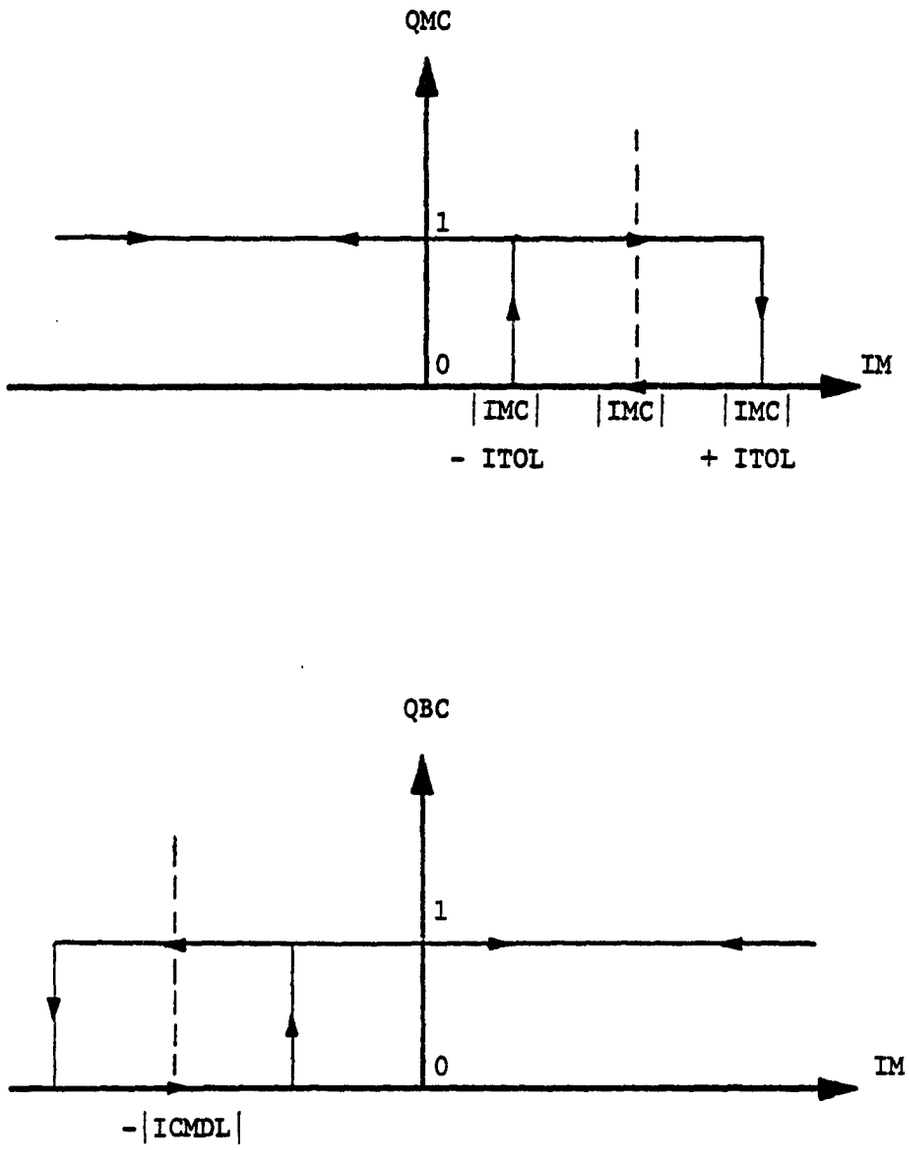

Figure 4.2-10. The Chopper Current Comparators QMC and QBC

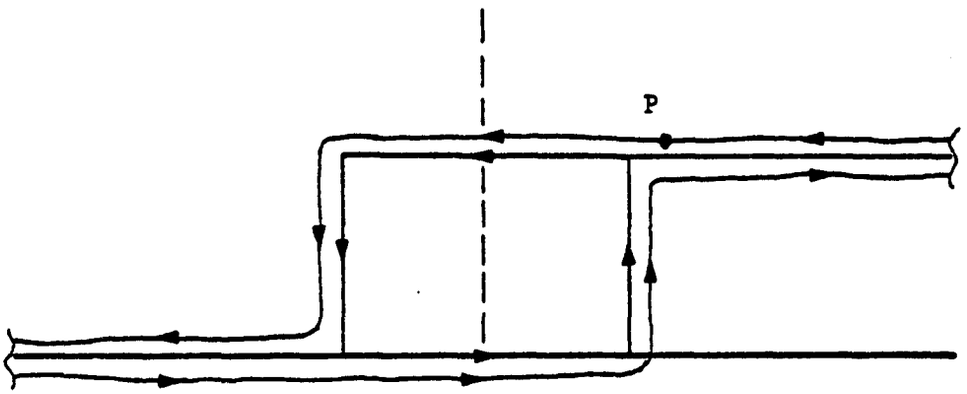

Figure 4.2-11. Operating Locus of the Point P about the Hysteresis Loop

QB. The switching commands for the remaining power conditioner transistors {Q1, . . . , Q6} of the inverter bridge are obtained next.

4.2.4 Inverter Control

Control of the six inverter transistors {Q1, . . . , Q6} is accomplished by six logical, switching commands, donated by Q(1) through Q(6). The switching commands are generated from the RPS logic signals (AA, BB, and CC) and from the logic signals FF and RGN. FF represents the sign of the commanded torque (current). FF is TRUE for ICMD1 positive and FALSE for ICMD1 negative. The logical variable, RGN, defined in equation (4.2-1) indicates whether or not the machine is functioning as a regenerative brake.

The boolean expressions which generate Q(1) through Q(6) from AA, BB, CC, FF, and RGN, References (1) and (2), are given below:

$$QAP1 = AA \cdot \overline{BB} \cdot FF + \overline{AA} \cdot CC \cdot \overline{FF} \tag{4.2-12}$$

$$QAN1 = \overline{AA} \cdot BB \cdot FF + AA \cdot \overline{CC} \cdot \overline{FF} \tag{4.2-13}$$

$$QBP1 = BB \cdot \overline{CC} \cdot FF + AA \cdot \overline{BB} \cdot \overline{FF} \tag{4.2-14}$$

$$QBN1 = \overline{BB} \cdot CC \cdot FF + \overline{AA} \cdot BB \cdot \overline{FF} \tag{4.2-15}$$

$$QCP1 = \overline{QAP1} \cdot \overline{QBP1} \tag{4.2-16}$$

$$QCN1 = \overline{QAN1} \cdot \overline{QBN1} \tag{4.2-17}$$

and finally

$$Q(1) = QAP1 \cdot \overline{RGN} \tag{4.2-18}$$

$$Q(2) = QBP1 \cdot \overline{RGN} \tag{4.2-19}$$

$$Q(3) = QCP1 \cdot \overline{RGN} \tag{4.2-20}$$

$$Q(4) = QAN1 \cdot \overline{RGN} \tag{4.2-21}$$

$$Q(5) = QBN1 \cdot \overline{RGN} \tag{4.2-22}$$

$$Q(6) = QCN1 \cdot \overline{RGN} \tag{4.2-23}$$

Notice that Q(1) through Q(6) are always OFF during regeneration. These

relationships between the input and output signals of the inverter controller during the motoring and plugging modes are clearly displayed in Figures (4.2-12) and (4.2-13) respectively.

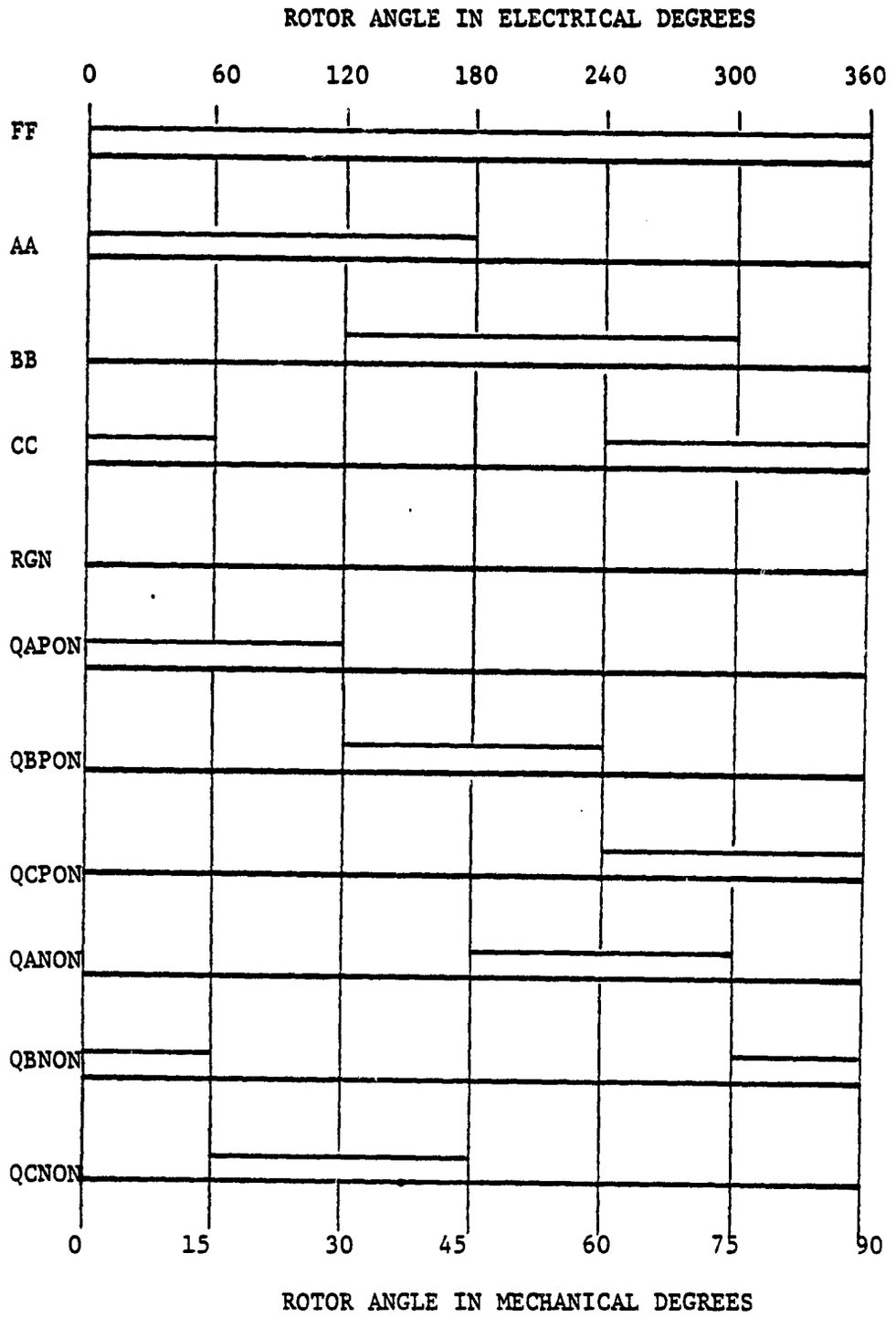

Figure 4.2-12. Inverter Control Signals - Motoring (+)
(Commutation Advance of 30°)

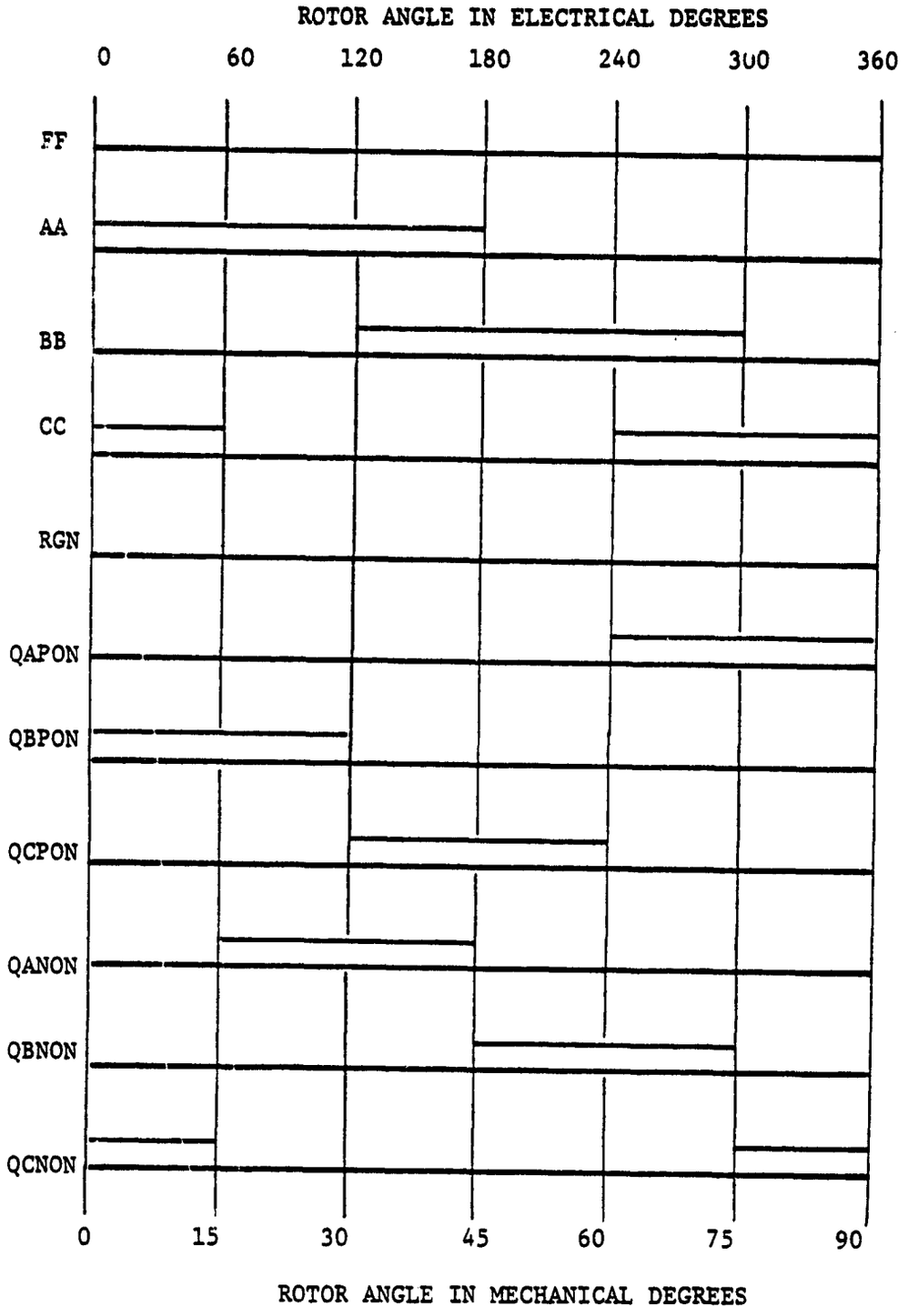

Figure 4.2-13. Inverter Control Signals - Plugging (+)
(Commutation Advance of 30°)

4.3 Derivation of the Velocity Loop State Equations

The velocity loop, which was introduced earlier in Section 4.1.4, is modeled here by means of the same state space approach used to represent the dynamics of the machine and power conditioner network. The transfer function form of this loop is shown in Figure (4.3-1). The state equations developed in this section are based upon this figure.

The transfer function representation of the velocity loop can be transformed into the signal flow graph of Figure (4.3-2). The outputs of the integrators (the 1/S branches) are denoted by the state variables: XV(1), XV(2), and XV(3). The remaining state variables, XV(4) and XV(5), are induced state variables at the outputs of the clamps, $C\ell_1$ and $C\ell_2$. The functions performed by these clamps are symbolized by $f_1(\cdot)$ and $f_2(\cdot)$, respectively. A description of these clamps has been given earlier, in Section 4.2.2.

The switches, SW_1 and SW_2 at the inputs of the clamps, close at the beginning of each integration interval. The data passed by these switches is immediately clamped for one entire integration time step by $C\ell_1$ and $C\ell_2$ respectively.

The differential equations which govern this network can be obtained by writing the equations for $\dot{XV}(1)$, $\dot{XV}(2)$, and $\dot{XV}(3)$ at inputs to the three integrators as follows:

$$\dot{XV}(1) = KE \cdot (PE - XV(3))/TAU1 - XV(1)/TAU1 \qquad (4.3\text{-}1)$$

$$\dot{XV}(2) = KRI \cdot XV(5) \qquad (4.3\text{-}2)$$

$$\dot{XV}(3) = KV \cdot RVEL/TAU2 - XV(3)/TAU2 \qquad (4.3\text{-}3)$$

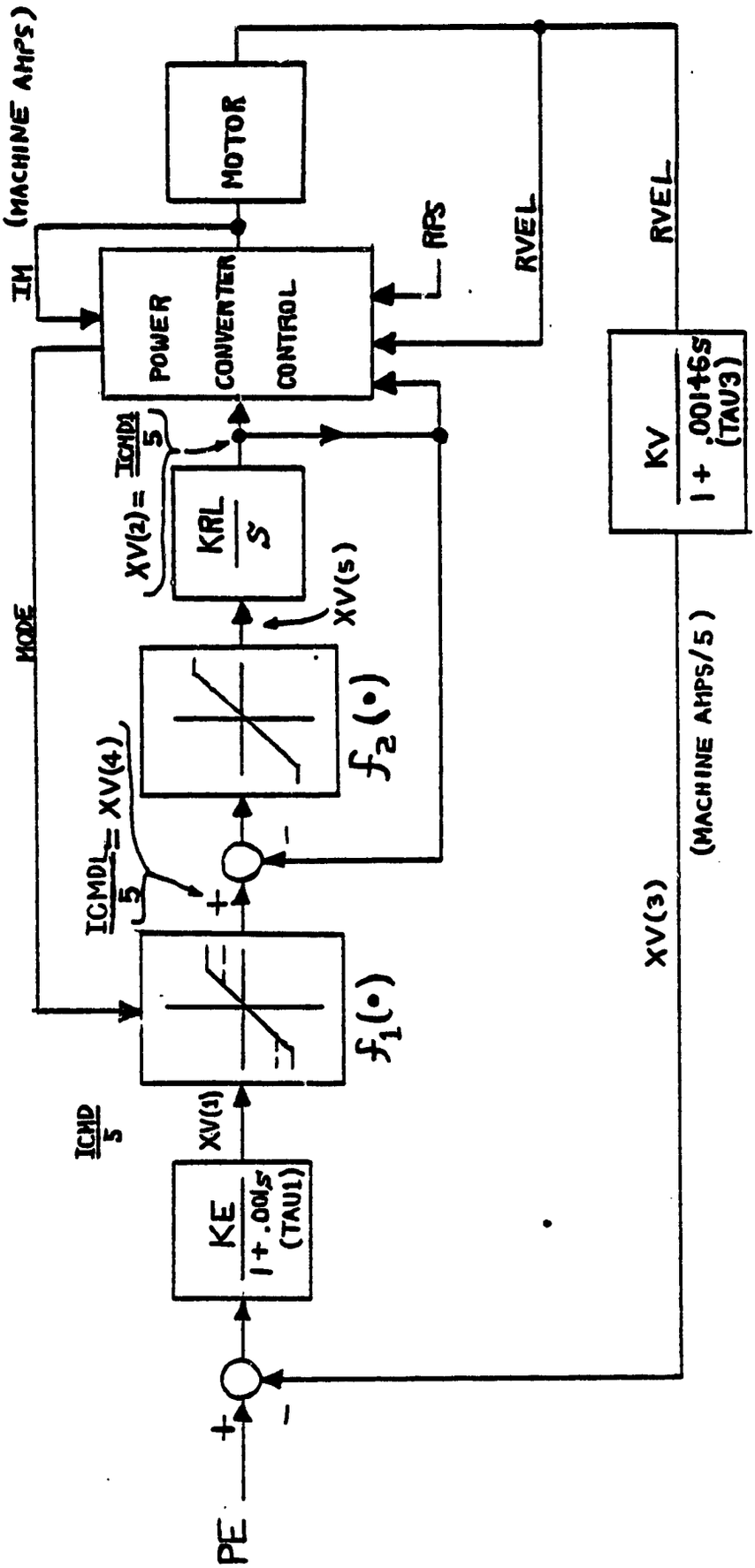

Figure 4.3-1. Signal Flow Diagram of the Velocity Loop.

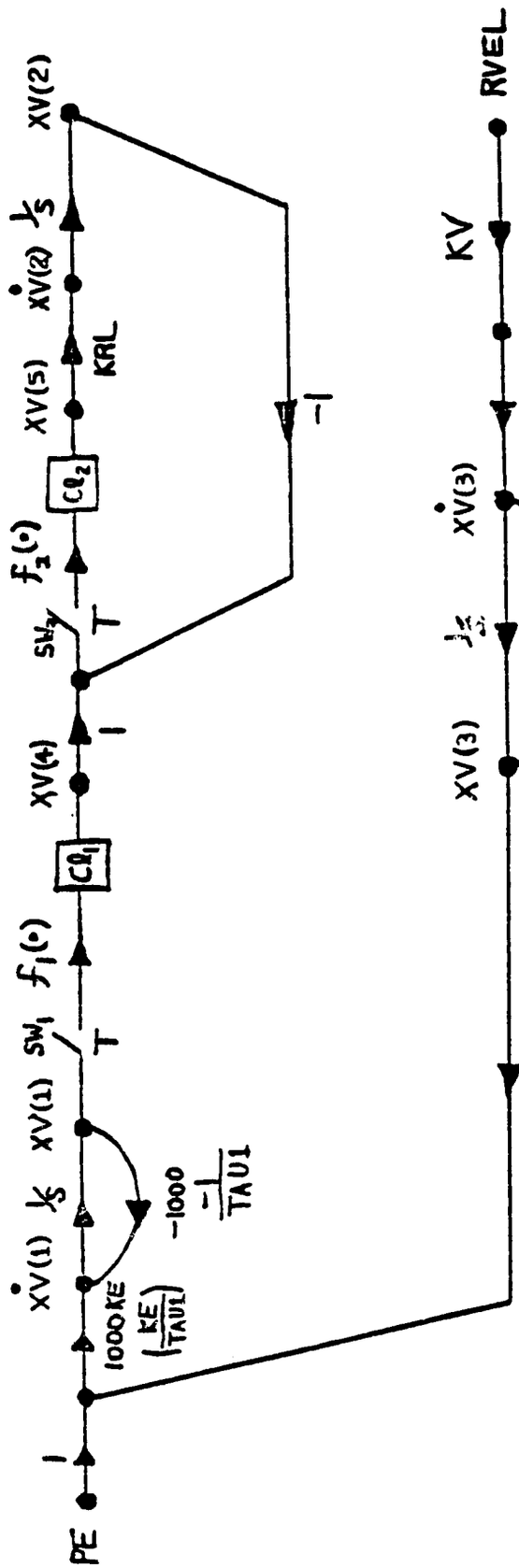

Figure 4.3-1. Signal Flow Diagram of the Velocity Loop.

The rate of change of the induced state variables with respect to time equals:

$$\dot{XV}(4) = 0 \tag{4.3-4}$$

$$\dot{XV}(5) = 0 \tag{4.3-5}$$

These five equations can be rewritten in matrix form as follows:

$$\begin{bmatrix} \dot{XV}(1) \\ \dot{XV}(2) \\ \dot{XV}(3) \\ \dot{XV}(4) \\ \dot{XV}(5) \end{bmatrix} = \begin{bmatrix} -\frac{1}{TAU1} & 0 & \frac{-KE}{TAU1} & 0 & 0 \\ 0 & 0 & 0 & 0 & KRL \\ 0 & 0 & -\frac{1}{TAU2} & 0 & 0 \\ 0 & 0 & 0 & 0 & 0 \\ 0 & 0 & 0 & 0 & 0 \end{bmatrix} \cdot \begin{bmatrix} XV(1) \\ XV(2) \\ XV(3) \\ XV(4) \\ XV(5) \end{bmatrix}$$

$$+ \begin{bmatrix} \frac{KE}{TAU1} & 0 \\ 0 & 0 \\ 0 & \frac{KV}{TAU2} \\ 0 & 0 \\ 0 & 0 \end{bmatrix} \cdot \begin{bmatrix} \tilde{PE} \\ RVEL \end{bmatrix}$$

or symbolically

$$\dot{\underline{x}}_v = \underline{A}_v \underline{x}_v + \underline{B}_v \underline{u}_v \tag{4.3-6}$$

The closing of switches SW_1 and SW_2 at time $t = t_k$ results in a transformation of the state variables from time $t = t_k^-$ to $t = t_k^+$ given by

$$XV(1)^+ = XV(1)^- \tag{4.3-7}$$

$$XV(2)^{+} = XV(2)^{-} \tag{4.3-8}$$

$$XV(3)^{+} = XV(3)^{-} \tag{4.3-9}$$

$$XV(4)^{+} = f_1[XV(1)^{-}] \tag{4.3-10}$$

$$XV(5)^{+} = f_2[XV(4)^{-}] \tag{4.3-11}$$

In matrix form these equations become

$$\underline{x}_v^{+} = \begin{bmatrix} 1 & 0 & 0 & 0 & 0 \\ 0 & 1 & 0 & 0 & 0 \\ f_1(\cdot) & 0 & 0 & 0 & 0 \\ 0 & 0 & 0 & f_2(\cdot) & 0 \end{bmatrix} \underline{x}_v^{-}$$

or symbolically

$$\underline{x}_v^{+} = \underline{V}\,\underline{x}_v^{-} \tag{4.3-12}$$

The interpretation of the state variables in terms of the velocity loop transfer functions is given in Figure (4.3-1).

The state equations for the mechanical and position loops are derived in the section which follows immediately.

4.4 DERIVATION OF THE STATE EQUATIONS FOR THE MECHANICAL AND POSITION LOOPS

The mechanical and position loops consists of the first order flap position loop, depicted in Figure (4.1-5), and the rotating masses of Figure (4.1-6).

The state equations for the rotating masses, with one or two active machines, can be obtained easily by representing this system by an equivalent mechanical network based upon the network elements of Figure (4.4-1). These elements are:

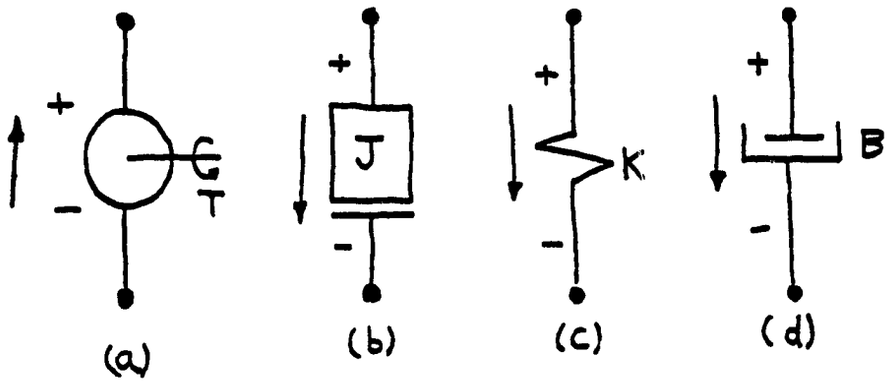

Figure 4.4-1 Network Elements of Mechanical Systems.

a) Torque, T (NT-M)
b) Moment of Inertia, J ($KG-M^2$)
c) Stiffness Coefficient, K (NT-M/RAD)
d) Viscous Damping Coefficient, B (NT-M/RAD/SEC)

The nodes of these branches correspond to the angular positions of the shafts, gears, rotors, etc. which make up the rotational system.

Using these elements, the rotational system of Figure (4.1-6) is represented as shown in Figure (4.4-2). The angles θ_M, θ_A, θ_C, θ_1, θ_0 and θ_F are defined in this figure. The change in the shaft torques through the different levels of the gearing is represented by the gear ratios between the various shaft torques.

The differential equations which describe this system are derived by summing the torques at the seven nodes designated by θ_M, θ_A, θ_C, θ_1, θ_0, $N3 \cdot \theta_F$, and θ_F in Figure (4.4-2). Performing these summations results in:

$$TM = JM \cdot \ddot{\theta}_M + T1 \qquad (4.4\text{-}1)$$

$$T2 = T3 \qquad (4.4\text{-}2)$$

$$T4 = T5 \qquad (4.4\text{-}3)$$

$$T6 = T7 \qquad (4.4\text{-}4)$$

$$T8 = (\theta_0 - N3 \cdot \theta_F)KACT \qquad (4.4\text{-}5)$$

$$T9 = -(N3 \cdot \theta_F - \theta_0)KACT \qquad (4.4\text{-}6)$$

$$T10 = JF \cdot \ddot{\theta}_F + BF \cdot \dot{\theta}_F + KF \cdot \theta_F \qquad (4.4\text{-}7)$$

Also

$$T2 = T1 \cdot N1 \qquad (4.4\text{-}8)$$

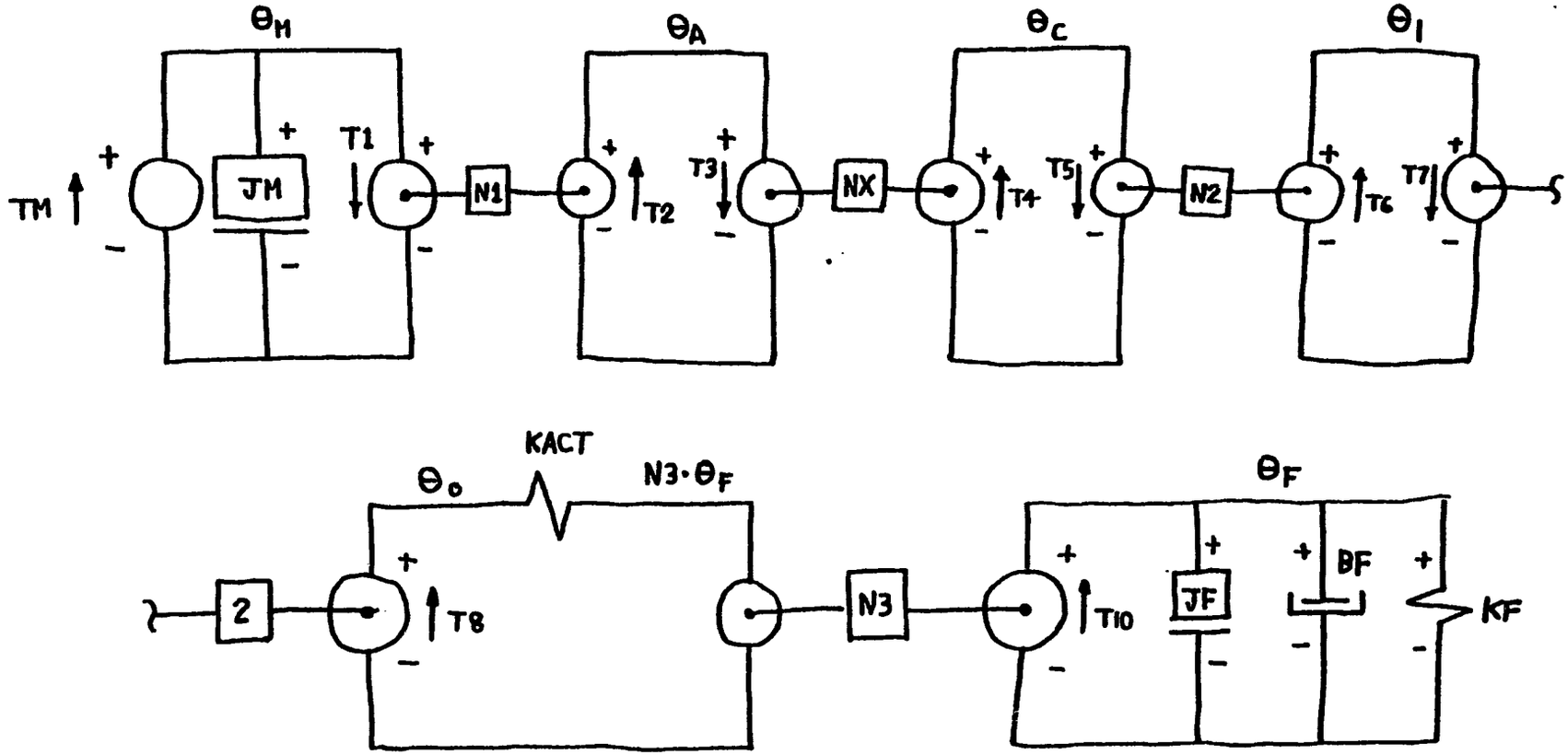

Figure 4.4-2. Network Model of the Rotating Masses.

$$T4 = T3 \cdot NX \tag{4.4-9}$$

$$T6 = T5 \cdot N2 \tag{4.4-10}$$

$$T8 = 2T7 \tag{4.4-11}$$

$$T10 = T9 \cdot N3 \tag{4.4-12}$$

Now the angle θ_o can be expressed in terms of θ_M as follows:

$$\theta_o = \frac{1}{2 \cdot NX \cdot N1 \cdot N2} \theta_M \tag{4.4-13}$$

By means of equations (4.4-8) through (4.4-13), one can rewrite equations (4.4-1) through (4.4-7) in terms of two second order differential equations in the variables θ_M and θ_F, as follows:

$$TM = JM \cdot \ddot{\theta}_M + TACT/2 \cdot NX \cdot N1 \cdot N2 \tag{4.4-14}$$

$$N3 \cdot TACT = JF \cdot \ddot{\theta}_F + BF \cdot \dot{\theta}_F + KF \cdot \theta_F \tag{4.4-15}$$

where

$$TACT = T9$$

These equations can be converted to the S-domain and therefore to a transfer function type block diagram. Taking the Laplace transforms of both sides of equations (4.4-14) and (4.4-15) and solving for $S\theta_M$ and $S\theta_F$ yields:

$$S\theta_M = \frac{TM - TACT/2 \cdot NX \cdot N1 \cdot N2}{SJM} \tag{4.4-16}$$

$$S\theta_F = N3 \cdot TACT - BF \cdot (S\theta_F) - (KF/S) \cdot (S\theta_F) \tag{4.4-17}$$

TACT can be expressed in terms of $S\theta_M$ and $S\theta_F$ by the Laplace transformed equations (4.4-5) and (4.4-13) as follows:

$$TACT = \frac{S\theta_M}{2 \cdot NX \cdot N1 \cdot N2} - N3 \cdot (S\theta_F)\frac{KACT}{S} \qquad (4.4\text{-}18)$$

Combining equations (4.4-16) through (4.4-18) with the block diagram of the position loop in Figure (4.1-5) results in the transfer function block diagram of the mechanical and position loops, Figure (4.4-3).

This block diagram can be readily translated into the signal flow graph of Figure (4.4-4). The state variables of this network, symbolized by XM(1) through XM(5), are the outputs of the integrators. Writing the equations at the inputs; $\dot{XM}(1)$ through $\dot{XM}(5)$, of the integrators yields (in matrix form):

$$\begin{bmatrix} \dot{XM}(1) \\ \dot{XM}(2) \\ \dot{XM}(3) \\ \dot{XM}(4) \\ \dot{XM}(5) \end{bmatrix} = \begin{bmatrix} 0 & \frac{-1}{4 \cdot N1 \cdot N2 \cdot JM} & 0 & 0 & 0 \\ \frac{KACT}{2 \cdot N1 \cdot N2 \cdot NX} & 0 & -N3 \cdot KACT & 0 & 0 \\ 0 & \frac{N3}{JF} & -\frac{BF}{JF} & -\frac{KF}{JF} & 0 \\ 0 & 0 & 1 & 0 & 0 \\ 0 & 0 & 0 & -\frac{KP \cdot KERR}{TAU3} & -\frac{1}{TAU3} \end{bmatrix} \cdot \begin{bmatrix} XM(1) \\ XM(2) \\ XM(3) \\ XM(4) \\ XM(5) \end{bmatrix}$$

$$+ \begin{bmatrix} \frac{1}{JM} & 0 \\ 0 & 0 \\ 0 & 0 \\ 0 & 0 \\ 0 & \frac{KERR}{TAU3} \end{bmatrix} \cdot \begin{bmatrix} TM \\ DC \end{bmatrix}$$

or symbolically as

$$\dot{x}_p = A_p\, x_p + B_p\, u_p \qquad (4.4\text{-}19)$$

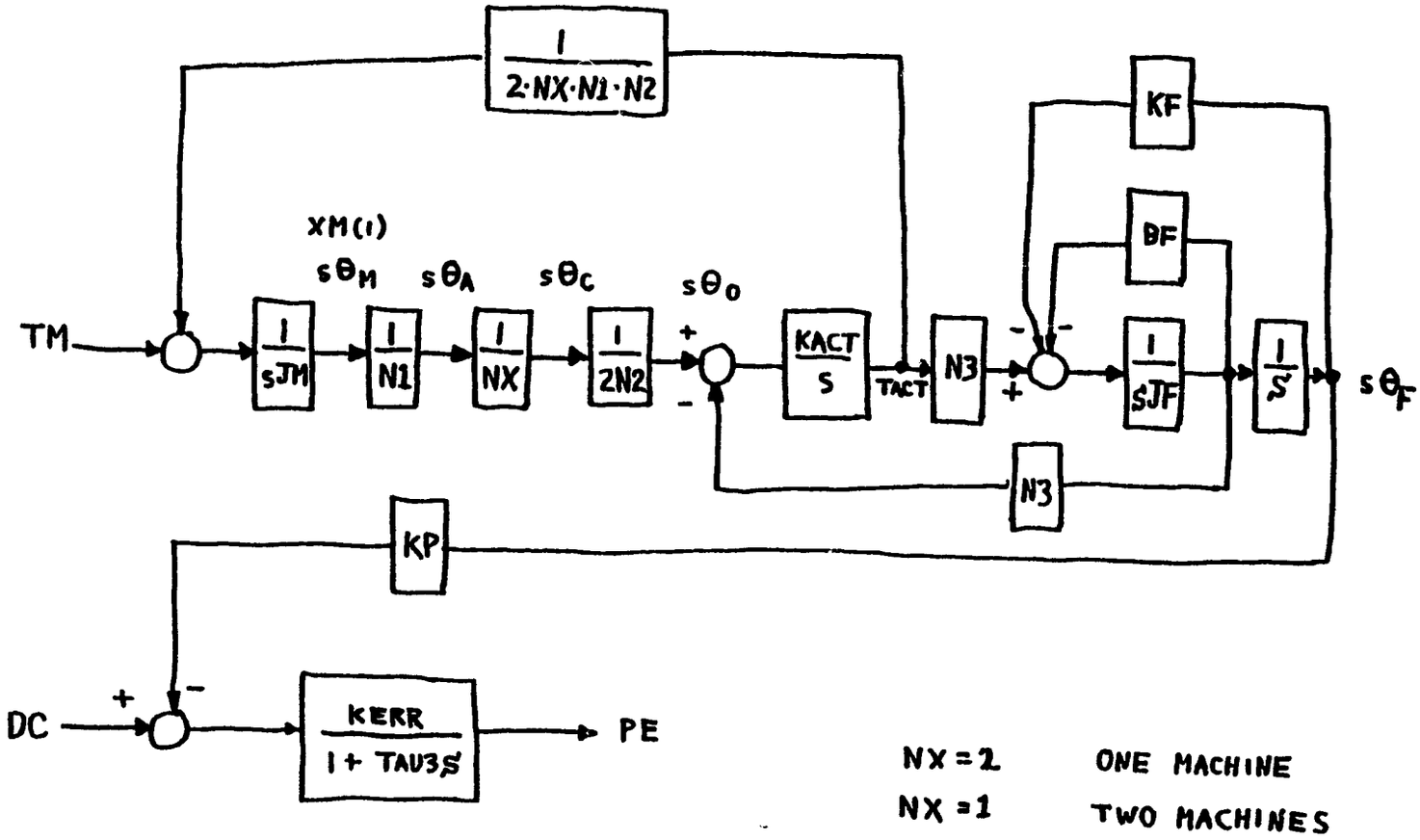

Figure 4.4-3. Transfer Functions of the Rotating Masses and Position Feedback Loop.

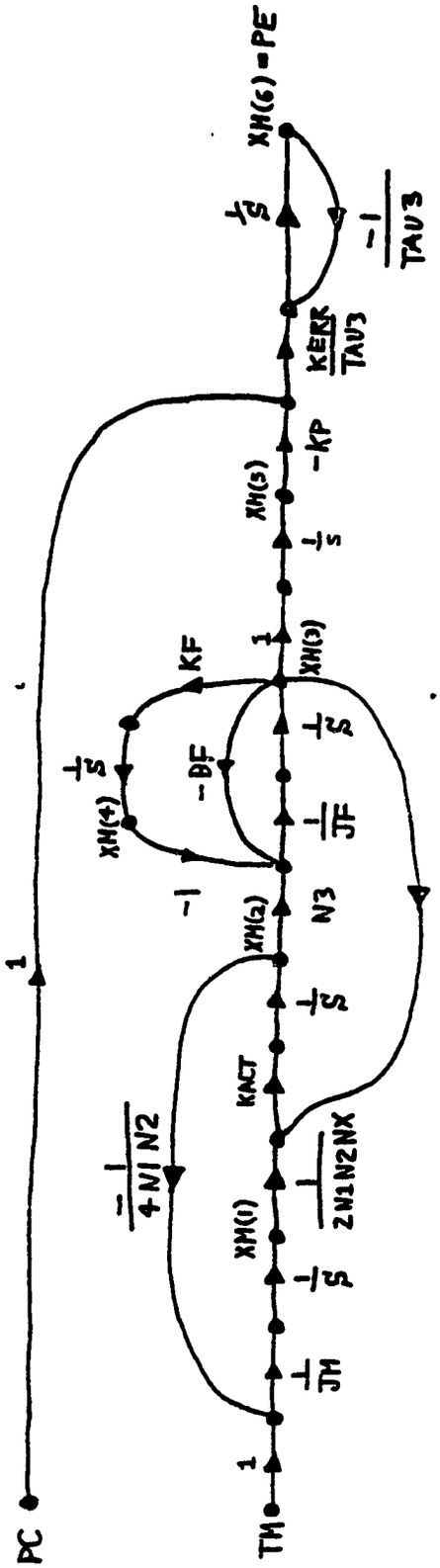

Figure 4.4-4. Signal Flow Diagram of the Rotating Masses and Position Feedback Loop.

The procedure used to integrate the EMA model forward in time is described next.

4.5 SOLUTION OF THE OVERALL EMA SYSTEM STATE EQUATIONS

The three basic subsystems of the EMA model developed in previous sections and chapters are described by the matrix state equations:

Equation (3.3-15) Power Conditioner and Machine Model
Equation (4.3-16) Velocity Loop Model
Equation (4.4-19) Mechanical and Position Loop Model

The integration of the resulting fourteenth order state model forward in time requires a solution technique capable of handling nonlinear differential equations as well as interfacing the different integration speeds used for the three subsystems. The solution procedure which performs these tasks is the topic of this section.

The signal paths between the various components of the EMA model as well as the component transfer functions (S-domain) are given in Figure (4.5-1). Notice that the power conditioner and machine models are not given in this diagram because of the nonlinear nature of these equations. The procedure used to integrate these equations forward in time is given in Section 3.5.

The integration of the three EMA subsystem models is accomplished by one of two time discretization schemes. In the first scheme, the three sets of differential equations are integrated forward in time at the same rate or time step. This scheme is illustrated in Figure (4.5-2a). Notice that each block shown represents one time step. The integration order is indicated by the numbers within the blocks.

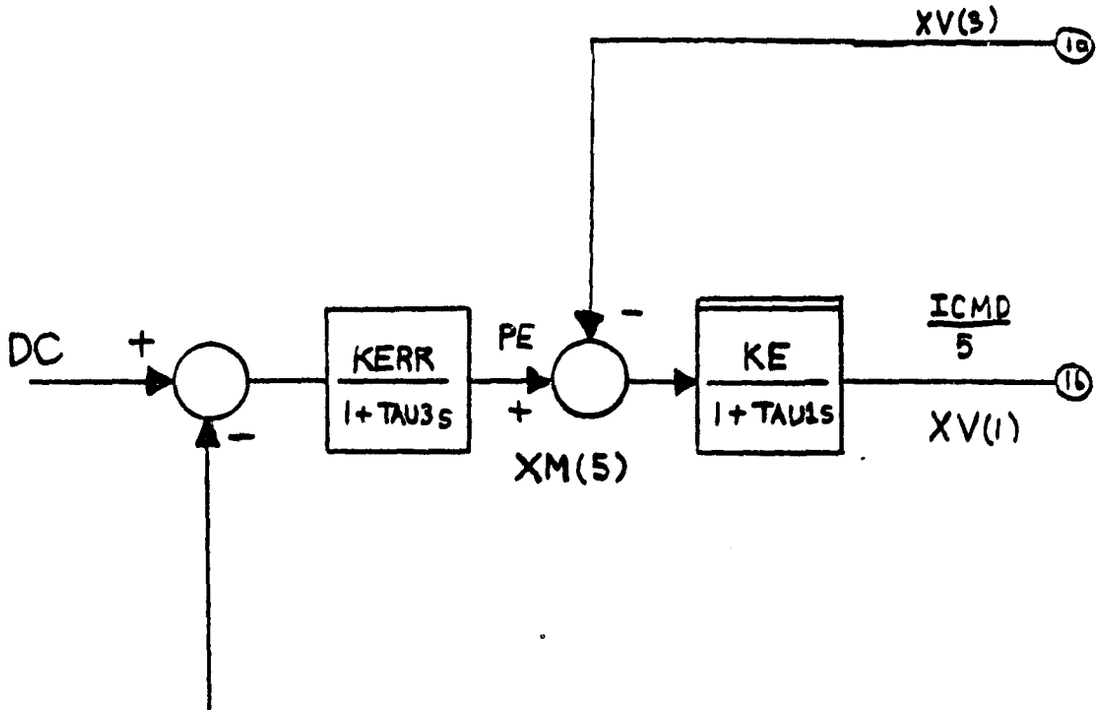

VELOCITY AND POSITION LOOP PARAMETERS

KP = 57.29577951 [deg/rad]

KE = 1. [Dimensionless]

KERR·KE = 85.1 [Amps/deg]

KV = 0.066845 [Amps/rad/S]

KRL = 379

Figure 4.5-1. Block Diagram of the One and Two Channel EMA Model

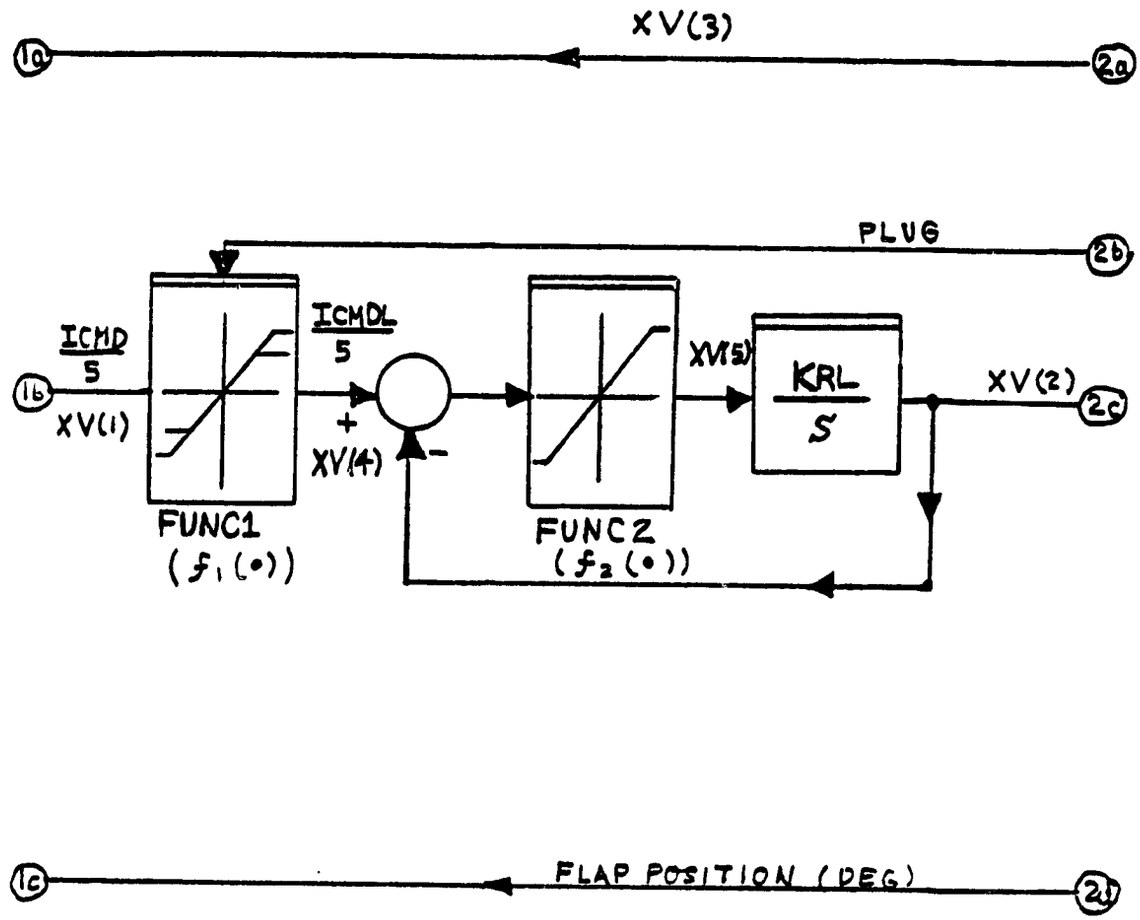

MECHANICAL LOOP PARAMETERS

KACT = 100,000 [in-lb/rad] = 11297.92 [NT-m/rad]

KF = 8.6×10^5 [in-lb/rad] = 97162.11 [NT-m/rad]

JM = .00842 [in-lb-s^2] = .00095126 [kg-m^2]

JF = 96.46 [in-lb-s^2] = 10.8977 [kg-m^2]

BF = 1821.6 [in-lb/rad/s] = 205.80291 [NT-m/rad/s]

N1 = 3.75 N2 = 1.5 N3 = 238.71

Figure 4.5-1. (cont)

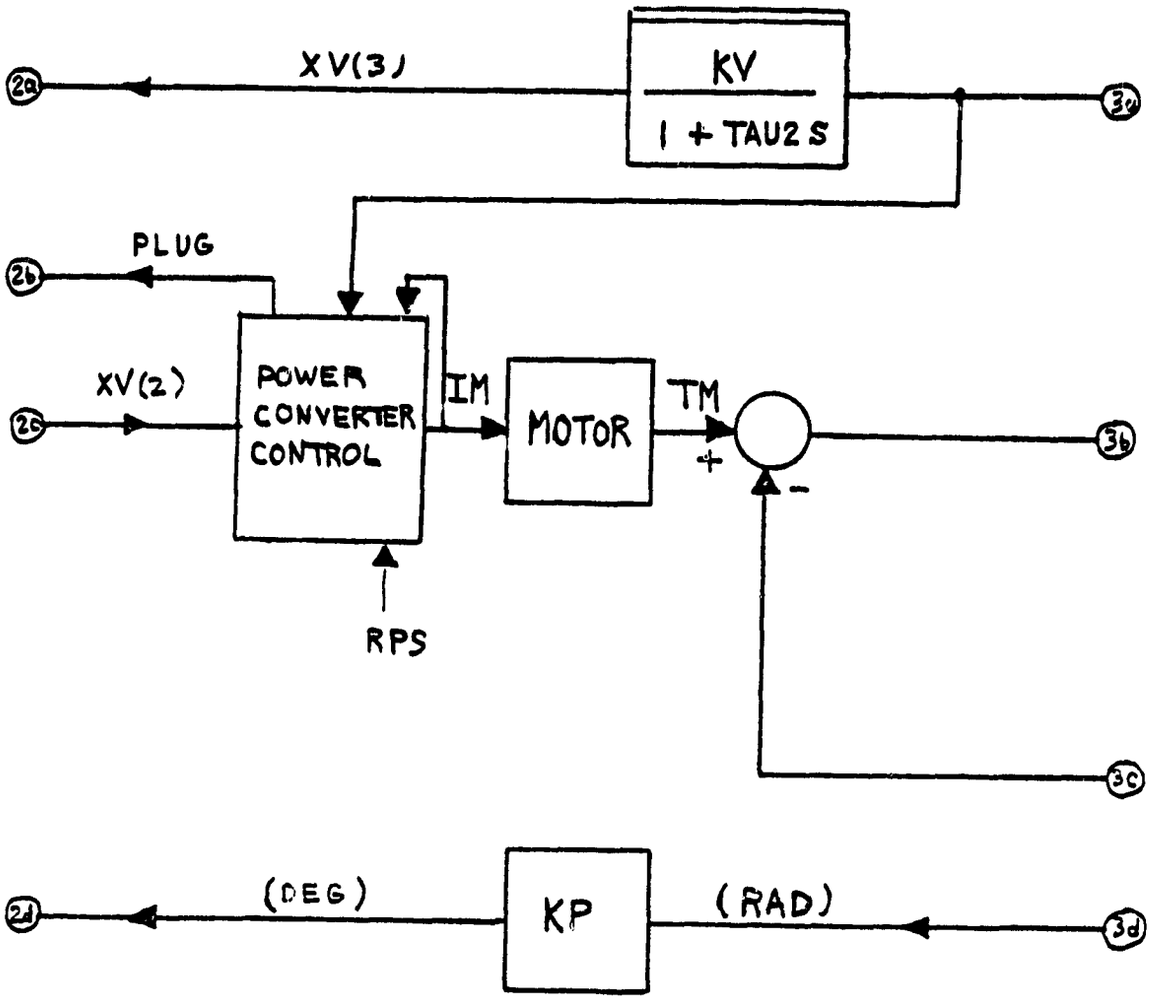

CONVERSION FACTORS (ENGLISH TO MKS)

$T\,[NT\text{-}m] = 0.1129792\ T\,[in\text{-}lb]$

$B\,[NT\text{-}m/rad/s] = 0.1129792\ B\,[in\text{-}lb/rad/s]$

$K\,[NT\text{-}m/rad] = 0.1129792\ K\,[in\text{-}lb/rad]$

$J\,[Kg\text{-}m^2] = 0.1129792\ J\,[in\text{-}lb\text{-}s^2]$

Figure 4.5-1. (cont)

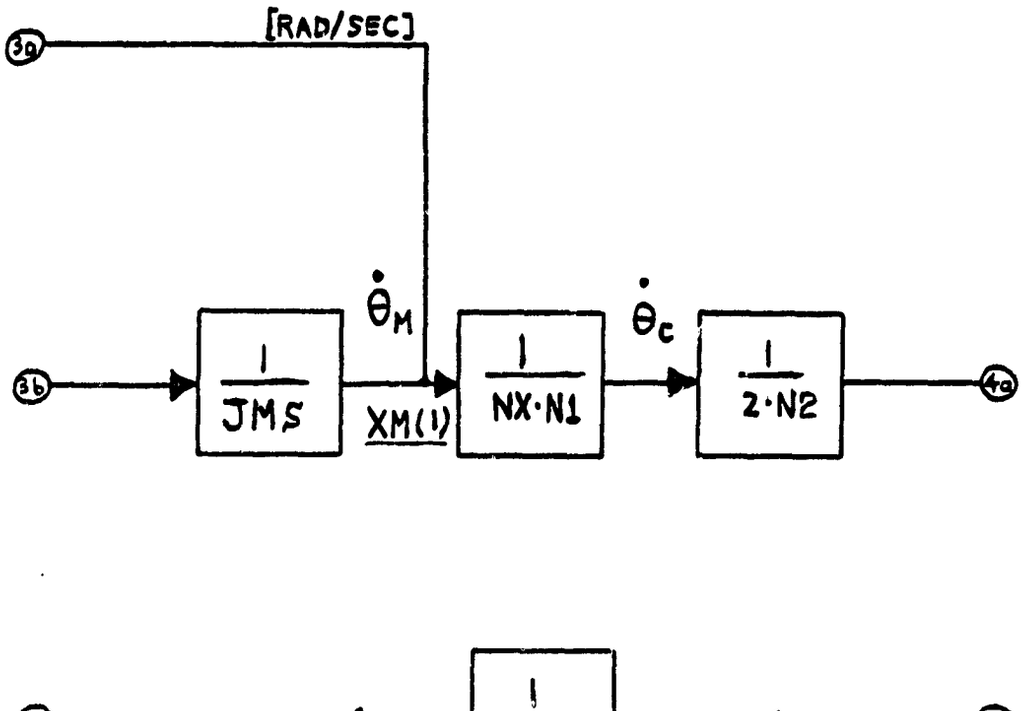

Figure 4.5-1. (cont)

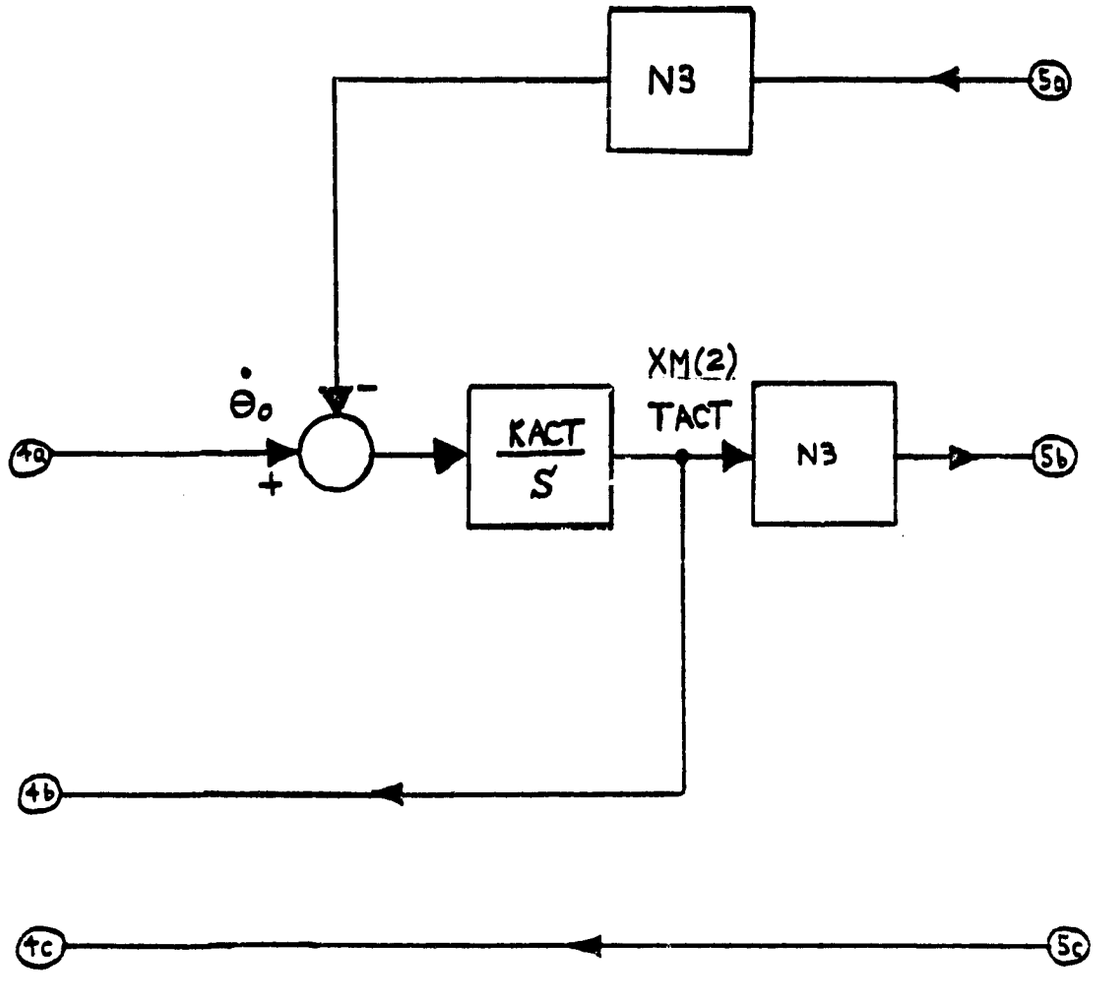

Figure 4.5-1. (cont)

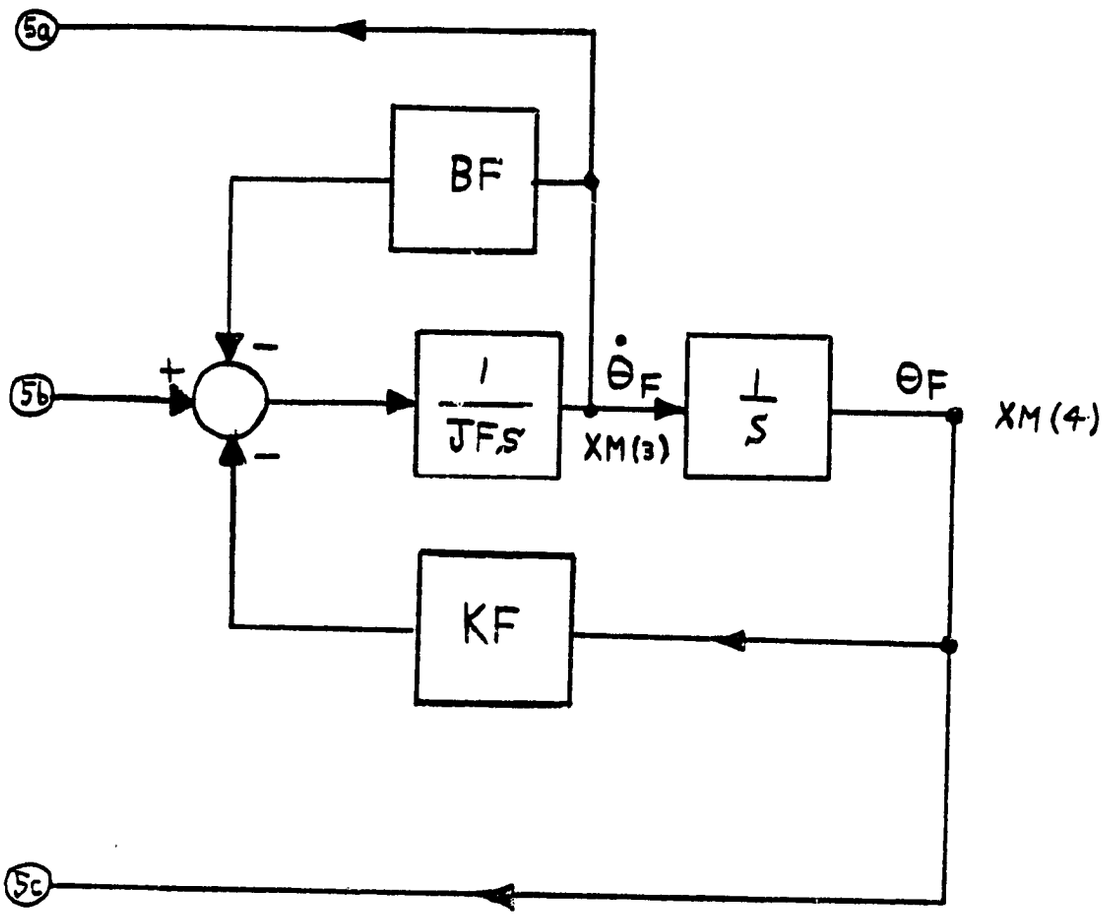

Figure 4.5-1. (cont)

This scheme is inefficient and could result in excessive roundoff since the time constants of the three blocks are widely separated. To reduce this inefficiency a second time discretization technique was adopted, Figure (4.5-2b). In this scheme, the time steps are scaled according to the relative speeds of the dynamics associated with the subsystems. Typical values of these time steps are:

Power Conditioner and Machine Model: 5-20 μs

Velocity Loop Model: 50-100 μs

Mechanical and Position Loop Model: 100-500 μs

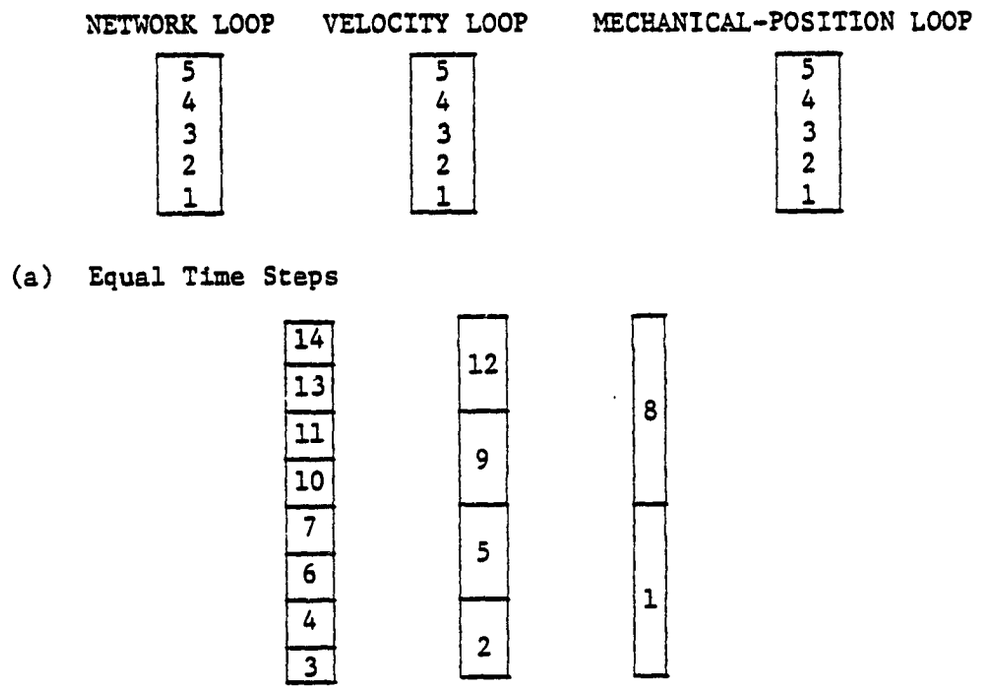

Figure (4.5-2) Integration Options for the EMA Model

The staggering of the time steps, which is evident from the order of integration (see Figure (4.5-2b), introduces a problem concerning the generation of the inputs for the slower integration loops. That is, some of the inputs for the faster loops are functions of the state variables of the slower loops. These inputs are generated by integrating the slowest loop first, and so on, and using linear interpolation to generate the proper input sequence for the fast loops. The interpolation scheme is illustrated by Figure (4.5-3). The solid points, (·), represent actual integration points in time, while the points marked by an (x) are interpolated.

The number of integrations required for a complete step response can be greatly reduced replacing the detailed power conditioner and machine model of equation (3.3-15) by the following:

$$TM = KT * ICMD1 \qquad (4.5\text{-}1)$$

where TM is the machine torque (Nt-m)
KT is the machine torque constant (Nt-m/amp)
and ICMD1 is the filtered current command (amps)

In addition, the rotor velocity is clamped at VMSAT = $\pm$9500 rpm to account for the velocity saturation which occurs during motoring because of increasing phase back emfs. This simplification of the EMA model reduces the order of the state equations from fourteenth to tenth and at the same time it allows the use of large time steps.

To further increase the program flexibility, an option has been added to allow steady state analysis of the power conditioner and machine network. Steady state, in this case. does not imply frequency domain analysis but rather it implies a constant torque command and a constant machine speed. These three program options

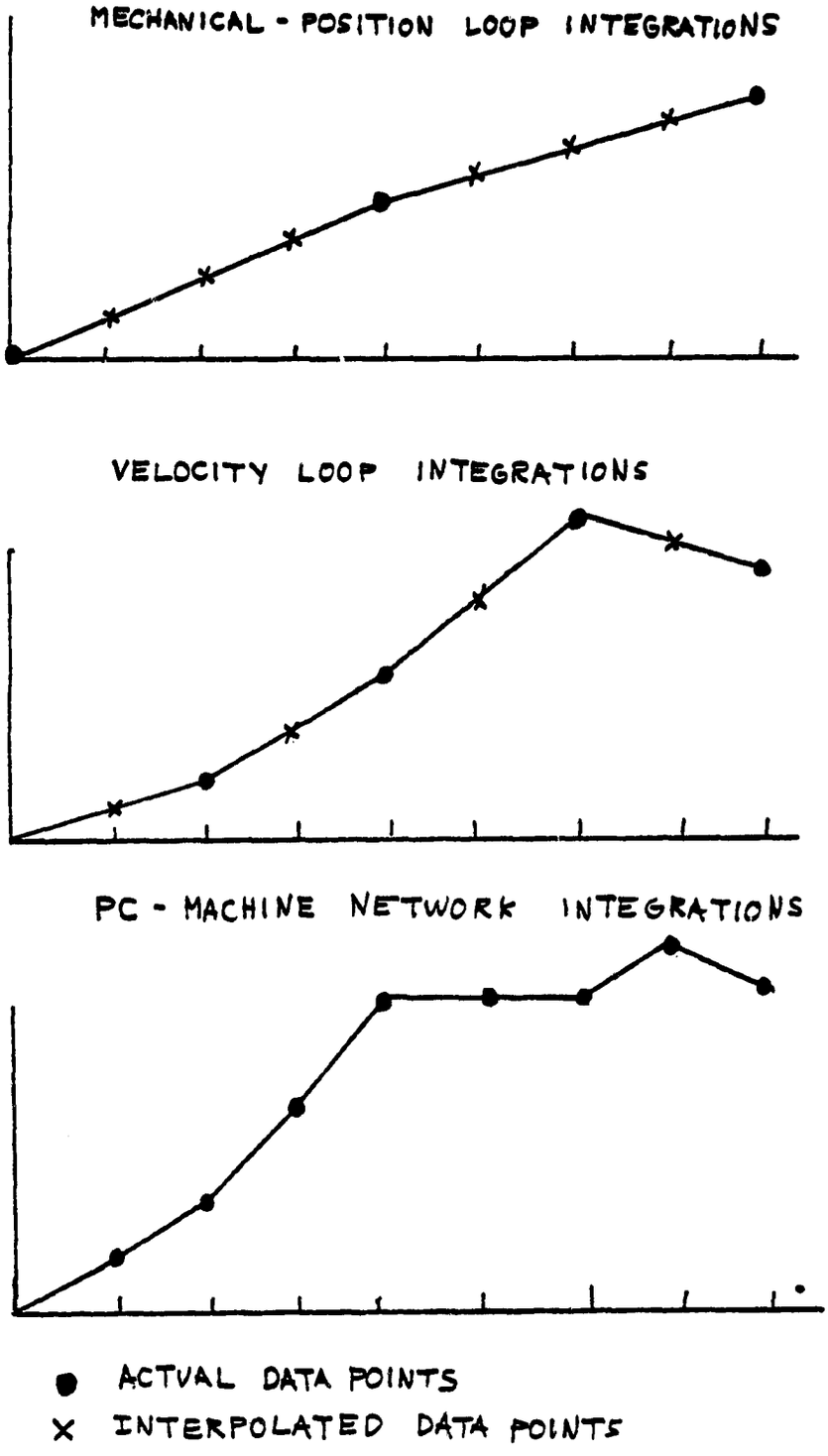

Figure 4.5-3. Interpolation of State Variables Backward in Time.